STABLE SPREADING OF ACOUSTIC PULSES DUE TO LAMINATED MICROSTRUCTURE.

A DISSERTATION
SUBMITTED TO THE DEPARTMENT OF SCIENTIFIC COMPUTING AND
COMPUTATIONAL MATHEMATICS
AND THE COMMITTEE ON GRADUATE STUDIES
OF STANFORD UNIVERSITY
IN PARTIAL FULFILLMENT OF THE REQUIREMENTS
FOR THE DEGREE OF
DOCTOR OF PHILOSOPHY

By
Knut Sølna
August 1998

I certify that I have read this dissertation and that in my opinion it is fully adequate, in scope and quality, as a dissertation for the degree of Doctor of Philosophy.

Prof. George C. Papanicolaou
(Principal Adviser)

I certify that I have read this dissertation and that in my opinion it is fully adequate, in scope and quality, as a dissertation for the degree of Doctor of Philosophy.

Prof. James Berryman

I certify that I have read this dissertation and that in my opinion it is fully adequate, in scope and quality, as a dissertation for the degree of Doctor of Philosophy.

Prof. Paul Switzer

Approved for the University Committee on Graduate Studies:

Preface

We consider acoustic pulse propagation in inhomogeneous media over relatively long propagation distances. Our main objective is to characterize the spreading of the travelling pulse due to microscale variations in the medium parameters. The pulse is generated by a point source and the medium is modeled by a smooth three dimensional background that is modulated by stratified random fluctuations. We refer to such media as *locally layered*.

A second objective is to establish a realistic model for the fine scale heterogeneities of the lithology from measurements and to explore how the theory of pulse spreading can be used to estimate the unknown parameters of the medium. We also explore how to eliminate pulse spreading, to the extent possible, by a suitable deconvolution process.

We show that, when the pulse is observed relative to its random arrival time, it *stabilizes* to the pulse shape determined by the slowly varying background convoluted with a Gaussian. The width of the Gaussian and the random travel time are determined by the medium parameters along the ray connecting the source and the point of observation. The ray is the one determined by classical high frequency asymptotics (geometrical optics). The analysis of this phenomenon involves the asymptotic solution of partial differential equations with randomly varying coefficients and is based on a novel representation of the field in terms of generalized plane waves that travel in opposite directions relative to the layering.

We show how the medium parameters can be estimated effectively from observations of the spreading of a pulse propagating through the medium. We do this for a purely layered model medium which is based on a statistical analysis of well-logs from

the North Sea. This analysis also reveals that, in this simplest case, the spreading of the pulse is accurately predicted by the theory.

Acknowledgements

I would like to express my deepest gratitude to my advisor Professor George C. Papanicolaou. His broad knowledge and interests have strongly enrichened my studies. I have appreciated his enthusiasm and energy in approaching new problems and his dedication and commitment to his students. I am also grateful to my previous advisors Professor Henning Omre and the late Professor Henrik H. Martens. They have all influenced my interests and values and I feel fortunate for having had the opportunity to work with them.

At Stanford I have also had the privilege of collaborating with Professors Gene Golub and Paul Switzer and have greatly enjoyed both their friendship and their academic advice.

I would like to thank Professor Joe Keller for his lucid lectures on wave propagation and for serving on my oral committee. His integrity and style of mathematics serves as a model for me.

I am also grateful to Dr. James Berryman for carefully reading my thesis and to Professor Jerry M. Harris for serving on my oral committee.

My studies at Stanford was made possible through financial support from The Research Council of Norway. I would like to extend my gratitude to Are Birger Carlson and the PROPETRO committee for their decision to support me.

During my stay at Stanford I have enjoyed the congenial and supportive atmosphere among the students in the SCCM program and I would like to thank them all for this. In particular I would like to thank Robert Lu and Hamid H. Samandari for their friendship and encouragement.

Finally, but above all, I would like to thank my parents for their love and support.

Contents

Chapter 1

Introduction

When an acoustic pulse propagates through an inhomogeneous medium, its shape and travel time are modified by fine scale heterogeneities. We will analyze in detail this phenomenon, in particular the way the modifications relate to the characterization of the inhomogeneities.

With increased resolution of seismic imaging methods it is important to determine when and how the probing pulse starts to interact with fine scale heterogeneity. For instance, in attempting to remove multiples Claerbout [14] points out that having correct amplitude and phase for these is important. The theory which we are about to describe explains how these are influenced by the microstructure. Serakiotou [42] exploits a simple version of the theory when designing a scheme for elimination of multiples. Amplitude information is also important in amplitude versus offset analysis and Widmaier et al. [55] suggest that the theory should be useful for this purpose.

We model the fine scale medium heterogeneities as random. Hence, deriving a description of the role of the fine scale heterogeneities involves the analysis of stochastic linear partial differential equations. The analysis will be based partly on the framework set forth in [3, 26, 36]. As pointed out by Keller [22] the reason for using stochastic equations is the belief that their solution represents physical phenomena which could not be investigated satisfactorily in any other way. In our case a description capturing all details of the scattering of the wave by all the heterogeneities of the earth's crust would be prohibitively complex. Moreover, the detailed structure

of the earth's crust is not known. Thus, we replace the actual fine scale variations by random variations whose statistics reflect those of the actual medium. As a result the propagating pulse becomes a random process. We shall see, however, that up to a random travel time correction, the accumulated effect of the fine scale layering can be described in a relatively simple, deterministic way.

In order to illustrate the main result we first consider, in the next section, the one dimensional purely layered case and review some pertinent literature. This case is well understood. So far however, only the purely one dimensional case has been analyzed. We generalize the theory to a medium that varies with respect to all three space coordinates. In the next section we also introduce a three dimensional model medium and give the main result of our theory describing pulse propagation in such a medium. The theory is derived in Chapter 2.

Whether or not the modeling of the medium captures the features that are important for pulse spreading can only be judged by comparing simulations with observations. In a second part of the thesis, described in Chapter 3, we carry out an investigation of this using well-logs from the North Sea. We also show how the theory can be used to effectively estimate parameters in the model medium. In Section 1.2 we give an introduction to Chapter 3.

1.1 The O'Doherty-Anstey approximation.

Wave pulses that propagate through finely *layered* media tend to spread and develop small scale fluctuations in their coda. The O'Doherty-Anstey theory [33] describes this spreading for such media. If the front of the pulse is observed relative to the random arrival time at some depth, it *stabilizes*. That is, statistical fluctuations around the deterministic mean pulse shape become negligible. This is a key property that was not noted in O'Doherty and Anstey's paper. In order to illustrate our main result concerning pulse propagation in media that are not restricted to layered ones we first consider the one dimensional purely layered case with a sound pulse impinging upon a heterogeneous halfspace $z > 0$. The halfspace $z < 0$ is homogeneous and the

pulse impinging at the surface is $p_0(t/\varepsilon^2)$. The pressure variations solve the wave equation in the heterogeneous halfspace

$$p_{zz} - \gamma^2(z)\, p_{tt} \;=\; 0$$

with the slowness $\gamma(z)$ modeled by

$$\gamma^2(z) \;=\; \gamma_0^2(1 + \varepsilon\, \nu(z/\varepsilon^2)). \tag{1.1}$$

The fluctuation ν is a statistically stationary process and represents the fine scale layering. Note that the impinging pulse is defined on the same scale as the fine scale medium heterogeneity. In this example there is no variation in the background medium and the amplitude of the fine scale variations is small, of order ε. We will consider more general models for which this is not the case. For short propagation distances the pulse travels essentially undistorted with a speed corresponding to the slowness γ_0. This is the effective medium approximation. However, for relatively long propagation distances, $z = z_1$ say, the effect of the fine scale layering becomes appreciable. The scattering associated with the layering gradually delays the pulse and changes its shape. The net effect can be described by

$$p(z_1, t_1 + \varepsilon^2 s) \;\sim\; [p_0(\cdot) \star \mathcal{H}(\cdot, z_1)](s) \qquad as \;\; \varepsilon \downarrow 0.$$

The pure propagation picture has been modified in a way we now explain.

Firstly, the travel time to depth z_1 for the approximation is random and given by

$$t_1 \;=\; \gamma_0 \int_0^{z_1} [1 + \varepsilon\, \nu(s/\varepsilon^2)/2]\, ds \tag{1.2}$$

which is obtained by adding a zero-mean random correction to the travel time associated with the deterministic or effective medium. The corrected arrival time is the first order Taylor approximation of $\tau_1 = \gamma_0 \int_0^{z_1} \sqrt{[1 + \varepsilon\ \nu(s/\varepsilon^2)]}\ ds$, the first arrival time at depth z_1.

Secondly, when we observe the pulse relative to its random arrival time we see a deterministic pulse shape, the original pulse convolved with the function $\mathcal{H}$. This function is

$$\mathcal{H}(s,z) \quad = \quad F^{-1}[e^{-z\omega^2 dF[h]}],$$

where F is the Fourier transform, $\star$ is convolution, $d = \gamma_0/8$ and $h(s) = E[\nu(0)\nu(s/2\gamma_0)]$ for $s > 0$ and 0 otherwise, with E denoting expectation. Based on this representation, one easily finds that

$$\begin{aligned} \partial_z \mathcal{H} &= d\ \partial_s^2[h(\cdot) \star \mathcal{H}(\cdot, z)](s) \\ \mathcal{H}(s,0) &= \delta(s). \end{aligned} \tag{1.3}$$

Thus, if z is large and $\mathcal{H}$ already relatively smooth such that $h(\cdot)$ can be considered as an impulse function, then $\mathcal{H}$ evolves essentially like a diffusion process and approaches a Gaussian pulse shape. The convolution of the pulse with $\mathcal{H}$ reflects its spreading which is caused by the fine scale random scattering which in a sense mixes the signal components and causes it to diffuse about its center. If the variance of the process ν is small or its spatial correlation relatively small it corresponds to the 'effective diffusion' in the above problem being small producing less spreading of the pulse. The function $\mathcal{H}$ is purely deterministic. Hence, if we observe the pulse relative to the random arrival time t_1, the pulse shape is also deterministic. This is what we call pulse stabilization.

The study of the effect of fine scale layering on a propagating pulse was initiated in [33] by O'Doherty and Anstey. On physical grounds they proposed a formula

which embodies somewhat implicitly the two effects mentioned above. They based their derivations on a discrete equal travel time representation of the medium. The first to give a mathematical account for the phenomenon in the continuous case were Banik et al. in [4] and [5]. They obtain the O'Doherty-Anstey formula using a mean-field approach, and applied it to investigate the pulse shaping associated with specific stochastic models for the heterogeneity. Resnick et al. [38] present an interesting alternative derivation of the formula, and were the first to approach the problem from an invariant imbedding point of view. However, the first rigorous account for the stabilization phenomenon was given by Burridge et al. in [12]. Here they derive the version of the formula which applies to an equal travel time discretized medium by using an averaging technique. Based on this result Burridge et al. performed a careful numerical investigation in [8] and [9] which showed that the formula generalizes to elastic wave propagation with obliquely travelling plane waves. Moreover, with this as their starting point they generalize the formula also to pulses generated by a point source over a layered medium in [10] by decomposing the source in terms of plane waves and using a stationary phase argument. Asch et al. [3] presents the first rigorous derivation of the formula in a continuous framework using invariant imbedding and by applying a limit theorem for stochastic ordinary differential equations. This analysis was generalized to reflections, rather than only the directly transmitted pulse, in [35] by Lewicki and Papanicolaou. Finally, in [28] Lewicki generalizes the O'Doherty-Anstey formula to certain rather general hyperbolic systems using an averaging approach.

In these last three reports the fluctuations in the medium were assumed to be continuous. Furthermore, in all of the above the fluctuations were assumed to be weak as in (1.1). The fact that the coupling to the fluctuations is weak is what allows one to probe the medium with a pulse on the same scale as the fluctuations, the scale ε^{-2}, and still observe stabilization. Recently, a different type of medium model has been considered. Here, the fluctuations are strong O(1) and not necessarily continuous. In this framework the source pulse is defined on the time scale t/ε rather than t/ε^2. Otherwise the pulse would interact strongly with every feature of the random medium and a characterization of the transmitted pulse in general terms would not be possible.

What enables one to push through the argument showing stabilization in this case are the rapid variations in the fluctuations. For this new scaling of the source there would be no pulse shaping associated with weak fluctuations. In the strong noise case with

$$\gamma^2(z) \;=\; \gamma_0^2(1+\nu(z/\varepsilon^2)),$$

the description (1.3) essentially prevails. Since the travelling pulse is broad compared to the fluctuations it does not 'feel' this detailed structure. Thus (1.3) is modified in that the convolution by h is replaced by multiplication with the integral of h, its magnitude as a distribution. Furthermore, the modification of the deterministic travel time is defined similarly as above, in this scaling

$$t_1 \;=\; \gamma_0 \int_0^{z_1} [1+\nu(s/\varepsilon^2)/2]\; ds.$$

This model was first analyzed by Burridge et al. in [11] and Clouet and Fouque in [15] using invariant imbedding approaches. Lewicki et al. generalize in [29] the results to certain rather general hyperbolic systems. Moreover, in [13] Chillan and Fouque extend the theory to the case with a point source over a strongly heterogeneous layered halfspace.

O'Doherty and Anstey's original paper was motivated by the need to characterize the effect of fine scale heterogeneity in seismic wave propagation. Realizing the importance of such a description a string of studies followed, aimed at a rigorous derivation of the formula and at extending it to more general medium models. However, all of these deal with a purely *layered* medium. To be able to describe wave propagation in an actual application it is necessary to somehow characterize the significance of lateral variation in the parameters. In this thesis we present a theory that generalizes the O'Doherty Anstey theory to a non-layered medium model of a certain kind. This

medium model has general three dimensional smooth, deterministic background variations which are modulated by stratified fine scale random fluctuations. Thus, on a micro scale we have a layered structure. The model is motivated by sedimentary rock formations where the sedimentary cycles create structures resembling a tilted stack of layers. On such local formations there are superposed, in general, coarse scale variations due to macroscopic geological events. We call such media *locally layered*.

The analysis in the locally layered case is fundamentally different, and more complicated than in the one dimensional case, due to the lateral variation in the parameters. We base the analysis on a new representation of the wave field in terms of locally up- and down-propagating waves, moreover, a novel way of specifying the interaction of these. This specific representation enable us to generalize the theory to locally layered media.

The main result can be stated as follows. A point source in a homogeneous halfspace generates a pulse impinging on a locally layered halfspace. The random layering modifies the transmitted pulse associated with the deterministic/effective medium when $\nu \equiv 0$. The random traveltime correction and the 'filter' modifying the pulse shape are given by (1.2) and (1.3), when these are generalized in the following way. The independent variable z and the integration path $(0, z_1)$ are replaced by the arc length parameter along a geometrical optics ray path and this path itself. The path is the one associated with solving the eiconal equation for the point source problem with the deterministic part of the medium parameters, see [23], which connects the source point and the point of observation. When the pulse travels obliquely relative to the layering, it 'sees' a fine scale structure with increased spatial correlation length. Thus (1.3) is also modified in that h is scaled suitably and becomes a function of the path argument. A precise statement of this result is stated in Section 2.5.

1.2 Modeling & estimation of microstructure.

In Chapter 3, we introduce and analyze a stochastic model for a layered medium based on a set of well-logs from the North Sea. Our motivation for the modeling is

twofold.

First, we want to examine whether the model for the medium which we used in the mathematical analysis is appropriate for describing pulse shaping, the transformation of the propagating pulse in a finely layered medium.

Second, we want to explore how accurate the pulse shaping approximation is when we use a model for the microstructure which is estimated from the well-logs. We also want to examine the actual degradation of the pulse and how this can be restored and, moreover, how we can estimate the parameters describing the microstructure by observing the degraded pulse.

Several authors have introduced models for the medium parameters corresponding to well-log measurements. In [7] Bølviken et al. model such parameters in terms of a hidden Markov chain and use this to design a scheme for automatic regime classification. In [25] Kneib models the acoustic velocity in terms of a nested exponential model. The different correlation ranges may be interpreted as corresponding to phenomena occurring on different scales. In [[50, 51, 58]], the macro and micro scales of modeled medium parameters, actually all scales, have been combined into a self similar, intrinsically stable process. In [18] and [57] the modeling is in terms of a stationary processes in the wide-sense. The model introduced in [52] has been used in several studies to generate synthetic media for use in wave propagation simulations. This model represents the medium in terms of the reflectivity process rather than the underlying acoustic parameters.

We propose a model that has the following characteristics. We model in terms of the primary acoustic variables, the density and compliance, and clearly distinguish between a micro- and a macro-scale. When the effects of the macro-scale modulations are taken out the model is statistically stationary.

The rationale for our modeling is that the medium representation is simple and its components have a clear physical interpretation which can be easily related to the measurements. It is also straight forward to simulate realizations from the model and a two scale model is desirable both from the point of view of analysis and applications. The analysis in the first chapter is based on a two scale framework which was set forth

in [3]. From an applications point of view it is natural to distinguish a macro-scale, which represents that part of the medium which can be estimated for instance by reflection seismology, from the micro-scale part that cannot be explicitly estimated, but whose statistics might possibly be estimated.

An important ingredient in the parameter estimation scheme that we use is an explicit model for the measurements tool, relating the well-logs to the physical parameters. This strongly influences the parameter estimates, but was not included in the cited papers.

O'Doherty and Anstey [33] observed that scattering associated with fine scale layering could account for a significant damping of the amplitude in seismic exploration and that such damping resembles the one associated with anelastic damping. Thus the effect of the fine scale layering was referred to as 'apparent attenuation' in the papers [40], [41] by Schoenberger and Levin. Based on a set of well-logs they examine numerically the effect of fine scale layering. Their results corroborated the aspect of the O'Doherty-Anstey formula which characterized the damping effect. Further simulations were carried out by Richards and Menke in [39], which however used media derived from a statistical models rather than from well-logs. They point out that the effect of 'apparent attenuation' is to redistribute energy rather than to remove it altogether. Moreover, a number of authors, [44] and [24], have explored how the O'Doherty-Anstey theory can be used for estimation of scattering attenuation without, however, exploiting the part of the theory that includes pulse stabilization.

We also carry out simulations. They confirm that as far as the pulse shaping is concerned it is appropriate to use the proposed model. Moreover, the theory accurately predicts the effect of the fine scale heterogeneity for realistic values of the medium parameters. We make explicit use of the *stabilization* phenomenon to design a deconvolution scheme that approximately removes the pulse shaping effect and to obtain robust estimates for certain medium parameters by observing the pulse shaping for a *single* transmitted pulse. We consider this to be the main contribution of the chapter.

1.3 Limitations.

The locally layered theory is a major step in generalizing the O'Doherty Anstey theory, but only a first step towards the analysis of the effects of microstructure in non-layered media because many important physical phenomena have been left out.

Intrinsic attenuation may often be more important than scattering associated with microstructure. In [11] the O'Doherty-Anstey approximation was derived for a layered medium in the prescence of intrinsic attenuation. The resulting approximation illustrates how the transmitted pulse is being modified depending on the values of the parameters that characterize the microstructure and the dissipation.

With waves propagating obliquely relative to the layering, mode conversion and anisotropy effects need to be analyzed. In the purely layered case the O'Doherty-Anstey approximation has been extended to rather general hyperbolic systems [29] describing for instance elastic wave propagation. Then the correlation of the parameters associated with the different modes of propagation becomes important.

It may also be necessary to have more general stochastic models for the microstructure to adequately represent a realistic medium. In particular it would be desirable to relax the assumption that the microstructure is stratified.

In the seismic exploration context a description of reflections associated with singularities or jumps in the macroscale medium component is important, but is not included in the current version of the locally layered theory. However, in the layered case a medium with such discontinuities has been considered [35].

In the data analysis we consider statistical variations of the acoustic parameters with respect to depth only. To assess the importance of some of the above mentioned phenomena this analysis needs to be extended, by looking, for instance, at lateral variations or correlations between the elastic parameters.

1.4 Plans.

The current and planned research activity focuses on addressing some of the above deficiencies.

First, we would like to generalize the pulse spreading theory to a wider class of models. As mentioned, the pulse shaping theory has been extended in the layered case to problems governed by rather general hyperbolic systems, and to media with dissipative mechanisms or a discontinuous background. We plan to do this also in the locally layered case.

Whether or not the theory generalizes when the fluctuations are *not* a function of one variable only, but have some lateral variation, is an important open question we also want to pursue.

In the one dimensional case the theory has been extensively tested with numerical simulations [12, 43], but this has not been done for non-layered problems. We believe that a time domain finite difference scheme that is adapted to the front of the wave is appropriate in this case.

Several authors [42, 55] have looked at applications of the *layered* O'Doherty-Anstey theory in seismic imaging. We want to pursue this based on its generalization to non-layered media. In particular developing tools for robust identification of the coherent components in a seismogram. The pulse shaping approximation characterizes how these are corrupted by microstructure. A theory for the fluctuations in the seismogram is derived in [3] and these can be analyzed using a flexible adaptive wavelet decomposition which was recently derived and implemented [30]. We aim at using such prior knowledge about the main character of the components in the seismogram combined with adaptive signal processing algorithms [30, 31] as tools when seismic traces are processed and combined in order to enhance their main features, the strong reflections.

1.5 Outline.

In the second chapter we generalize the O'Doherty-Anstey approximation to locally layered media, both for strongly and weakly fluctuating media. In the first section we present the formulation of the problem and the governing equations. In Section 2.2 we review briefly the high frequency approximation of the deterministic problem. In

Sections 2.3 and 2.4 we discuss the results in the one-dimensional case, that is the case with a purely layered medium and an impinging vertical plane wave. Then in Section 2.5, we state the O'Doherty-Anstey approximation for a locally layered medium when the impinging pulse is being generated by a point source. In Sections 2.6 and 2.7, we derive the results presented in Section 2.5. First, in Section 2.6, we derive the result in the purely layered case. We obtain the approximation by combining the method of stationary phase and invariant imbedding. In Section 2.7 we introduce the modification of the high frequency formulation which enables us to generalize the analysis of Section 2.6 to the locally layered case.

In the third chapter we estimate layered models for the fine scale heterogeneity based on a set of well logs from the North Sea. We also consider applications of the O'Doherty-Anstey theory. In Sections 3.1 and 3.2 we review briefly the acoustic equations and also the O'Doherty-Anstey approximation for a Goupillaud or equal travel time medium. In Section 3.3, we present the well-logs and the stochastic model for the medium. In Section 3.4 we simulate numerically acoustic wave propagation through realizations of the model medium and discuss possible applications of the O'Doherty-Anstey theory. In Section 3.5 we consider the effect of fluctuations in the density parameter and collect some concluding remarks in Section 3.6.

Chapter 2

Pulse shaping due to microstructure.

In this chapter we analyze the spreading of a spherical acoustic pulse as it propagates in a locally layered halfspace. A smooth, macroscopic three dimensional background variation is modulated by a fine scale random layering which need not be plane on the macro scale. We show that when the propagating pulse is observed relative to its random travel time it stabilizes to a shape determined by the slowly varying, deterministic background, convolved with a Gaussian. The width of the Gaussian and the random travel time are determined by the medium parameters along the ray connecting the source and the point of observation; the ray is defined according to geometrical optics.

For short propagation distances, on the order of several pulse lengths, the approximation coincides with the classical effective medium approximation.

A full numerical validation of the three dimensional case is complicated and has not been carried out.

2.1 The acoustic equation and scaling.

We consider acoustic wave propagation in three space dimensions. Let $\boldsymbol{u}(\boldsymbol{x}, z, t)$ and $p(\boldsymbol{x}, z, t)$ be the acoustic velocity and pressure satisfying the equation of continuity

of momentum and mass

$$\begin{aligned} \rho\ \boldsymbol{u}_t + \nabla p &= \boldsymbol{F}_\varepsilon(\boldsymbol{x}, z, t) \\ K_\varepsilon^{-1}(\boldsymbol{x}, z)\ p_t + \nabla \cdot \boldsymbol{u} &= 0, \end{aligned} \tag{2.1.1}$$

where t is time, z is depth into the medium and $\boldsymbol{x} = (x_1, x_2)$ are the horizontal coordinates. Note that z is defined so as to increase with depth. Furthermore, ρ and K_ε^{-1} are material properties, density and compliance, respectively. Above and in the sequel boldface indicates a vectorial quantity. The geometry of the problem is shown in Figure 2.1. A point source, modeled by $\boldsymbol{F}_\varepsilon$, is located in the homogeneous half space $z < 0$ and initiates a pulse impinging on the heterogeneous halfspace. The focus of the thesis is to characterize how the heterogeneities transform the pulse as it travels. That is, to identify the convolving function indicated by a question mark in Figure 2.1. In the above model we have introduced the small dimensionless parameter ε. The role of this parameter is to distinguish phenomena occurring on different scales. We let the compliance, K_ε^{-1}, have a two scale structure. Its mean varies on a macroscopic scale while it is being randomly modulated on a microscopic scale. We find it convenient to order the various length scales relative to the macroscopic scale of the compliance corresponding to the macroscopic propagation distance which is an O(1) quantity.

We will consider two qualitatively different models for the character of the material properties, corresponding to two different choices in the definition of K_ε^{-1} in terms of ε.

First, we consider what we refer to as a *locally layered strongly heterogeneous* random medium. In this case the material properties, density and compliance are modeled by

$$\begin{aligned} \rho(\boldsymbol{x}, z) &\equiv \rho_0 \\ K_\varepsilon^{-1}(\boldsymbol{x}, z) &= \begin{cases} K_0^{-1} & z \in (-\infty, 0] \\ K_1^{-1}(\boldsymbol{x}, z)(1 + \nu(\Phi(\boldsymbol{x}, z)/\varepsilon^2)) & z \in (0, \infty) \end{cases}, \end{aligned} \tag{2.1.2}$$

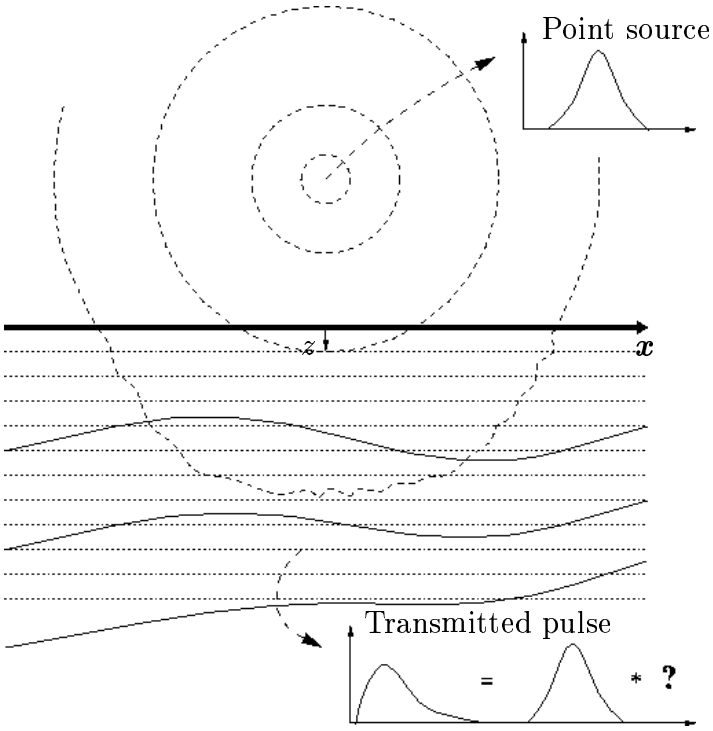

Figure 2.1: The physical problem.

where the mean K_1^{-1} is a smooth and positive function. The fluctuation ν modulating the compliance is a zero-mean, stationary stochastic process bounded below by $(-1+d)$, with d a positive constant. It is assumed to have a rapidly decaying correlation function. Note that the random modulation includes the smooth function Φ. This model can be transformed, by a change of variables as in Appendix C, to the more special one in which the modulation term is a function of depth only. Hence, in the sequel we assume $\nu = \nu(z/\varepsilon^2)$. The fluctuation embodies the random character of the medium. The forcing is due to a point source given by

$$\boldsymbol{F}_\varepsilon(\boldsymbol{x}, z, t) \;=\; \varepsilon\, f(t/\varepsilon)\delta(\boldsymbol{x})\delta(z - z_s)\boldsymbol{e}, \tag{2.1.3}$$

where f is a pulse shape function, $\boldsymbol{e}$ is the source directivity vector and the source

location is $(\mathbf{0}, z_s)$, with $z_s < 0$. In order to simplify formulas we will assume a vertical source $\boldsymbol{e} = (\mathbf{0}, 1)'$ and the matched medium case, that is $K_1^{-1}(\boldsymbol{x}, 0) \equiv K_0^{-1}$. The ε scaling of the source magnitude has been introduced only to make the transmitted pulse an $O(1)$ quantity.

What sets the above model apart from previously considered models is that the mean compliance K_1^{-1} is a function of all space coordinates; thus we consider wave propagation which is truly three dimensional. Furthermore, that the fluctuation process ν is a function of the level surfaces of Φ. On the finest scale of the model, the scale of the fluctuations, the medium variations are essentially one-dimensional. We therefore refer to the model as locally layered. The rationale for denoting the model as strongly heterogeneous is that the amplitude of the random modulation is $O(1)$, and not small. Note also that the source is on a time scale intermediate between that of the fluctuations and that of the background medium. In this scaling the effect of the macroscopic features of the medium on the propagating wave can be analyzed by a high frequency approximation, while the propagation relative to the microstructure can be understood in terms of averaging of stochastic equations.

Second, we consider a scaling in which the density and compliance are modeled by

$$\begin{aligned} \rho(\boldsymbol{x}, z) &\equiv \rho_0 \\ K_\varepsilon^{-1}(\boldsymbol{x}, z) &= \begin{cases} K_0^{-1} & z \in (-\infty, 0] \\ K_1^{-1}(\boldsymbol{x}, z)(1 + \varepsilon\nu(\Phi(\boldsymbol{x}, z)/\varepsilon^2)) & z \in (0, \infty) \end{cases}, \end{aligned} \tag{2.1.4}$$

and refer to this as a *locally layered weakly heterogeneous* random medium. In this case the source is taken to be

$$\boldsymbol{F}_\varepsilon(\boldsymbol{x}, z, t) = \varepsilon^2 \, f(t/\varepsilon^2)\delta(\boldsymbol{x})\delta(z - z_s)\boldsymbol{e}. \tag{2.1.5}$$

This model differs from (2.1.2) & (2.1.3) only in that the amplitude of the random

fluctuations is $O(\varepsilon)$, and that the source is defined on the same scale as the fluctuations, the finest scale of the model. Such a scaling is not appropriate in the strongly heterogeneous case because the pulse will interact strongly with every feature of the particular realization of the random modulation. In the weakly heterogeneous case, this scaling is appropriate because the coupling between the propagating pulse and the random process ν is weak and an asymptotic characterization of the transmitted pulse can be obtained.

In both of the above cases we assume that the medium is initially at rest

$$\begin{aligned} f(t) &= 0 \quad \text{for} \quad t \in (-\infty, 0] \\ p(\boldsymbol{x}, z, t) &= 0 \qquad \text{“} \\ \boldsymbol{u}(\boldsymbol{x}, z, t) &= \mathbf{0} \qquad \text{“}. \end{aligned} \tag{2.1.6}$$

The analysis can be extended to the case in which the density, ρ, is given by

$$\rho(\boldsymbol{x}, z) = \begin{cases} \rho_o & z \in (-\infty, 0] \\ \rho_1(\boldsymbol{x}, z)(1 + \eta(z/\varepsilon^2)) & z \in (0, \infty) \end{cases},$$

in the strongly heterogeneous case and similarly in the weakly heterogeneous case. Here, η is a fluctuation process with the same properties as ν.

Finally, when the mean compliance K_1^{-1} and the fluctuations ν are functions of depth z only, then the random medium is purely layered and this situation has been extensively studied, see for example [3], [15] and [35].

Here, for ease of presentation, we will deal exclusively with the models defined by (2.1.1) – (2.1.3) & (2.1.4) – (2.1.5) and the layered versions thereof.

2.2 High frequency wave propagation.

When there are no fluctuations, $\nu \equiv 0$, we can analyze (2.1.1) in the high frequency approximation. We will obtain the approximation for the transmitted pulse in the random case as a modification of the deterministic one. In this section we review the deterministic case since this serves to motivate our approach in later sections. We carry out the calculations with respect to the strongly heterogeneous model. The result in the weakly heterogeneous case is completely analogous. Note that, for the model at hand, the deterministic case corresponds to using effective medium parameters; see [3].

2.2.1 Point source case.

Consider the deterministic version of the strongly heterogeneous model defined in (2.1.1) – (2.1.3) & (2.1.6). In view of the form of the source pulse, we define the scaled Fourier transform as

$$\hat{p}(\mathbf{x}, z, \omega) \;=\; \int p(\mathbf{x}, z, s) e^{i\omega s/\varepsilon} ds.$$

By elimination of $\boldsymbol{u}$ in (2.1.1) we find that the time transformed pressure solves, in the effective medium/deterministic case,

$$\triangle \hat{p} + (\omega/\varepsilon)^2 \gamma_1^2 \; \hat{p} \;=\; \varepsilon^2 \hat{f}(\omega) \delta(\boldsymbol{x}) \delta'(z - z_s) \tag{2.2.1}$$

where the effective medium slowness is

$$\gamma_1(\boldsymbol{x}, z) \;=\; \sqrt{E[K_\varepsilon^{-1}(\boldsymbol{x}, z)] \; \rho} = \sqrt{K_1^{-1}(\boldsymbol{x}, z) \; \rho}. \tag{2.2.2}$$

The high frequency approximation for the point source problem associated with the reduced wave equation

$$\mathcal{L}u \equiv \triangle u + (\omega/\varepsilon)^2 \gamma_1^2 u = -\delta(\boldsymbol{x})\delta(z - z_s), \tag{2.2.3}$$

has the form

$$u \sim A\, e^{i\omega\varphi/\varepsilon}. \tag{2.2.4}$$

The phase φ is the travel time to a given point in the medium. Thus we have centered the Fourier components with respect to travel time. The amplitude A describes how the source pulse is transformed as it travels. Substituting (2.2.4) in (2.2.3) we find that away from the source the phase, φ, solves the eiconal equation

$$(\nabla\varphi)^2 = \gamma_1^2, \tag{2.2.5}$$

and A satisfies

$$2\nabla\varphi \cdot \nabla A + \triangle\varphi A - i\varepsilon/\omega\triangle A = 0. \tag{2.2.6}$$

The leading order approximation for the amplitude is obtained by requiring it to solve the first order transport equation, that is

$$2\nabla\varphi \cdot \nabla A_0 + \triangle\varphi A_0 = 0. \tag{2.2.7}$$

In order to obtain correct initial conditions we consider (2.2.3) in a neighborhood of the source and match the approximation with the free space Green's function of the homogeneous case, the homogeneous parameters being those at the source point. Thus, we choose $\varphi = 0$ at the source and increasing isotropically away from this point. The eiconal equation is solved by the method of characteristics. An example

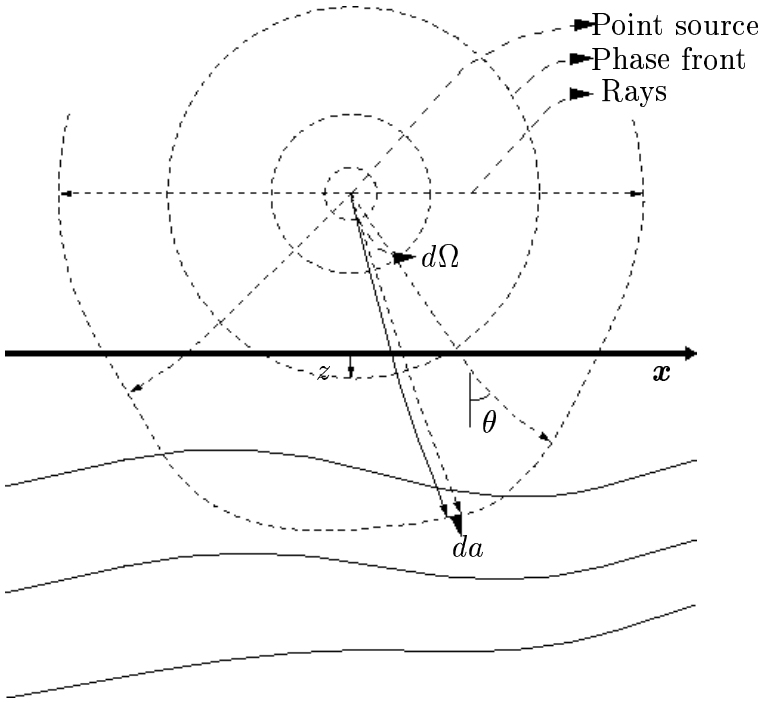

Figure 2.2: Rays associated with propagation from a point source.

showing a possible configuration of characteristic rays orthogonal to the phase fronts $\varphi = constant$ is shown in Figure 2.2. Making use of the source point condition to find also the value of the amplitude at the source point, $A_0(0)$, we arrive at the following approximation for u

$$\begin{aligned} u &\sim A_0(0)\, e^{-\int_\Gamma (\triangle\varphi/(2\gamma_1))\ ds}\ e^{i\omega\varphi/\varepsilon} \\ &= \frac{\sqrt{(d\Omega/da)(\gamma_0/\gamma_1)}}{4\pi}\, e^{i\omega\varphi/\varepsilon} \qquad as\ \ \varepsilon \downarrow 0. \end{aligned}$$

Here γ_0 is the slowness at the source point $(\mathbf{0}, z_s)$ and Γ the ray segment corresponding to the solid line in Figure 2.2, the ray from the source point to the point of observation. Moreover, we made use of the identity

$$e^{-\int_\Gamma \triangle\varphi/(2\gamma_1)ds} \;=\; \sqrt{(d\Omega/da)(\gamma_0/\gamma_1)},$$

derived in detail in [23]. Here, $d\Omega$ is an element of solid angle of the initial directions of rays about the ray path passing through $(\boldsymbol{x}, z)$ and da is the associated element of area on the phasefront.

Since

$$\mathcal{L}[-\varepsilon^2 \hat{f}\ \partial_z u] \;=\; \varepsilon^2 \hat{f}(\omega)\delta(\boldsymbol{x})\delta'(z - z_s),$$

the leading order asymptotic approximation for p is

$$p(\boldsymbol{x}, z, \varphi + \varepsilon s) \;\sim\; \frac{\varphi_z\ \sqrt{(d\Omega/da)(\gamma_0/\gamma_1)}}{4\pi}\ f'(s) \qquad as\ \ \varepsilon \downarrow 0. \tag{2.2.8}$$

In the sequel we need some assumptions about the phase φ associated with the slowness γ_1. We assume that φ is uniquely defined, that the path Γ is nowhere horizontal and that φ is a smooth function in a neighborhood of this path.

Before we turn to the O'Doherty-Anstey theory we briefly consider the high frequency approximation in the one dimensional case, that is for a purely layered medium with an impinging horizontal plane wave.

2.2.2 One dimensional case.

We consider an impinging vertical plane wave and a purely layered medium. The governing equations with appropriate scaling are in the deterministic case

$$\rho\ u_t + p_z \;=\; f(t/\varepsilon)\ \delta(z - z_s) \tag{2.2.9}$$

$$K_1^{-1}(z)\ p_t + u_z \ = \ 0.$$

We define the scaled Fourier transform as above

$$\hat{p}(z,\omega) \ = \ \int p(z,s) e^{i\omega s/\varepsilon} ds,$$

and obtain from (2.2.9) that for $z > 0$

$$\hat{p}_{zz} + (\omega/\varepsilon)^2\ \gamma_1^2\ \hat{p} \ = \ 0. \tag{2.2.10}$$

where

$$\gamma_1(z) \ = \ \sqrt{E[K_\varepsilon^{-1}(z)]\ \rho} = \sqrt{K_1^{-1}(z)\ \rho}. \tag{2.2.11}$$

The leading order high-frequency approximation now amounts to obtaining an asymptotic approximation for $\hat{p}$ in the form

$$\hat{p}(z,\omega) \ \sim \ A(z,\omega) e^{i\omega\varphi(z)/\varepsilon} \qquad as \ \ \varepsilon \downarrow 0, \tag{2.2.12}$$

and then requiring (2.2.10) to be satisfied to first order. In this approximation $\varphi(z)$, the phase, is the travel time from the source and A, the amplitude term, governs the magnitude of the transmitted signal. We find that

$$\begin{aligned} \varphi(z) \ &= \ \tau_1(z) = \int_{z_s}^{z} \gamma_1(s) ds \\ A(z,\omega) \ &= \ A(0,\omega)\sqrt{\gamma_0/\gamma_1(z)} \end{aligned} \tag{2.2.13}$$

with $\tau_1(z)$ the effective medium travel time to depth z, and with $\gamma_0 = \gamma_1(0)$. Note

that the pulse impinging on the heterogeneous halfspace, $z > 0$, does not depend on the value of γ_1 in this halfspace. We can therefore find $A(0,\omega)$ by comparison with the purely homogeneous case when $\gamma(z) \equiv \gamma_0$. Upon backtransforming (2.2.12) in time and substituting the value for $A(0,\omega)$ we obtain

$$p(z, \tau_1(z) + \varepsilon s) \quad \sim \quad 2^{-1}\sqrt{\gamma_0/\gamma_1(z)}\; f(s) \equiv p_0(z,s) \qquad as \quad \varepsilon \downarrow 0. \quad (2.2.14)$$

Thus the phase term τ_1 provides a centering with respect to the travel-time and the amplitude term scales the pulse in terms of variations in the slowness. We see that the high-frequency approximation expresses the propagating wave in terms of a down-travelling wave mode only. In the simplest case discussed above, the approximation is just a translation of the source pulse scaled by a geometric factor. As we saw above, for wave propagation in two and three dimensions the geometric factor also reflects dispersion and confluence of the the characteristic rays of the wave, whereas the phase is the travel time along characteristic rays.

For long propagation distances, scattering by the random fluctuations in the medium parameters causes an appreciable statistical coupling between up- and down-travelling modes. In order to account for this coupling we will, in the next section where we consider the purely layered random case, modify the ansatz (2.2.12) so as to include an up-travelling wave mode as well as a down-travelling wave mode, and show how the O'Doherty-Anstey comes about from this coupling.

2.3 Strongly heterogeneous layered media.

We will review in this section the O'Doherty-Anstey theory in the purely one-dimensional strongly heterogeneous case. That is, when a horizontal plane-wave is impinging upon the layered halfspace $z > 0$. The governing equations with appropriate scaling are

$$\rho\; u_t + p_z \quad = \quad F_\varepsilon(z,t) \qquad (2.3.1)$$

$$K_\varepsilon^{-1}(z)\ p_t + u_z \ = \ 0,$$

with

$$\begin{aligned} \rho(z) &\equiv \rho_0 \\ K_\varepsilon^{-1}(z) &= \begin{cases} K_0^{-1} & z \in (-\infty, 0] \\ K_1^{-1}(z)(1+\nu(z/\varepsilon^2)) & z \in (0,\infty) \end{cases} \\ F_\varepsilon(z,t) &= f(t/\varepsilon)\delta(z-z_s). \end{aligned}$$

We seek an asymptotic in ε approximation of the transmitted pressure. The first step in our analysis is to convert (2.3.1) into a stochastic integro-differential equation for the time harmonic amplitudes of the down-going wave mode of the travelling pulse. Then we show how an approximation of the transmitted pulse follows from an asymptotic approximation of the solution of this integro-differential equation.

2.3.1 Decomposition in terms of up- and down-travelling modes.

In this section we consider the random medium model defined in (2.3.1). In Section 2.6 we will generalize this analysis to the case when we probe a layered medium with a point source. First define the scaled Fourier transform by

$$\begin{aligned} \hat{p}(z,\omega) &= \int p(z,s)e^{i\omega s/\varepsilon}ds \\ \hat{u}(z,\omega) &= \int u(z,s)e^{i\omega s/\varepsilon}ds. \end{aligned}$$

In the positive halfspace the transformed version of (2.3.1) is

$$\begin{aligned} -i\omega/\varepsilon\ \rho\ \hat{u} + \hat{p}_z &= 0 \\ -i\omega/\varepsilon\ K_\varepsilon^{-1}(z)\ \hat{p} + \hat{u}_z &= 0, \end{aligned} \tag{2.3.2}$$

with $\hat{p}$ solving

$$\hat{p}_{zz} + (1+\nu)(\omega/\varepsilon)^2 \, \gamma_1^2(z) \, \hat{p} \;\; = \;\; 0. \tag{2.3.3}$$

We parameterize $\hat{p}$ in terms of up- and down-travelling wave components as

$$\hat{p} \;\; = \;\; Ae^{i\omega\tau_1/\varepsilon} + Be^{-i\omega\tau_1/\varepsilon} \tag{2.3.4}$$

where $A = A(z,\omega)$, $B = B(z,\omega)$ and τ_1 is defined in (2.2.13). Note that in defining the pressure we introduced two degrees of freedom. Therefore, letting the pressure solve (2.3.3), we need an additional constraint on the amplitudes beyond (2.3.4). Substituting (2.3.4) in (2.3.2) we obtain

$$\begin{aligned} \hat{u} \;\; = \;\; & \gamma_1/\rho \, [Ae^{i\omega\tau_1/\varepsilon} - Be^{-i\omega\tau_1/\varepsilon}] \\ & - i\varepsilon/(\omega\rho)[A_z e^{i\omega\tau_1/\varepsilon} + B_z e^{-i\omega\tau_1/\varepsilon}]. \end{aligned} \tag{2.3.5}$$

Recall the interpretation of A and B as amplitudes of the up- and down-propagating wave modes. Since the local scattering occurs on the scale $\mathrm{O}(\varepsilon^{-2})$ with respect to depth z, the fluctuations in A and B will in general have a spatial support of $O(\varepsilon^2)$. For the velocity to depend only on the amplitudes we require

$$A_z e^{i\omega\tau_1/\varepsilon} + B_z e^{-i\omega\tau_1/\varepsilon} \;\; = \;\; 0.$$

This is the additional constraint on the amplitudes. We thus arrive at the ansatz

$$\hat{p} \;\; = \;\; Ae^{i\omega\tau_1/\varepsilon} + Be^{-i\omega\tau_1/\varepsilon} \tag{2.3.6}$$

$$0 \;\; = \;\; A_z e^{i\omega\tau_1/\varepsilon} + B_z e^{-i\omega\tau_1/\varepsilon}, \tag{2.3.7}$$

with $\hat{p}$ solving (2.3.3).

The above formulation is a special case of the one discussed in [3]. In this paper the ansatz

$$\begin{aligned} \hat{p} &= \xi_1^{1/2}[\overline{A}e^{i\omega\tau_1/\varepsilon} - \overline{B}e^{-i\omega\tau_1/\varepsilon}] \\ \hat{u} &= \xi_1^{-1/2}[\overline{A}e^{i\omega\tau_1/\varepsilon} + \overline{B}e^{-i\omega\tau_1/\varepsilon}], \end{aligned} \tag{2.3.8}$$

is used. The effective impedance ξ_1 is defined by $\xi_1 = \rho/\gamma_1$, and is a constant multiple of the effective wave speed. In view of (2.3.5) we see that this corresponds exactly to the ansatz we formulated in (2.3.6) – (2.3.7).

2.3.2 The amplitude equations.

We now proceed to obtain equations governing the evolution of the amplitudes with respect to depth. Substituting (2.3.6) in (2.3.3) we obtain

$$\begin{aligned} [2\gamma_1 A_z + \gamma_{1,z}A - i(\varepsilon/\omega)A_{zz}]e^{i\omega\tau_1/\varepsilon} - [2\gamma_1 B_z + \gamma_{1,z}B + i(\varepsilon/\omega)B_{zz}]e^{-i\omega\tau_1/\varepsilon} \\ = i(\omega/\varepsilon)\gamma_1^2\ \nu[Ae^{i\omega\tau_1/\varepsilon} + Be^{-i\omega\tau_1/\varepsilon}], \end{aligned}$$

moreover, from (2.3.7) it follows that

$$[\gamma_1 A_z e^{i\omega\tau_1/\varepsilon} - \gamma_1 B_z e^{-i\omega\tau_1/\varepsilon}] - i(\varepsilon/\omega)[A_{zz}e^{i\omega\tau_1/\varepsilon} + B_{zz}e^{-i\omega\tau_1/\varepsilon}] \;=\; 0.$$

Combining the above two relations we find that

$$\begin{aligned} [\gamma_1 A_z + \gamma_{1,z}A]e^{i\omega\tau_1/\varepsilon} - [\gamma_1 B_z + \gamma_{1,z}B]e^{-i\omega\tau_1/\varepsilon} \\ = i(\omega/\varepsilon)\gamma_1^2\ \nu[Ae^{i\omega\tau_1/\varepsilon} + Be^{-i\omega\tau_1/\varepsilon}]. \end{aligned} \tag{2.3.9}$$

Finally, adding/subtracting a multiple γ_1 of (2.3.7) to/from (2.3.9), we obtain the equations

$$\begin{aligned} 2\gamma_1 A_z + \gamma_{1,z} A &= i(\omega/\varepsilon)\gamma_1^2\ \nu[A + Be^{-2i\omega\tau_1/\varepsilon}] + \gamma_{1,z} B e^{-2i\omega\tau_1/\varepsilon} \\ 2\gamma_1 B_z + \gamma_{1,z} B &= -i(\omega/\varepsilon)\gamma_1^2\ \nu[Ae^{2i\omega\tau_1/\varepsilon} + B] + \gamma_{1,z} A e^{2i\omega\tau_1/\varepsilon}. \end{aligned} \tag{2.3.10}$$

In order to obtain a simpler representation we introduce the transformation

$$\begin{aligned} \alpha &= A\ e^{\int_0^z [d[\ln[\sqrt{\gamma_1}]]/dz - i(\omega/\varepsilon)\gamma_1\nu/2]ds} \\ \beta &= B\ e^{\int_0^z [d[\ln[\sqrt{\gamma_1}]]/dz + i(\omega/\varepsilon)\gamma_1\nu/2]ds}. \end{aligned} \tag{2.3.11}$$

This corresponds to compensating for a random travel time introduced by the fluctuations and, moreover, the geometric effect on a macroscopic scale. We then arrive at the amplitude equations

$$\begin{aligned} d\alpha/dz &= \zeta\beta \\ d\beta/dz &= \overline{\zeta}\alpha, \end{aligned} \tag{2.3.12}$$

with

$$\zeta(z,\omega) = [i\omega\gamma_1(z)\nu(z/\varepsilon^2)/(2\varepsilon) + \frac{d[\ln[\sqrt{\gamma_1(z)}]]}{dz}\ ]e^{-2i\omega\tau_\varepsilon/\varepsilon}, \tag{2.3.13}$$

where

$$\tau_\varepsilon(z) = \int_{z_s}^{z} \gamma_1(s)(1 + \nu(s/\varepsilon^2)/2)\ ds. \tag{2.3.14}$$

Note that α is 'centered' with respect to a frame moving with a slowness τ_ε that is

slightly different from the effective medium slowness τ_1. The random fluctuations in the medium parameters cause a slight travel time correction. The appropriate centering is therefore with respect to τ_ε rather than with the effective medium travel time. That we have obtained the right parameterization for the amplitudes now manifests itself by the fact that the system is purely off-diagonal.

The amplitude coupling associated with the term '$d[\ln[\sqrt{\gamma_1}]]/dz$' in (2.3.12) can be ignored since we are considering a high frequency approximation relative to the background. In the effective medium approximation we also ignore the stochastic coupling between the amplitudes, that is, the coupling due to the term '$i\omega\gamma_1\nu/(2\varepsilon)$'. However, as we show in the next section, this stochastic coupling causes a small modulation of the pulse on the average which becomes appreciable for propagation distances on the order of the slowly varying background.

In general the wave-energy will be localized to a region below the surface, and we obtain from (2.3.12) the expression

$$\beta(z,\omega) \;=\; -\int_z^\infty \overline{\zeta(s,\omega)}\alpha(s,\omega)\; ds$$

for the up-going amplitude and the stochastic integro-differential equation

$$\frac{d\alpha}{dz}(z,\omega) \;=\; -\int_z^\infty \zeta(z,\omega)\overline{\zeta(s,\omega)}\alpha(s,\omega)\; ds \tag{2.3.15}$$

for the down-going amplitude. This integro-differential equation is a special case of the one considered in the more general point source case discussed in Section 2.5. In the next section, we will offer a simple heuristic argument showing how the solution of (2.3.15) can be characterized for small ε.

2.3.3 Stabilization of the pulse.

Take the expected value of (2.3.15) to obtain

$$\frac{dE[\alpha(z,\omega)]}{dz} \;=\; -\int_z^\infty E[\zeta(z,\omega)\overline{\zeta(s,\omega)}\alpha(s,\omega)]ds.$$

Recall that the effective medium approximation suggests that the transformation of the travelling pulse, due to the random fluctuations of the medium parameters, occurs on a scale which is slow relative to that of the random fluctuations. The heuristic argument now rests on the following approximation motivated by this observation

$$E[\zeta(z,\omega)\overline{\zeta(s,\omega)}\alpha(s,\omega)] \;\sim\; E[\zeta(z,\omega)\overline{\zeta(s,\omega)}]E[\alpha(s,\omega)] \quad as \;\; \varepsilon \downarrow 0 \;\; (2.3.16)$$

and, furthermore, the observation that formally for $z > 0$

$$E[\zeta(z,\omega)\overline{\zeta(s,\omega)}] \;\sim\; 2\,\omega^2 D(z)\delta(z-s) \qquad as \;\; \varepsilon \downarrow 0, \qquad (2.3.17)$$

with $D(z) = \gamma_1^2(z)l/4$. The correlation length l being defined by

$$l \;\equiv\; \int_0^\infty E[\nu(0)\nu(s)]ds. \qquad (2.3.18)$$

Hence, assuming $E[\alpha(z,\omega)]$ smooth, we expect, based on the above discussion

$$E[\alpha(z,\omega)] \;\sim\; a(z,\omega) \qquad as \;\; \varepsilon \downarrow 0,$$

with a solving for $z > 0$

$$\frac{da}{dz}(z,\omega) \;=\; -\omega^2 D(z)a(z,\omega). \qquad (2.3.19)$$

From (2.3.6) and (2.3.11) we find for the downpropagating pressure pulse

$$\begin{aligned} p_d(z,t) &= e^{-\int_0^z \frac{d[\ln[\sqrt{\gamma_1(s)}]}{ds}}/(2\pi) \int \alpha(z,\omega)\, e^{i\omega(\tau_\varepsilon - t)/\varepsilon}\, d\omega \\ &= \sqrt{\gamma_0/\gamma_1(z)}/(2\pi) \int \alpha(z,\omega)\, e^{i\omega(\tau_\varepsilon - t)/\varepsilon}\, d\omega, \end{aligned} \tag{2.3.20}$$

and define a random process by substituting the approximation for α defined by (2.3.19) into (2.3.20)

$$X(z,t) = \sqrt{\gamma_0/\gamma_1(z)}/(2\pi) \int A(0,\omega) e^{-\omega^2 \int_0^z D(s)ds}\, e^{i\omega(\tau_\varepsilon - t)/\varepsilon}\, d\omega.$$

We 'center' with respect to the random phase and use the time scaling of the source and consider

$$Y(z,s) \equiv (p_d(z, \varepsilon s - \tau_\varepsilon) - X(z, \varepsilon s - \tau_\varepsilon)),$$

that is, we 'open a window at the random arrival time'. Then

$$\begin{aligned} E[Y(z,s)^2] \sim\ & \gamma_0/(4\pi^2\gamma_1(z)) \int\int \{E[\alpha(z,\omega_1)\alpha(z,\omega_2)] \\ & - A(0,\omega_1)A(0,\omega_2) e^{-(\omega_1^2+\omega_2^2)\int_0^z D(s)ds}\}\, e^{-i(\omega_1+\omega_2)s}\, d\omega_1 d\omega_2 \qquad as\ \ \varepsilon \downarrow 0, \end{aligned}$$

using the approximation (2.3.19). Observe that

$$\begin{aligned} \frac{dE[\alpha(z,\omega_1)\alpha(z,\omega_2)]}{dz} &= -\int_z^\infty \{E[\zeta(z,\omega_1)\overline{\zeta(s,\omega_1)}\alpha(s,\omega_1)\alpha(z,\omega_2)] \\ &\quad + E[\zeta(z,\omega_2)\overline{\zeta(s,\omega_2)}\alpha(z,\omega_1)\alpha(s,\omega_2)]\}\, ds. \end{aligned}$$

If we again make an assumption about 'locality' as in (2.3.16) we find

$$E[\alpha(z,\omega_1)\alpha(z,\omega_2)] \quad \sim \quad h(z,\omega_1,\omega_2) \qquad as \quad \varepsilon \downarrow 0,$$

with h solving for for $z > 0$

$$\frac{dh}{dz}(z,\omega_1,\omega_2) \quad = \quad -(\omega_1^2+\omega_2^2)D(z)h(z,\omega_1,\omega_2). \tag{2.3.21}$$

The above argument suggests that $Y \sim 0$. This is the remarkable stabilization aspect of the O'Doherty-Anstey approximation. The variability of the time-centered transmitted *time pulse* which follows from the approximation (2.3.19) is negligible for small ε. Note that since α is complex it does not follow from (2.3.21) that the time-harmonic amplitude itself stabilizes; in fact it does not. Therefore the above result cannot be obtained by considering the evolution of the different harmonic amplitudes in isolation, which is done for instance in [44].

The stabilization aspect follows rigorously by the results of Appendix E.3, and was first derived in [11] and [15].

2.3.4 The O'Doherty-Anstey approximation.

As in the effective medium case the up-travelling pulse amplitude B is small. We therefore obtain by comparison with (2.2.12) – (2.2.14)

The O'Doherty-Anstey approximation in
one dimensional strongly heterogeneous case:

Let p solve the problem (2.3.1), then with probability one

$$p(z,\tau_\varepsilon+\varepsilon s) \quad \sim \quad [p_0(z,\cdot)\star\mathcal{N}(z,\cdot)](s) \qquad as \quad \varepsilon \downarrow 0. \tag{2.3.22}$$

The high frequency approximation based on the effective medium parameters, p_0, is

defined in (2.2.14) and τ_ε by (2.3.14). The pulse shaping function $\mathcal{N}$ solves

$$\begin{aligned} \mathcal{N}_z &= D(z)\,\mathcal{N}_{ss} \\ \mathcal{N}(0,s) &= \delta(s), \end{aligned}$$

obtained from (2.3.19). Thus, $\mathcal{N}(z,\cdot)$ is a Gaussian pulse of squared width $2\int_0^z D(s)ds = l/2\int_0^z \gamma_1^2(s)ds$, with the correlation length l defined by (2.3.18) and the slowness γ_1 by (2.2.11).

Assume now that the slowness is constant. Upon the change of variables $\mathcal{Z} = z/(\varepsilon^2 l)$ and $\mathcal{T} = s/(\gamma_1 \varepsilon l)$ we find that $\mathcal{N}$ solves

$$\begin{aligned} \mathcal{N}_{\mathcal{Z}} &= (1/4)\,\mathcal{N}_{\mathcal{T}\mathcal{T}} \\ \mathcal{N}(0,\mathcal{T}) &= \delta(\mathcal{T}), \end{aligned} \tag{2.3.23}$$

and in terms of these variables $\mathcal{N}$ as a function of $\mathcal{T}$ is a Gaussian pulse of squared width $\mathcal{Z}/2$. Thus, if we refer to the correlation length of the fluctuations on the original spatial scale, $\varepsilon^2 l$, as 'the correlation length', we can conclude that when the pulse has reached N correlation lengths into the medium, the spatial support of the convolving pulse is $\sqrt{N}$ correlation lengths. Here we define spatial support as the interval containing 99 % of the pulse energy.

Also, note that despite the fact that the fluctuations appear to induce an attenuation of the pulse, the L_1 norm of the approximation is conserved if the pulse impinging on the surface is a positive function of time. This is because $\mathcal{N}$ is a probability distribution.

The approximation (2.3.23) modifies the usual high frequency approximation for the effective medium in two important ways.

First, the arrival time of the transmitted pulse, defined as the center of the impulse response is random and given by $\tau_\varepsilon(z) = \int_{z_s}^z \gamma_1(s)(1+\nu(s/\varepsilon^2)/2)\,ds$. The first arrival time is given by $\tau(z) = \int_{z_s}^z \gamma_1(s)\sqrt{(1+\nu(s/\varepsilon^2))}\,ds$. Since the function $\sqrt{1+x}$ is

concave down and has slope 1/2 at the origin $\tau(z) < \tau_\varepsilon(z)$. Moreover by the central limit theorem

$$\varepsilon^{-1}[\tau_\varepsilon(z) - \tau_1(z)] \;=\; \varepsilon^{-1}\int_0^z \gamma_1(s)\;\nu(s/\varepsilon^2)/2ds \to X \qquad as \;\; \varepsilon \downarrow 0,$$

with X a Gaussian random variable. Therefore, we see that the discrepancy between the center of the impulse response and the effective medium arrival time is a mean-zero $O(\varepsilon)$ random quantity, and is hence on the scale of the probing pulse.

Second, the scattering associated with the fluctuations causes a smearing of the travelling pulse. The asymptotic characterization of this phenomenon at depth z, is through a convolution with the Gaussian pulse $\mathcal{N}(z,\cdot)$. The convolution is on the scale of the probing pulse, and hence interacts strongly with its shape. The width of the Gaussian pulse is defined in terms of the correlation length of the modulating process ν and the medium parameters in the interval $[0,z]$ only, and does not depend on the particular realization. Hence, the smearing is deterministic. Observe that even though a small fraction of the pulse has reached much deeper into the medium than the pulse center, the leading order pulse shape when the center reaches depth z depends only on the medium parameters in the interval $[0,z]$. This is in accordance with intuition. The pulse shaping, though only visible after a long travelling distance, is a local phenomenon. The random modulation of the medium parameters, on the finest scale of the model, causes energy to be scattered over to the up-propagating wave mode, but this energy is quickly scattered back again due to the fluctuations. Hence, only a small amount of energy is carried by the up-propagating wave mode but it is important because the continuous random channeling of energy gradually delays the pulse relative to the first arrival and causes its shape to diffuse and approach a Gaussian. The support of the main pulse is $O(\varepsilon)$ and hence only the parameters in the interval $[0,z]$ are important. Note that if there is a lot of structure in the fluctuations, that is, strong correlations, then l will be relatively large. Moreover, l scales with the second moment of the fluctuations. Hence, coherence and strong variability in the random modulation implies that the random scattering is associated with a stronger

smearing of the pulse.

Finally, note that since $\mathcal{N}(z,t)$ is strictly positive for all t, the approximation (2.3.23), being a diffusive transport approximation, actually violates causality. However, since this concerns only the tail which is of exponential decay, it is still a valid asymptotic approximation.

2.4 Weakly heterogeneous layered media.

We now turn our attention to the weakly heterogeneous case. The heuristic argument leading to an approximation of the transmitted pulse in the weakly heterogeneous case is but a slight modification of the one in the strongly heterogeneous case. The governing equations pertaining to the weakly heterogeneous case are as in (2.3.1). However, now the source and the medium parameters are given by

$$\begin{aligned} \rho(z) &\equiv \rho_0 \\ K_\varepsilon^{-1}(z) &= \begin{cases} K_0^{-1} & z \in (-\infty, 0] \\ K_1^{-1}(z)(1+\varepsilon\nu(z/\varepsilon^2)) & z \in (0,\infty) \end{cases} \\ F_\varepsilon(z,t) &= f(t/\varepsilon^2)\delta(z-z_s). \end{aligned}$$

2.4.1 The amplitude equations.

In the weakly heterogeneous case we define the Fourier transform by

$$\begin{aligned} \hat{p}(z,\omega) &= \int p(z,s)e^{i\omega s/\varepsilon^2}ds \\ \hat{u}(z,\omega) &= \int u(z,s)e^{i\omega s/\varepsilon^2}ds. \end{aligned}$$

By an exact analogue of the argument presented in the previous section, we find that the appropriate ansatz now is

$$\begin{aligned} \hat{p} &= Ae^{i\omega\tau_1/\varepsilon^2} + Be^{-i\omega\tau_1/\varepsilon^2} \\ 0 &= A_z e^{i\omega\tau_1/\varepsilon^2} + B_z e^{-i\omega\tau_1/\varepsilon^2}, \end{aligned}$$

the difference being the order of ε appearing in the exponent. Proceeding as before we obtain upon the change of variables

$$\begin{aligned} \alpha &= A\ e^{\int_{z_s}^{z}[d[\ln[\sqrt{\gamma_1}]/dz - i(\omega/\varepsilon)\gamma_1\ \ \nu/2]ds} \\ \beta &= B\ e^{\int_{z_s}^{z}[d[\ln[\sqrt{\gamma_1}]/dz + i(\omega/\varepsilon)\gamma_1\ \ \nu/2]ds}, \end{aligned}$$

that the amplitudes satisfy

$$\begin{aligned} d\alpha/dz &= \zeta\beta \\ d\beta/dz &= \overline{\zeta}\alpha, \end{aligned} \tag{2.4.1}$$

now with

$$\zeta(z) = [i\omega\gamma_1(z)v(z/\varepsilon^2)/(2\varepsilon) + \frac{d[\ln[\sqrt{\gamma_1(z)}]}{dz}]\ e^{-2i\omega\tau_\varepsilon(z)/\varepsilon^2}. \tag{2.4.2}$$

It follows that α satisfies (2.3.15), as before, with ζ defined as above. Note that in this case we define

$$\tau_\varepsilon = \int_{z_s}^{z} \gamma_1(1 + \varepsilon\nu/2)\ ds. \tag{2.4.3}$$

2.4.2 Stabilization of the pulse.

In the weakly heterogeneous case we motivate the approximation (2.3.16) by the fact that the coupling between the propagating pulse and the random process ν is weak. Formally, we obtain for $z > 0$

$$E[\zeta(z)\overline{\zeta(s)}] \sim 2\,\omega^2 D(z,\omega)\delta(z-s) \qquad as \;\; \varepsilon \downarrow 0$$

with $D(z,\omega) = \gamma_1^2(z)\bar{l}(z,\omega)/4$, and where $\bar{l}$ is defined by

$$\begin{aligned} \bar{l}(z,\omega) &\equiv \int_0^\infty E[\nu(0)\nu(s)]e^{i\omega 2\gamma_1(z)s}ds \\ &\equiv \int_0^\infty C(s)e^{i\omega 2\gamma_1(z)s}ds. \end{aligned}$$

Hence, the 'diffusion parameter' $D(z,\omega)$ depends on the spatial auto-covariance function of the process ν and not only the correlation length as was the case above. Again for $E[\alpha(z,\omega)] \sim a(z,\omega) as \;\; \varepsilon \downarrow 0$. The mean amplitude solves

$$\frac{da}{dz}(z,\omega) = -\omega^2 D(z,\omega)a(z,\omega). \tag{2.4.4}$$

Since the probing pulse is defined on the same scale as the fluctuations, the pulse 'sees' the whole correlation structure, not only the correlation length as in the strongly heterogeneous case. The same argument as presented in Section 2.3.3 leads to the conclusion that the transmitted time pulse stabilizes around the pulse that follows from the approximation (2.4.4).

2.4.3 The O'Doherty-Anstey approximation.

Based on the above observations we now state the O'Doherty-Anstey approximation in the one dimensional weakly heterogeneous case. We also discuss the result and contrast it to the corresponding one in the strongly heterogeneous case.

The O'Doherty-Anstey approximation in
one dimensional weakly heterogeneous case:

Let p solve the weakly heterogeneous version of the problem (2.3.1),
then with probability one

$$p(z, \tau_\varepsilon + \varepsilon^2 s) \sim [p_0(z,\cdot) \star \mathcal{H}(z,\cdot)](s) \qquad as \;\; \varepsilon \downarrow 0. \tag{2.4.5}$$

The high frequency approximation based on the effective medium parameters, p_0, is defined in (2.2.14) and τ_ε by (2.4.3). The pulse shaping function $\mathcal{H}$ solves

$$\begin{aligned} \partial_z \mathcal{H}(z,s) &= (\gamma_1(z)/8)\partial_s^2[h(z,\cdot) \star \mathcal{H}(z,\cdot)](s) \\ \mathcal{H}(0,s) &= \delta(s) \end{aligned} \tag{2.4.6}$$

with

$$h(z,s) = \begin{cases} 0 & s \in (-\infty, 0] \\ C(s/2\gamma_1(z)) & s \in (0,\infty) \end{cases}.$$

We obtained (2.4.6) by backtransforming (2.4.4) in time.

In order to obtain the correct travel time for p we need to take into account the centering of the pulse $\mathcal{H}$. To obtain a more transparent expression for $\mathcal{H}$ we write it as

$$\begin{aligned} \mathcal{H}(z,t) &= F^{-1}[e^{-\omega^2 \int_0^z \gamma_1^2(s)\bar{l}(s,\omega)/4 \ ds}] \\ &= F^{-1}[e^{-i\omega C(0)/8 \int_0^z \gamma_1(s)ds + az(-1+\int_0^\infty f(u;z) \ \exp(i\omega u)du)}], \end{aligned} \tag{2.4.7}$$

where the the second equation was obtained using integration by parts. Above, F^{-1} denotes the unscaled inverse Fourier transform and we used the notation

$$\begin{aligned} a &\equiv -C'(0^+)/16 \\ f(u;z) &\equiv \begin{cases} 0 & u \in (-\infty, 0] \\ -(C'(0^+)z)^{-1} \int_0^z C''(u/2\ \gamma_1(s))/(2\ \gamma_1(s))ds & u \in (0,\infty) \end{cases} . \end{aligned}$$

In defining f we made the assumption that $C'(0^+) < 0$. Note that $\int_0^\infty f(u;z)du = 1$, and that if $\gamma_1(z) \equiv \gamma_1$ the function $f(u;z)$ is just a scaled version of the second derivative of the covariance function of ν.

Let $\varepsilon\nu_k$ be the value of the medium fluctuations in layer k of a *discretely* layered medium. Then pulse propagation is described by a sequence of interface reflection coefficients, which is approximately proportional to the sequence $\varepsilon(\nu_k - \nu_{k-1})$. For the discrete medium the analog of f is the autocovariance of the interface reflections. This is explained in more detail in Chapter 3.

In the weakly heterogeneous case one can show that

$$\tau(z) = \tau_\varepsilon(z) - (\varepsilon^2 C(0)/8) \int_0^z \gamma_1(s)ds + O(\varepsilon^3 \sqrt{\log\log \varepsilon^{-1}}).$$

Thus, in view of (2.4.7), we find

$$p(z, \tau(z) + \varepsilon^2 s) \sim [p_0(z,\cdot) \star \tilde{H}(z,\cdot)](s) \qquad as \ \ \varepsilon \downarrow 0,$$

with $\tilde{\mathcal{H}}$ being defined by

$$\begin{aligned}\tilde{\mathcal{H}}(z,s) &= F^{-1}[e^{az(-1+\int_0^\infty f(u;z)\ \exp(i\omega u)du)}] \\ &= p_0(z)\ \delta(s) + \sum_{n=1}^{\infty} p_n(z) f^{n*}(s;z).\end{aligned}$$

Here, $p_n(z)$ is the discrete Poisson distribution with parameter az. The above representation shows, since $f(s;z) = 0$ for $s < 0$, that in this case we have obtained a strictly causal approximation. If $f \geq 0$, which is the case if for instance ν is exponentially correlated, we obtain a characterization of $\tilde{\mathcal{H}}$ as the distribution of a random sum. Then f^{n*} approaches the Gaussian distribution by the central limit theorem. The width and centering of $\tilde{\mathcal{H}}$ will be defined in terms of the first and second moments of f which are

$$\begin{aligned}m_1(z) &= \int_0^\infty u f(u;z)du = -2C(0)/(zC'(0^+)) \int_0^z \gamma_1(s)\ ds \\ m_2(z) &= \int_0^\infty u^2 f(u;z)du = -8l/(zC'(0^+)) \int_0^z \gamma_1^2(s)\ ds.\end{aligned}$$

Making use of the formulas for the moments of a random sum we obtain the delay, μ, and squared width, σ^2, of $\tilde{\mathcal{H}}$ as

$$\begin{aligned}\mu &= az\ m_1(z) = C(0)/8 \int_0^z \gamma_1(s)\ ds \\ \sigma^2 &= az\ (m_2(z) - m_1^2(z)) + az\ m_1^2(z) \\ &= az\ m_2(z) = l/2 \int_0^z \gamma_1^2(s)\ ds.\end{aligned}$$

Consider now the special case when $\gamma_1(z) \equiv \gamma_1$ and when the fluctuations are exponentially correlated, that is, the covariance of the fluctuations is given by $E[\nu(0)\nu(s)] = C(0)e^{-s/r}$. Then we obtain $\tilde{\mathcal{H}}$ explicitly as

$$\tilde{\mathcal{H}}(\mathcal{Z},\mathcal{T}) = \lambda\ e^{-\mathcal{Z}}[\delta(\mathcal{T}) + e^{-\mathcal{T}}\ \sqrt{\mathcal{Z}/\mathcal{T}}\ I_1(\sqrt{\mathcal{Z}\mathcal{T}})], \tag{2.4.8}$$

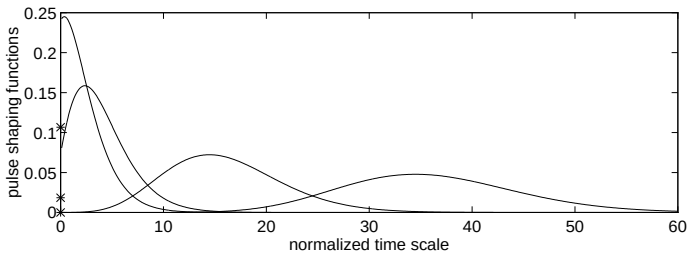

Figure 2.3: The pulse shaping function $\tilde{\mathcal{H}}$ plotted as a function of normalized time $\mathcal{T}$ for a set of different relative travel lengths $\mathcal{Z}$.

with $\mathcal{Z} = z[C(0)/(16r)]$, $\mathcal{T} = s/(2\gamma_1 r) \equiv s\lambda$ and I_1 is the modified Bessel function of order 1. In Figure 2.3 we show $\tilde{\mathcal{H}}$ for different relative propagation distances, that is, for $\sqrt{\mathcal{Z}} \in \{1.5, 2, 4, 6\}$. As the wave penetrates deeper into the medium we see that the associated pulse-shaping function looses its impulsive character and approaches a Gaussian pulse. The parts of the impulses having 'tunneled' through the medium are indicated by stars.

A simpler characterization of $\tilde{\mathcal{H}}$ can be obtained in the low frequency limit. In this limit '$\exp(i\omega u)$' will be nearly constant over the support of f. We therefore get the approximation

$$\begin{aligned}
\tilde{\mathcal{H}}(z,t) &= F^{-1}[e^{az(-1+\int_0^\infty f(u;z)\ \exp(i\omega u)du)}] \\
&\approx F^{-1}[e^{az(-1+\int_0^\infty f(u;z)\ (1+i\omega u-\omega^2u^2/2)du)}] \\
&= F^{-1}[e^{i\omega(az\ m_1(z))-(\omega^2/2)(az\ m_2(z))}]
\end{aligned}$$

and thus can approximate $\tilde{\mathcal{H}}$ by a Gaussian pulse centered at '$az\ m_1(z)$' and having square width '$az\ m_2(z)$' in conformity with the above results. In the low-frequency limit we obtain

Low frequency limit of The O'Doherty-Anstey approximation in one dimensional weakly heterogeneous case:

Let p solve the weakly heterogeneous version of the problem (2.3.1), then with probability one

$$p(z, \tau_\varepsilon(z) + \varepsilon^2 s) \approx [p_0(z,\cdot) \star \mathcal{N}(z,\cdot)](s) \qquad as \quad \varepsilon \downarrow 0$$

with $\mathcal{N}(z,\cdot)$ a Gaussian pulse of squared width $l/2 \int_0^z \gamma_1^2(s)ds$. Note that this approximation is also valid in the limit when $\mathcal{Z}$ becomes large, by a generalization of the central limit theorem, page 265 [16].

We now compare this approximation with the asymptotics in the strongly heterogeneous case given in (2.3.22). First, observe that the deterministic pulse shaping in the two cases is defined in the same way, through convolution with a Gaussian pulse of squared width $l/2 \int_0^z \gamma_1^2(s)\ ds$. This convolution is furthermore defined on the scale of the probing pulse. Second, in both cases the travel time correction relative to the effective medium travel time is a random quantity on the scale of the probing pulse.

In the next section we return to consider three dimensional wave propagation. In Section 2.5 we state the O'Doherty-Anstey approximation associated with the model (2.1.1). The approximation can be interpreted as a combination of the high frequency asymptotics of Section 2.2 with the one-dimensional O'Doherty-Anstey approximation discussed above.

2.5 Results for spherical waves.

We state the versions of the O'Doherty-Anstey approximation that apply to a locally layered medium. The results will be derived in Sections 2.6 and 2.7.

2.5.1 Locally layered strongly heterogeneous media.

Let $\boldsymbol{u}, p$ solve (2.1.1)–(2.1.3) & (2.1.6). Furthermore, let φ solve the eiconal equation (2.2.5) associated with $\gamma_1(\boldsymbol{x}, z)$ and a point source at $(\mathbf{0}, z_s)$. Assume that the ray segment Γ between the surface $z = 0$ and the observation point $(\boldsymbol{x}, z)$ of the

characteristic ray actually going through $(\boldsymbol{x}, z)$ is nowhere horizontal; see Figure 2.2. Furthermore, assume that φ is smooth in a neighborhood of this path. Then for $z > 0$, with probability one, the transmitted pressure admits pathwise the asymptotic characterization

$$p(\boldsymbol{x}, z, \varphi + \chi_\varepsilon + \varepsilon s) \;\sim\; [G_f \star \mathcal{N}](s) \qquad as \;\; \varepsilon \downarrow 0. \tag{2.5.1}$$

The function $G_f(\boldsymbol{x}, z, (t-\varphi)/\varepsilon)$ denotes the exact transmitted pressure in the deterministic case when $\nu \equiv 0$. The high frequency approximation for G_f is given in (2.2.8). The pulse shaping function $\mathcal{N}$ is the centered Gaussian distribution whose square width V *depends on the spatial location.* Moreover

$$\begin{aligned} \chi_\varepsilon &= \int_\Gamma \gamma_1 \nu/2 \; du \\ V &= (l/2) \int_\Gamma \gamma_1^2 \; \cos(\theta)^{-1} \; du \\ l &\equiv \int_0^\infty E[\nu(0)\nu(u)] \; du, \\ \gamma_1 &= \sqrt{K_1^{-1}\rho} \end{aligned} \tag{2.5.2}$$

with u being arc-length along the path Γ and $\cos(\theta(\boldsymbol{x}, z)) = \varphi_z/|\nabla\varphi|$, the angle between Γ and the vertical direction.

The pulse shaping function $\mathcal{N}$ is the solution of the diffusion equation

$$\begin{aligned} \mathcal{N}_u &= D\, \mathcal{N}_{ss} \\ \mathcal{N}|_{z=0} &= \delta(s), \end{aligned}$$

where $\mathcal{N}_u = [\gamma_1^{-1}\nabla\varphi] \cdot \nabla\mathcal{N}$ and the characteristic ray parameter, u, plays the role of the 'time variable'. The 'diffusion coefficient' is

$$D(\boldsymbol{x}, z) \quad = \quad l\ \gamma_1^2(\boldsymbol{x}, z)/(4\cos(\theta(\boldsymbol{x}, z))).$$

Thus, we have obtained an approximation which is a generalization of the analogous one in the one dimensional case discussed in Section 2.3. It is a generalization in that the random travel time correction χ_ε and the square width of the modulating pulse, V, are defined as integrals over the geometrical optics path Γ, which in the purely layered horizontal plane-wave case is $(\mathbf{0}, (0, z))$. The interpretation of the effect of the random modulation of the compliance, given in Section 2.3, therefore prevails. That is, it induces a deterministic smearing of the transmitted pulse shape through convolution with the heat kernel and, furthermore, a small random travel time correction. The discussion concerning the travel time therefore also prevails. Note the slight generalization of the integral expressions defined by the term $\cos(\theta)$. This means that when the pulse propagates with a shallow angle relative to the layering its smearing becomes stronger. This is in accordance with our previous observations, since the pulse then 'sees' a fluctuation process with stronger spatial correlation. Note that if we straighten the path Γ and let the correlation length depend on depth as $l/\cos(\theta)$, allowing for a generalization in which the correlation length of the fluctuations varies on the macroscopic depth scale, the above pulse shaping is defined just as in the one-dimensional case.

2.5.2 The weakly heterogeneous case.

Under the same assumptions as above

$$p(\boldsymbol{x}, z, \tau + \varepsilon^2 s) \quad \sim \quad [G_f \star \mathcal{H}](s) \qquad as \quad \varepsilon \downarrow 0, \tag{2.5.3}$$

with

$$\tilde{\mathcal{H}}(\boldsymbol{x}, z, s) \;=\; p_0(\boldsymbol{x}, z)\ \delta(s) + \sum_{n=1}^{\infty} p_n(\boldsymbol{x}, z) F^{n*}(s; \boldsymbol{x}, z)$$

and where a and F are defined by

$$\begin{aligned} a &\equiv -C'(0^+)/16 \qquad (2.5.4)\\ F(s; \boldsymbol{x}, z) &\equiv \begin{cases} 0 & s \in (-\infty, 0] \\ -(1/C'(0^+)b) \int_\Gamma \cos(\theta)^{-3} & \\ \times C''(s/(2\ \gamma_1\ \cos(\theta))/(2\ \gamma_1 \cos(\theta))\ du & s \in (0, \infty) \end{cases} \\ b &= \int_\Gamma \cos(\theta)^{-3}\ du \end{aligned}$$

with θ and γ_1 being evaluated along the path of integration. As before, we make the reasonable assumption that $C'(0^+) < 0$, where C is the covariance function of the fluctuations. We use the notation $p_n(\boldsymbol{x}, z)$ for the discrete Poisson distribution with parameter '$a \cdot b$'. The result holds pathwise with probability one.

In the low frequency limit we obtain the approximation

$$p(\boldsymbol{x}, z, \varphi + \varepsilon\chi_\varepsilon + \varepsilon^2 s) \;\approx\; [G_f \star \mathcal{N}](s) \qquad as\ \ \varepsilon \downarrow 0, \qquad (2.5.5)$$

with

$$V \;=\; (l/2) \int_\Gamma \gamma_1^2\ \cos(\theta)^{-1}\ ds.$$

Hence, the convolving pulse is defined as in the strongly heterogeneous case. The arrival time is now approximated by $\tau_\varepsilon = \varphi + \varepsilon\chi_\varepsilon$ with χ_ε defined in (2.5.2).

We see that the two approximations differ only in their scaling. When time is scaled by ε^{-1} and ε^{-2} in the strong and weak noise cases, respectively, we can replace

the question mark in Figure 2.1, modulo the effective medium response, by a Gaussian pulse of squared width V time shifted by $\varepsilon^{-1}\chi_\varepsilon$.

2.5.3 Approximation for purely layered media.

In the purely layered case the above simplifies because the phase and ray paths can be written more explicitly. For the approximations (2.5.1) and (2.5.3) we get the following expressions for the quantities involved

$$\begin{aligned}
\chi_\varepsilon &= \int_0^z \gamma_1 \nu/2 \ \cos(\theta)^{-1} \ du \\
V &= (l/2) \int_0^z \gamma_1^2 \ \cos(\theta)^{-2} \ du \\
F(s;\boldsymbol{x},z) &\equiv \begin{cases} 0 & s \ \in \ (-\infty, 0] \\ -(1/C'(0^+)b) \int_0^z \cos(\theta)^{-4} & \\ \times C''(s/(2\ \gamma_1\ \cos(\theta))/(2\ \gamma_1 \cos(\theta))\ du & s \ \in \ (0,\infty) \end{cases} \\
b &= \int_0^z \cos(\theta)^{-4} \ du \\
\cos(\theta) &= \sqrt{1 - c\gamma_1^2}.
\end{aligned}$$

with u being the depth variable. The constant c is defined so that

$$\int_{z_s}^z [(c\ \gamma_1(s)^2)^{-1} - 1]^{-1/2} \ ds = ||\boldsymbol{x}||.$$

The approximation in the point source case for a strongly heterogeneous purely layered media was first obtained by Chillan and Fouque in [13].

2.5.4 The homogeneous case.

In the special case of a uniform background medium, that is $\gamma_1(\boldsymbol{x}, z) = \gamma_1$, the asymptotic approximation becomes

$$\begin{aligned} p(\boldsymbol{x}, z, \varphi + \chi_\varepsilon + \varepsilon s) &\sim [G_f \star \mathcal{N}](s) \\ &\sim \frac{\gamma_1 \cos(\theta)}{4\pi r} [f' \star \mathcal{N}](s) \qquad as \;\; \varepsilon \downarrow 0, \end{aligned} \tag{2.5.6}$$

with

$$\begin{aligned} \varphi &= \gamma_1 r \\ \chi_\varepsilon &= (\gamma_1/2) \int_0^z \nu \; ds \;\; \cos(\theta)^{-1} \\ V &= (\gamma_1^2 \; l \; z/2) \;\; \cos(\theta)^{-2} \\ \cos(\theta) &= (z - z_s)/r \end{aligned}$$

in the strongly heterogeneous case. Again, we see that the random layering is felt more strongly when the wave propagates with a shallower angle θ relative to the layering.

In the weakly heterogeneous case the approximation becomes

$$\begin{aligned} p(\boldsymbol{x}, z, \tau + \varepsilon^2 s) &\sim [G_f \star \mathcal{H}](s) \\ &\sim \frac{\gamma_1 \cos(\theta)}{4\pi r} [f' \star \mathcal{H}](s) \qquad as \;\; \varepsilon \downarrow 0, \end{aligned} \tag{2.5.7}$$

with

$$\mathcal{H}(\boldsymbol{x}, z, s) = p_0(\boldsymbol{x}, z) \; \delta(s) + \sum_{n=1}^{\infty} p_n(\boldsymbol{x}, z) g^{n*}(s)$$

where

$$g(s) \equiv \begin{cases} 0 & s \in (-\infty, 0] \\ -C''(s/2\ \gamma_1\ \cos(\theta))/(2\ \gamma_1\ \cos(\theta))/C'(0^+) & s \in (0, \infty) \end{cases}$$

and $p_n(\boldsymbol{x}, z)$ is the discrete Poisson distribution with parameter '$az\cos(\theta)^{-2}$', a being defined in (2.5.4). In the low-frequency limit we obtain the approximation

$$p(\boldsymbol{x}, z, \varphi + \varepsilon\chi_\varepsilon + \varepsilon^2 s) \approx [G_f \star \mathcal{N}](s) \qquad as \ \ \varepsilon \downarrow 0. \tag{2.5.8}$$

In [10] Burridge et al. discuss pulse shaping in the constant background, weakly heterogeneous elastic case, with the above acoustic model as a special case.

If we specialize their result to the acoustic case it matches the expression (2.5.8) apart from the random travel time correction which they did not include.

Note that the constant background effective medium case is so simple that we can solve it explicitly and find

$$\begin{aligned} G_f &= \frac{\gamma_1 \cos(\theta)}{4\pi r}\ f'(s) + \frac{\sqrt{\varepsilon}\cos(\theta)}{4\pi r^2}\ f(s) \\ &\sim \frac{\cos(\theta)\gamma_1}{4\pi r}\ f'(s) \qquad as \ \ \varepsilon \downarrow 0 \end{aligned}$$

with all quantities defined as above.

2.6 Analysis for spherical waves in layered media.

In this section we derive the O'Doherty-Anstey approximation in the purely layered case stated in Section 2.5. The rationale for considering the purely layered case first is to set the stage for solving the locally layered case, which we do in the next section. Although fundamentally different from a global perspective, the scattering process associated with the locally layered case will resemble locally the one associated with

the purely layered case. Thus we aim at a parameterization of the locally layered case in which the local scattering is captured much as in the purely layered case to be discussed shortly, while global aspects of the wave propagation phenomenon are captured as in the high frequency approximation discussed in Section 2.2.

We first consider the model defined in (2.1.1) – (2.1.6) when

$$\gamma_1 \equiv \gamma_1(z). \tag{2.6.1}$$

This differs from the one considered in Sections 2.3 and 2.4 only in that there we considered an impinging plane wave, whereas we now consider a spherical wave. The main implication of the assumption (2.6.1) is that the analysis becomes one dimensional since it allow us to apply the Fourier transform not only with respect to time, but also with respect to the horizontal spatial dimensions. This corresponds to decomposing the source in obliquely travelling plane wave components, and for each of these the analysis is as in the one dimensional case discussed in Section 2.3 and 2.4. Moreover we obtain the leading order contribution to the Fourier integral over the plane wave components, the O'Doherty-Anstey approximation in the purely layered case, by a stationary phase argument. The analysis is in terms of the strongly heterogeneous model. However, the result in the weakly heterogeneous case follows similarly as indicated in Section 2.6.4.

2.6.1 Decomposition in terms of up- and down-travelling wave components.

In this section we obtain the version of the ansatz (2.3.6)–(2.3.7) which is appropriate for the model at hand. As mentioned above we transform the system (2.1.1) also with respect to the horizontal spatial dimensions. Thus we express the pressure as

$$p = (1/2\pi\varepsilon) \int \tilde{p}\, e^{-i\omega t/\varepsilon}\, d\omega$$

$$
\begin{aligned}
&= (1/2\pi\varepsilon)\int\int\int \hat{p}\; e^{i\omega\boldsymbol{\kappa}\cdot\boldsymbol{x}/\varepsilon}\; e^{-i\omega t/\varepsilon}\; d\boldsymbol{\kappa}\; d\omega \\
&= (1/2\pi\varepsilon)\int\int [A\; e^{i\omega\tau_1/\varepsilon} + B\; e^{-i\omega\tau_1/\varepsilon}]\; e^{i\omega\boldsymbol{\kappa}\cdot\boldsymbol{x}/\varepsilon}\; e^{-i\omega t/\varepsilon} d\boldsymbol{\kappa} d\omega, \qquad (2.6.2)
\end{aligned}
$$

where $A = A(z, \boldsymbol{\kappa}, \omega)$, $B = B(z, \boldsymbol{\kappa}, \omega)$, and we decomposed the wave-field in terms of up- and down-travelling wave parts. The phase component τ_1 is defined by $\tau_1 = \int_{z_s}^{z} \sqrt{\gamma_1^2(s) - \kappa^2}\; ds$.

In subsequent sections we will be able to eliminate the up-propagating wave component, B, and obtain an equation for the amplitude A which is a slight modification of (2.3.15).

As in the one dimensional case we introduce two degrees of freedom in defining the pressure. Thus, we need to introduce an additional constraint on the amplitudes, beyond (2.6.2), so as to make the solution of A unique for appropriate boundary data and, furthermore, so that A appropriately represents the down-propagating part of the harmonic component of the pressure. Since the medium is purely layered and the amplitudes are independent of the horizontal space argument we obtain the appropriate ansatz as a generalization of (2.3.6) – (2.3.7) concerning the one-dimensional case. The same argument as presented there can be used with the ansatz

$$
\begin{aligned}
\hat{p} &= A\; e^{i\omega\tau_1/\varepsilon} + B\; e^{-i\omega\tau_1/\varepsilon} \qquad (2.6.3) \\
0 &= A_z\; e^{i\omega\tau_1/\varepsilon} + B_z\; e^{-i\omega\tau_1/\varepsilon}. \qquad (2.6.4)
\end{aligned}
$$

The Fourier transformed pressure, $\hat{p}$, solves the reduced wave equation obtained from (2.1.1) by elimination of $\boldsymbol{u}$

$$
\hat{p}_{zz} + (\omega/\varepsilon)^2([\gamma_1^2 - \boldsymbol{\kappa}^2] + \gamma_1^2\nu)\hat{p} = 0. \qquad (2.6.5)
$$

The purely layered case was studied in [3]. In this paper the pressure and the

vertical component of the velocity were represented by the ansatz (2.3.8). This formulation corresponds to the ansatz (2.6.3) – (2.6.4).

2.6.2 The amplitude equations.

We proceed to obtain the equations for the amplitudes which follow from the ansatz (2.6.3) – (2.6.4). Using the same arguments as in Section 2.3 we derive the amplitude equations

$$\begin{aligned} 2\tau_{1,z}A_z + \tau_{1,zz}A &= i(\omega/\varepsilon)\gamma_1^2\ \nu\{A + B\ e^{-2i\omega\tau_1/\varepsilon}\} + \tau_{1,zz}B\ e^{-2i\omega\tau_1/\varepsilon} \\ 2\tau_{1,z}B_z + \tau_{1,zz}B &= -i(\omega/\varepsilon)\gamma_1^2\ \nu\{A\ e^{2i\omega\tau_1/\varepsilon} + B\} + \tau_{1,zz}A\ e^{2i\omega\tau_1/\varepsilon}, \end{aligned} \tag{2.6.6}$$

Here $\tau_{1,z} = \sqrt{\gamma_1(z)^2 - \boldsymbol{\kappa}^2}$, and (2.3.10) corresponds to the case $\boldsymbol{\kappa} = \mathbf{0}$. In these amplitude equations the terms '$\tau_{1,zz}A$' and '$\tau_{1,zz}B$' govern the main behavior of the solution and correspond to the geometrical effect in the high frequency approximation of the deterministic case. Moreover, the stochastic coupling, defined by the terms involving the fluctuations ν, is not purely off-diagonal. This reflects the fact that the random fluctuations affect the travel time of the propagating pulse. By a change of the dependent variable we obtain amplitude equations where these effects have been compensated for. Thus, let

$$\begin{aligned} \alpha &= A\ e^{\int_0^z [\tau_{1,zz}/(2\gamma_1) - i(\omega/\varepsilon)\gamma_1\ \nu/2]\cos(\theta)^{-1}\ ds} \\ \beta &= B\ e^{\int_0^z [\tau_{1,zz}/(2\gamma_1) + i(\omega/\varepsilon)\gamma_1\ \nu/2]\cos(\theta)^{-1}\ ds}. \end{aligned}$$

The angle θ is defined by

$$\cos(\theta) = \tau_{1,z}/\gamma_1 = \sqrt{1 - \boldsymbol{\kappa}^2/\gamma_1^2}. \tag{2.6.7}$$

We arrive then at the following pair of amplitude equations

$$\begin{aligned} d\alpha/dz &= \zeta\beta \\ d\beta/dz &= \overline{\zeta}\alpha, \end{aligned} \tag{2.6.8}$$

with

$$\zeta(z) = \cos(\theta)^{-1}[i\omega\gamma_1(z)\nu(z/\varepsilon^2)/(2\varepsilon) + \tau_{1,zz}/(2\ \gamma_1(z))]\ e^{-2i\omega\tau_\varepsilon/\varepsilon},$$

and

$$\tau_\varepsilon(z) = \int_{z_s}^{z} \gamma_1(s)(1 - \boldsymbol{\kappa}^2/\gamma_1^2(s) + \nu(s/\varepsilon^2)/2)\cos(\theta(s))^{-1}\ ds. \tag{2.6.9}$$

We can eliminate β from the first equation and obtain a stochastic integro-differential equation for the downgoing amplitude

$$\frac{d\alpha}{dz}(z) = -\int_z^\infty \zeta(z)\overline{\zeta(s)}\ \alpha(s)ds, \tag{2.6.10}$$

which is a generalization of (2.3.15). Here we suppressed the dependence on ω and $\boldsymbol{\kappa}$, and used the boundary condition

$$\lim_{z\to\infty} \beta = 0. \tag{2.6.11}$$

2.6.3 Stabilization of the pulse.

In this section we derive an asymptotic expression for the transmitted pressure at an arbitrary point $(\boldsymbol{x}, z)$ in the medium. Recall that the pressure is expressed in terms of the integral (2.6.2). Based on the stochastic integro-differential equation (2.6.10) we first obtain an approximation for the wave amplitude A. Upon substitution of this

in (2.6.2) and observing that the upgoing wave-field is asymptotically negligible we arrive at an approximation of the transmitted pressure. However, this approximation is in terms of an integral expression over slownesses. We then make use of a stationary phase argument to go from an integral expression over wave components to an expression involving one component only. Furthermore, we show that the resulting approximation is but a slight modification of the high frequency approximation of the deterministic case. This representation makes explicit the effect of the random modulation of the compliance on the transmitted pulse shape and travel time.

By a straightforward calculation we obtain that for all $\overline{\alpha} \in C$

$$\int_z^\infty E[\zeta(z)\overline{\zeta(s)}]\ \overline{\alpha}(s)\ ds \quad \sim \quad \omega^2\gamma_1^2 l/(4\cos(\theta)^2)\ \overline{\alpha}(z) \qquad as \ \ \varepsilon \downarrow 0,$$

and assuming 'locality' as in the layered case we find $E[\alpha] \sim a \ \ as \ \ \varepsilon \downarrow 0$ with a solving for $z > 0$

$$da/dz \ = \ -\omega^2 \cos(\theta)^{-1} D\ a, \tag{2.6.12}$$

where

$$D \ = \ \gamma_1^2 l/(4\cos(\theta)), \tag{2.6.13}$$

which is a generalization of (2.3.19).

Recall the integral expression for the transmitted pressure

$$p \ = \ (1/2\pi\varepsilon) \int\int [A\ e^{i\omega\tau_1/\varepsilon} + B\ e^{-i\omega\tau_1/\varepsilon}]\ e^{i\omega \boldsymbol{\kappa}\cdot\boldsymbol{x}/\varepsilon}\ e^{-i\omega t/\varepsilon} d\boldsymbol{\kappa}. \tag{2.6.14}$$

As before the reflected amplitude will be small and

$$p \sim (1/2\pi\varepsilon)\int\int\int A\, e^{i\omega(S^+-t)/\varepsilon}\, d\boldsymbol{\kappa}\, d\omega \qquad as \;\; \varepsilon \downarrow 0, \tag{2.6.15}$$

where we introduced the notation

$$S^+ = \boldsymbol{\kappa}\cdot\boldsymbol{x} + \tau_1. \tag{2.6.16}$$

Note that S^+ solves the eiconal equation associated with γ_1 and, furthermore, corresponds to the plane wave phase in the halfspace $z < 0$. Thus (2.6.15) represents propagation of incoming plane waves.

Substituting the asymptotic approximation for the mean of α defined by (2.6.12) in the integral expression (2.6.15) we arrive at the stochastic process

$$X = \int\int\int \overline{A}\, e^{-(\omega^2\int_0^z D\cos(\theta)^{-1}ds)}\, e^{i\omega(S^+ + \chi_\varepsilon - t)/\varepsilon}\, d\boldsymbol{\kappa}\, d\omega \tag{2.6.17}$$

with

$$\begin{aligned} \overline{A} &= (2\pi\varepsilon)^{-1}\, \mathcal{A}\, e^{-\int_0^z \cos(\theta)^{-1}\tau_{1,zz}/(2\gamma_1)\cos(\theta)^{-1}\, ds} \\ \chi_\varepsilon &= \int_0^z \gamma_1\, \nu/2\, \cos(\theta)^{-1}\, ds \\ \mathcal{A} &= \omega^2\hat{f}(\omega)/(8\pi^2). \end{aligned} \tag{2.6.18}$$

Note that $D \equiv 0$ and $\chi_\varepsilon \equiv 0$ in the deterministic case when $\nu \equiv 0$. As in the one-dimensional case we find the wave field impinging on the heterogeneous halfspace, and hence $\mathcal{A}$, by comparison with the homogeneous case. In this case the incoming field is parameterized in terms of plane waves and we derive the expression for $\mathcal{A}$ in Appendix E.1. Consider

$$\Delta_N \;=\; \sum_{n=1}^{N}(X-p)^2(t_n),$$

with $0 < t_i < t_{i+1}$. By direct computation we get

$$E[\Delta_N] = \int\int\,(\sum_{n=1}^{N} e^{-i(\omega_1+\omega_2)t_n/\varepsilon})\int\int\int\int\; e^{i\omega_1 S^+(\boldsymbol{x},z,\boldsymbol{\kappa}_1)/\varepsilon}\; e^{i\omega_2 S^+(\boldsymbol{x},z,\boldsymbol{\kappa}_2)/\varepsilon}$$
$$\times\,\overline{A}(z,\boldsymbol{\kappa}_1,\omega_1)\;\overline{A}(z,\boldsymbol{\kappa}_2,\omega_2)\;E[\mathcal{R}(z,\boldsymbol{\kappa}_1,\omega_1)\mathcal{R}(z,\boldsymbol{\kappa}_2,\omega_2)]\;d\omega_1 d\omega_2 d\boldsymbol{\kappa}_1 d\boldsymbol{\kappa}_2$$

with

$$\mathcal{R} \;=\; e^{i\omega\chi_\varepsilon/\varepsilon}(\alpha-a).$$

It follows from the results in Appendix E.3 that

$$E[\mathcal{R}(z,\boldsymbol{\kappa}_1,\omega_1)\mathcal{R}(z,\boldsymbol{\kappa}_2,\omega_2)] \;\sim\; 0 \qquad as\;\; \varepsilon\downarrow 0 \tag{2.6.19}$$

and that by dominated convergence

$$E[\Delta_N] \;\sim\; 0 \qquad as\;\; \varepsilon\downarrow 0.$$

Thus the stochastic process X is an asymptotic approximation of the downgoing pressure at $(\boldsymbol{x},z)$. In fact, with probability one, we have pathwise convergence. Consider now the asymptotic evaluation of the integral

$$I \;=\; \int\int \overline{A}\; e^{-(\omega^2\int_0^z D\cos(\theta)^{-1}\;ds)}\; e^{i\omega(S^+ +\chi_\varepsilon)/\varepsilon}\; d\boldsymbol{\kappa}.$$

If we ignore the random perturbation of the phase, that is the χ_ε term, this integral can be evaluated by a standard stationary-phase argument. From the law of the iterated logarithm of probability theory it follows that with probability 1

$$\limsup_{\varepsilon \downarrow 0} |\chi_\varepsilon(\boldsymbol{x}, z, \boldsymbol{\kappa})| \;\; \leq \;\; C\, \varepsilon\, \sqrt{\log\log \varepsilon^{-1}}. \tag{2.6.20}$$

for some constant $C > 0$. Consequently, to leading order the term χ_ε does not contribute to the phase. In Appendix E.5 we verify that we thus can ignore χ_ε when computing the stationary phase point in the method of stationary phase. Therefore we obtain

$$\begin{aligned} p \;\sim\; & \\ & \int (-i2\pi\varepsilon/\omega)\; \Delta^{-1/2}\; \overline{A}\; e^{-(\omega^2 \int_0^z D\cos(\theta)^{-1} ds)}\; e^{i\omega(S^+ + \chi_\varepsilon - t)/\varepsilon}\; d\omega \qquad as \;\; \varepsilon \downarrow 0 \end{aligned} \tag{2.6.21}$$

see [6]. The quantity $\Delta = \Delta(\boldsymbol{x}, z, \boldsymbol{\kappa})$ is the determinant of the Hessian of S^+ with respect to $\boldsymbol{\kappa}$. Note that the above expression is evaluated at the stationary phase point $\overline{\boldsymbol{\kappa}}$ defined as in Appendix E.4. In Appendix E.2 we show how we can obtain the high frequency approximation (2.2.8) when the source is parameterized by incoming plane wave components at the surface $z = 0$ as in (2.6.15). Now, in view of (E.2.4) and (2.2.8) we find that

$$\begin{aligned} & p(\boldsymbol{x}, z, \varphi + \chi_\varepsilon + \varepsilon s) \;\sim \\ & \quad (4\pi)^{-1}\; \varphi_z\; \sqrt{(d\Omega/da)(\gamma_0/\gamma_1)}\; [f' \star \mathcal{N}_V](s) \qquad as \;\; \varepsilon \downarrow 0, \end{aligned}$$

where $\mathcal{N}$ is the Gaussian distribution of square width V defined by

$$V \;\; = \;\; 2\int_0^z D\cos(\theta)^{-1}\; ds \;\; = \;\; (l/2)\int_0^z \gamma_1^2/\cos(\theta)^2\; ds,$$

and we have finally derived the layered version of the result (2.5.1), which was our objective.

Actually, from the approximation (2.6.21) it follows directly, in view of the stationary phase result, that

$$\begin{aligned} p &\sim \int [e^{-(\omega^2 \int_{z_s}^{z} D ds)} \; e^{i\omega\chi_\varepsilon/\varepsilon}](\overline{\boldsymbol{\kappa}}) \\ &\quad \times \int\int \overline{A} \; e^{i\omega S^+/\varepsilon} \; e^{-i\omega t/\varepsilon} \; d\boldsymbol{\kappa} \; d\omega \\ &\sim [\overline{p} \star \mathcal{N}_{\varepsilon^2 V}](t - \chi_\varepsilon) \quad as \quad \varepsilon \downarrow 0 \end{aligned}$$

with $\overline{p}$ being the exact transmitted pressure in the deterministic case. Consequently, the pressure is found as a deterministic pulse shape, with a random correction of the travel time.

2.6.4 Modification of analysis in weakly heterogeneous case.

We review briefly here the modifications of the above analysis which allow us to handle the weakly heterogeneous case.

The ansatz now becomes

$$\hat{p} = A \; e^{i\omega\tau_1/\varepsilon^2} + B \; e^{-i\omega\tau_1/\varepsilon^2} \tag{2.6.22}$$

$$0 = A_z \; e^{i\omega\tau_1/\varepsilon^2} + B_z \; e^{-i\omega\tau_1/\varepsilon^2}. \tag{2.6.23}$$

Introducing the change of variables

$$\alpha = A \; e^{\int_{z_s}^{z} \cos(\theta)^{-1}[\tau_{1,zz}/(2\gamma_1) - i(\omega/\varepsilon)\gamma_1 \;\; \nu/2] \cos(\theta)^{-1} ds}$$

we find that $E[\alpha] \sim a \;\; as \;\; \varepsilon \downarrow 0$, with a solving

$$da/dz \;=\; -\omega^2 \cos(\theta)^{-1} D\; a.$$

However, now

$$D \;=\; \bar{l}\gamma_1^2/(4\cos(\theta))$$

with

$$\bar{l}(z,\omega) \;\equiv\; \int_0^\infty E[\nu(0)\nu(s)] e^{i\omega 2\gamma_1(z)\cos(\theta(z))s} ds.$$

The result in Section 2.5 for the weakly heterogeneous layered case can be obtained from the above formulation by modifying the arguments of the previous section.

Next we generalize the above analysis and derive the O'Doherty-Anstey approximation in the locally layered case, as stated in Section 2.5.

2.7 Analysis for locally layered media.

We consider now the locally layered model defined in Section 2.1. We derive the O'Doherty-Anstey approximation only in the strongly heterogeneous case. The result in the weakly heterogeneous case follows essentially from the same arguments, allowing for modifications like those outlined in Section 2.6.4. The model we consider is thus

$$\begin{aligned} \rho\; \boldsymbol{u}_t + \nabla p &= \boldsymbol{F}_\varepsilon(\boldsymbol{x}, z, t) \\ K_\varepsilon^{-1}(\boldsymbol{x}, z)\; p_t + \nabla \cdot \boldsymbol{u} &= 0, \end{aligned} \tag{2.7.1}$$

with

$$\begin{aligned} \rho(\boldsymbol{x}, z) &\equiv \rho_0 \\ K_\varepsilon^{-1}(\boldsymbol{x}, z) &= \begin{cases} K_0^{-1} & z \in (-\infty, 0] \\ K_1^{-1}(\boldsymbol{x}, z)(1 + \nu(z/\varepsilon^2)) & z \in (0, \infty) \end{cases} . \end{aligned} \tag{2.7.2}$$

We start our treatment of (2.7.1) by deriving generalizations of the transport equations given in (2.6.6). In the purely layered case the amplitudes do not vary horizontally. In the locally layered case we seek a formulation in which the amplitudes vary only slowly in the horizontal directions. As in the purely layered case, the amplitudes will vary rapidly, on the finest scale of the model, in the depth direction z. This premise, that the amplitudes vary slowly horizontally, is important in order to obtain simple expressions for the asymptotic approximations of the partial differential equations describing the evolution of the amplitudes.

In order to motivate our approach in the locally layered case, we now briefly return to the purely layered case.

2.7.1 The purely layered case revisited.

Rewrite the expression (2.6.2) for the pressure in the layered case as

$$p = (1/2\pi\varepsilon) \int \int [A\ e^{i\omega S^+/\varepsilon} + B\ e^{-i\omega S^-/\varepsilon}]\ e^{-i\omega t/\varepsilon} d\boldsymbol{\kappa}\ d\omega, \tag{2.7.3}$$

where $A = A(z, \boldsymbol{\kappa}, \omega)$, $B = B(z, \boldsymbol{\kappa}, \omega)$ and

$$S^\pm = \boldsymbol{\kappa} \cdot \boldsymbol{x} \pm \tau_1.$$

Note that the conjugate harmonic argument $\boldsymbol{\kappa}$ can also be interpreted as the horizontal slowness of an incoming plane wave. The phases $S^\pm$ solve the eiconal equation associated with the deterministic part of the medium

$$(\nabla S^{\pm})^2 \;=\; \gamma_1^2, \tag{2.7.4}$$

and furthermore are respectively up- and down-going plane wave phases in the homogeneous part of the medium

$$S^{\pm} \;=\; \boldsymbol{\kappa}\cdot\boldsymbol{x} \pm \sqrt{\gamma_1^2 - \boldsymbol{\kappa}^2}\,(z - z_s). \tag{2.7.5}$$

We refer to $S^{\pm}$ as generalized plane wave phases, and τ_1 corresponds to the travel time from the source for these. It follows that

$$\hat{p}_{down} \;=\; \int\int A\; e^{i\omega S^{+}/\varepsilon}\; d\boldsymbol{\kappa} \tag{2.7.6}$$

constitutes a decomposition of the impinging pulse in terms of obliquely travelling plane waves. A possible ray configuration for S^+ is shown in Figure 2.4, rays are denoted Γ^+. The phase fronts will be orthogonal to these. It can be shown that $S^-(\boldsymbol{x}, z, \boldsymbol{\kappa}) \equiv -S^+(\boldsymbol{x}, z, -\boldsymbol{\kappa})$. Thus, if we change the direction of the rays in Figure 2.4, we obtain the rays associated with $S^-(\boldsymbol{x}, z, -\boldsymbol{\kappa})$. The formulation (2.7.3) can be seen as a generalization of the high frequency ansatz (2.2.4) in that we have included the reflected ray field. In contrast to the high frequency approximation, analysis based on this formulation will capture the modulation of the propagating pulse due to a local random coupling between the up- and down-propagating wave-fields, the scattering process which induces the pulse modulation we want to characterize. In the purely layered case, the problem decouples and becomes essentially one dimensional. The physical interpretation of this is that because of ray symmetry only amplitude pairs with the same horizontal slowness $\boldsymbol{\kappa}$ at the surface interact through scattering, see Figure 2.5. Equivalently, we can consider each Fourier component of $\hat{p}$ in isolation. We shall now see how this picture generalizes in the locally layered case.

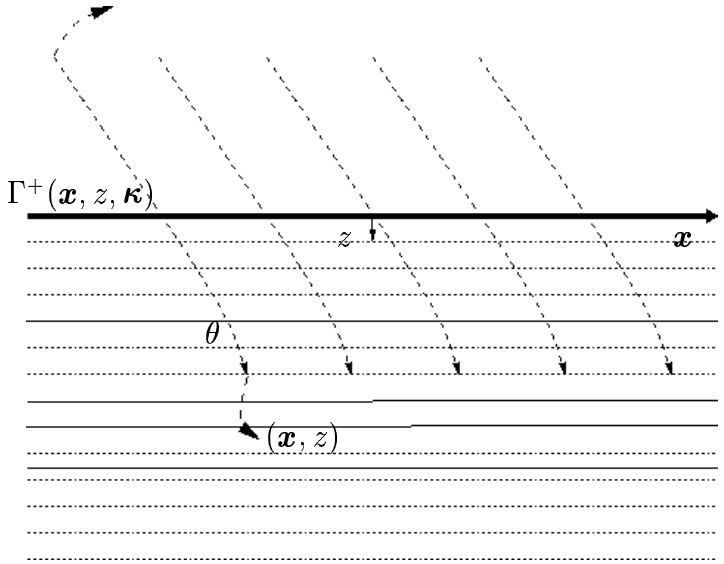

Figure 2.4: Rays associated with forward propagating plane wave.

2.7.2 Decomposition in terms of generalized plane wave components.

We seek to generalize the amplitude equations (2.6.6) to the locally layered case. We insist on retaining the parameterization (2.6.2) for the time-transformed pressure

$$\hat{p} \;=\; \int\int [A\; e^{i\omega S^+/\varepsilon} + B\; e^{i\omega S^-/\varepsilon}] d\boldsymbol{\kappa}, \tag{2.7.7}$$

but hasten to point out that this is not a standard step since the medium now is varying horizontally. The phases S^+ and S^- are defined as in the layered case. They solve the eiconal equation (2.7.4) associated with γ_1 and with initial conditions at the surface defined by (2.7.5). However, because the medium parameters vary horizontally, the associated rays will not be parallel in the halfspace $z > 0$ as they are in the purely layered case illustrated in Figure 2.4. Furthermore, the general ray picture shows that the amplitudes depend also on the horizontal argument and wave components with different horizontal slowness vectors at the surface *interact* as they

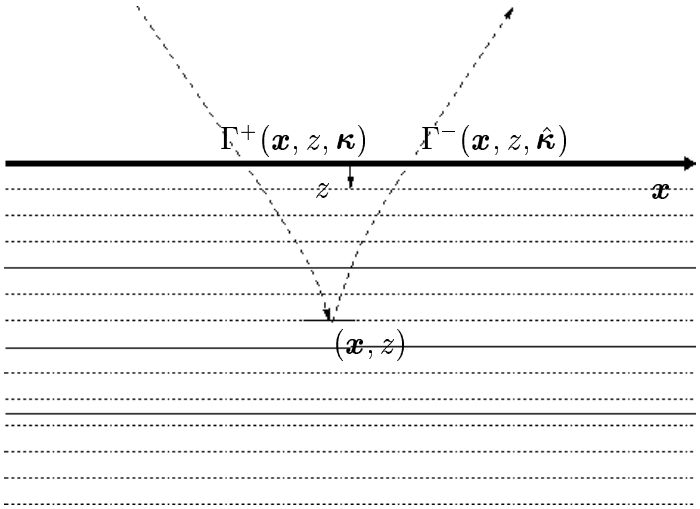

Figure 2.5: The reflected ray in purely layered case.

propagate.

As before we need to complement the ansatz (2.7.7) with an additional constraint. The amplitudes will vary in general on the scale of the local scattering, the scale ε^{-2}, though according to our premise only in the z-direction. We can therefore repeat the argument applied in the purely layered case in order to obtain the second part of the ansatz. Thus we arrive at the representation

$$\hat{p} = \int\int [A\ e^{i\omega S^+/\varepsilon} + B\ e^{i\omega S^-/\varepsilon}] d\boldsymbol{\kappa} \tag{2.7.8}$$

$$0 = \int\int [A_z\ e^{i\omega S^+/\varepsilon} + B_z\ e^{i\omega S^-/\varepsilon}] d\boldsymbol{\kappa}, \tag{2.7.9}$$

with $A = A(\boldsymbol{x}, z, \boldsymbol{\kappa}, \omega)$, $B = B(\boldsymbol{x}, z, \boldsymbol{\kappa}, \omega)$. The Fourier transformed pressure, $\hat{p}$, solves the reduced wave equation obtained from (2.1.1) by elimination of $\boldsymbol{u}$

$$\triangle \hat{p} + (\omega/\varepsilon)^2 \gamma_1^2 (1+\nu)\hat{p} = 0. \tag{2.7.10}$$

Note that the representation (2.7.8) – (2.7.9) makes sense only with the integral over the slownesses. Since different modes interact at different depths we cannot consider each mode in isolation and thereby obtain equations describing the evolution of the amplitudes with respect to depth. Thus, the situation is different from that of the previous section where the decoupling of generalized plane wave components makes it possible to obtain asymptotic approximations for the amplitudes by standard techniques, using stochastic ordinary differential equations. To cope with the more general scattering picture we introduce a mapping in the slowness domain. This enables us to derive stochastic integro-differential equations for the amplitudes, similar to the ones of the previous section.

2.7.3 Mapping of slowness vector.

In the locally layered case the rays associated with a given surface slowness vector will in general form a complicated ray pattern. The rays, defined as the characteristic directions associated with the solution of the eiconal equation, are parallel at the surface but do not remain so at depth due to the general background medium. Recall that the fine-scale modulation of the compliance is a function of the depth variable z only. Hence, at this level scattering couples the up- and down-going modes whose ray-paths have angles of incidence with respect to the z-direction which are equal and coplanar. See Figure 2.6 for a two-dimensional example. If the down-going ray path corresponds to the surface slowness vector $\boldsymbol{\kappa}$, we denote the slowness vector corresponding to the reflected path satisfying this law of reflection by $\hat{\boldsymbol{\kappa}}(\boldsymbol{\kappa}; \boldsymbol{x}, z)$. Note that the mapping is a function of the space argument. In the sequel we will make us of the following notation for a function $f = f(\boldsymbol{x}, z, \boldsymbol{\kappa})$ evaluated at the image/inverse image of $\boldsymbol{\kappa}$

$$\begin{aligned} \hat{f} &= f(\boldsymbol{x}, z, \hat{\boldsymbol{\kappa}}(\boldsymbol{\kappa}; \boldsymbol{x}, z)) \\ \check{f} &= f(\boldsymbol{x}, z, \hat{\boldsymbol{\kappa}}^{-1}(\boldsymbol{\kappa}; \boldsymbol{x}, z)). \end{aligned}$$

From the definition of this mapping it follows that $\nabla_\perp S^+ = \widehat{\nabla_\perp S^-}$ and $S_z^+ = -\widehat{S_z^-}$,

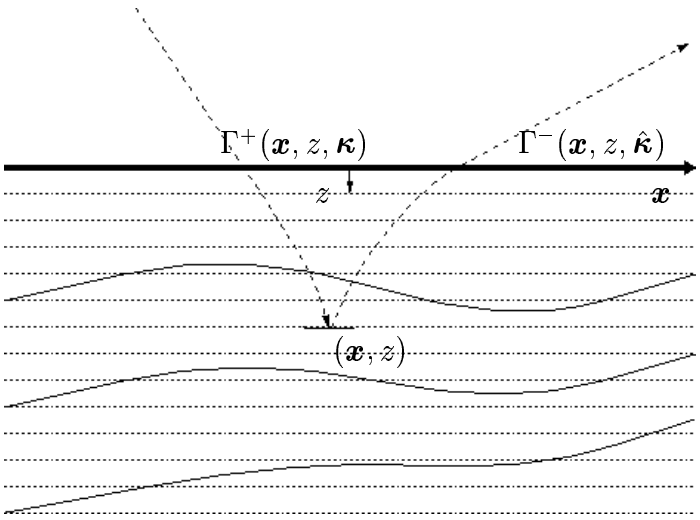

Figure 2.6: Ray coupling through slowness mapping.

and that $\hat{\boldsymbol{\kappa}}^{-1}(\boldsymbol{\kappa}; \boldsymbol{x}, z)) = -\hat{\boldsymbol{\kappa}}(-\boldsymbol{\kappa}; \boldsymbol{x}, z))$. Figure 2.6 illustrates that we have generalized the ray picture of Figure 2.5 of the purely layered case by introducing a mapping in the slowness domain. The above described scattering picture is a slight idealization of the one we use in the analysis presented in Appendix D, but captures the essential aspects of the ray geometry needed to describe the evolution of the front.

2.7.4 The mode coupling amplitude equations.

In this section we proceed to obtain the equations for the amplitudes which follows from the ansatz (2.7.8) – (2.7.9). In doing this we will make use of the mapping for the slownesses defined above. First we substitute (2.7.8) in (2.7.10) to obtain

$$\begin{aligned}\int\int [\{2\nabla S^+ \cdot \nabla A + \triangle S^+ A - i(\varepsilon/\omega)\triangle A\} e^{i\omega S^+/\varepsilon} \\ +\{2\nabla S^- \cdot \nabla B + \triangle S^- B - i(\varepsilon/\omega)\triangle B\} e^{i\omega S^-/\varepsilon} \\ - i(\omega/\varepsilon)\gamma_1^2\ \nu\{A\ e^{i\omega S^+/\varepsilon} + B\ e^{i\omega S^-/\varepsilon}\}] d\boldsymbol{\kappa} &= 0.\end{aligned}$$

From (2.7.9) we find that

$$\begin{aligned}\int\int[\{S_z^+A_z\ e^{i\omega S^+/\varepsilon}+S_z^-B_z\ e^{i\omega S^-/\varepsilon}\}\\ -i\omega/\varepsilon\{A_{zz}\ e^{i\omega S^+/\varepsilon}+B_{zz}\ e^{i\omega S^-/\varepsilon}\}]d\boldsymbol{\kappa} &= 0.\end{aligned}$$

We now combine the above two integral relations

$$\begin{aligned}\int\int[\{S_z^+A_z+2\nabla_\perp S^+\cdot\nabla_\perp A+\triangle S^+A-i(\varepsilon/\omega)\triangle_\perp A\}e^{i\omega S^+/\varepsilon}\\ +\{S_z^-B_z+2\nabla_\perp S^-\cdot\nabla_\perp B+\triangle S^-B-i(\varepsilon/\omega)\triangle_\perp B\}e^{i\omega S^-/\varepsilon}\\ -i(\omega/\varepsilon)\gamma_1^2\ \nu\{A\ e^{i\omega S^+/\varepsilon}+B\ e^{i\omega S^-/\varepsilon}\}]d\boldsymbol{\kappa} &= 0.\end{aligned}\tag{2.7.11}$$

In the standard high frequency approximation we use the high frequency character of the problem to solve for each mode separately. For the model at hand the 'high frequency' fluctuations in the medium parameters cause a coupling between modes. To articulate this coupling we rewrite (2.7.9) and (2.7.11) as

$$\begin{aligned}\int\int[\{S_z^+A_z+2\nabla_\perp S^+\cdot\nabla_\perp A+\triangle S^+A-i(\varepsilon/\omega)\triangle_\perp A\}e^{i\omega S^+/\varepsilon}\\ +\{\widehat{S^-}_z\hat{B}_z+2\widehat{\nabla_\perp S^-}\cdot\widehat{\nabla_\perp}B+\widehat{\triangle S^-}\hat{B}-i(\varepsilon/\omega)\widehat{\triangle_\perp}B\}e^{i\omega\hat{S}^-/\varepsilon}\ J\\ -i(\omega/\varepsilon)\gamma_1^2\ \nu\{A\ e^{i\omega S^+/\varepsilon}+\hat{B}\ e^{i\omega\hat{S}^-/\varepsilon}\ J\}]d\boldsymbol{\kappa}=0\\ \int\int[A_z\ e^{i\omega S^+/\varepsilon}+\hat{B}_z\ e^{i\omega\hat{S}^-/\varepsilon}\ J]d\boldsymbol{\kappa}=0,\end{aligned}$$

with J denoting the Jacobian of the transformation $\boldsymbol{\kappa}\mapsto\hat{\boldsymbol{\kappa}}(\boldsymbol{\kappa};\boldsymbol{x},z)$

$$J(\boldsymbol{x},z,\boldsymbol{\kappa}) = |\partial\hat{\boldsymbol{\kappa}}(\boldsymbol{\kappa};\boldsymbol{x},z)/\partial\boldsymbol{\kappa}|.$$

At this point we require the integral kernels of the above two integral relations to be zero since then the appropriate local interaction between up- and down-propagating

components are enforced. By adding/subtracting a multiple of S_z^+ ($= -\hat{S}_z^-$) times the second kernel to/from the first we obtain the generalized amplitude equations

$$\begin{aligned} 2\nabla S^+ \cdot \nabla A + \triangle S^+ A - i(\omega/\varepsilon)\gamma_1^2 \ \nu\{A + \hat{B}\ e^{i\omega(\hat{S}^- - S^+)/\varepsilon}\ J\} \\ = i(\varepsilon/\omega)\triangle_\perp A - \hat{R}^-\ e^{i\omega(\hat{S}^- - S^+)/\varepsilon}\ J \qquad (2.7.12) \\ 2\nabla S^- \cdot \nabla B + \triangle S^- B - i(\omega/\varepsilon)\gamma_1^2 \ \nu\{B + \check{A}\ e^{i\omega(\check{S}^+ - S^-)/\varepsilon}\ \check{J}^{-1}\} \\ = i(\varepsilon/\omega)\triangle_\perp B - \check{R}^+\ e^{i\omega(\check{S}^+ - S^-)/\varepsilon}\ \check{J}^{-1}, \qquad (2.7.13) \end{aligned}$$

with

$$\begin{aligned} R^+ &= 2\nabla_\perp S^+ \cdot \nabla_\perp A + \triangle S^+ A - i(\varepsilon/\omega)\triangle_\perp A \qquad (2.7.14) \\ R^- &= 2\nabla_\perp S^- \cdot \nabla_\perp B + \triangle S^- B - i(\varepsilon/\omega)\triangle_\perp B. \qquad (2.7.15) \end{aligned}$$

This is a generalization of (2.6.6). If we compare the above amplitude equations with the corresponding ones in the high frequency case given in (2.2.6), we see that, apart from a stochastic coupling, the amplitude equation for A has been changed in that only the horizontal rather than the full Laplacian of A appears. By considering the amplitude pair rather than a forward propagating component only, we have eliminated the component of the Laplacian in the direction in which the micro scale structure will cause it to be rapidly varying. According to our premise, the amplitudes are still slowly varying in the horizontal directions, the directions in which the medium varies only on a macroscopic scale.

In these amplitude equations the terms '$\triangle S^+ A$' and '$\triangle S^- B$' govern the main behavior of the solution and contain the geometrical effect in the high frequency effective medium approximation. As in the purely layered case the stochastic coupling, defined by the terms involving the fluctuations ν, is not purely off-diagonal. This is because the random fluctuations affect the travel time of the propagating pulse. By a change of the dependent variable we now obtain amplitude equations where these effects have been compensated for

$$\begin{aligned} \alpha &= A\, e^{\int_{\Gamma^+}[\triangle S^+/(2\gamma_1)-i(\omega/\varepsilon)\gamma_1\ \nu/2]ds} \\ \beta &= B\, e^{\int_{\Gamma^-}[\triangle S^-/(2\gamma_1)-i(\omega/\varepsilon)\gamma_1\ \nu/2]du}, \end{aligned}$$

where the path Γ^+ is defined as before, and Γ^- is similarly defined, however with respect to S^-, see Figure 2.6.

We then arrive at the following pair of amplitude equations

$$\begin{aligned} d\alpha/ds &= i(\omega/2\varepsilon)\gamma_1\ \nu\ \hat{\beta}\ e^{\Phi^+-\hat{\Phi}^-}\ J \\ &\quad + \{i(\varepsilon/\omega)\triangle_\perp A\ e^{i\omega S^+/\varepsilon+\Phi^+} - \hat{R}^-\ e^{i\omega\hat{S}^-/\varepsilon+\Phi^+}\ J\}/(2\gamma_1) \\ d\beta/du &= i(\omega/2\varepsilon)\gamma_1\ \nu\ \check{\alpha}\ e^{-\check{\Phi}^++\Phi^-}\ \check{J}^{-1} \\ &\quad + \{i(\varepsilon/\omega)\triangle_\perp B\ e^{i\omega S^-/\varepsilon+\Phi^-} - \check{R}^+\ e^{i\omega\check{S}^+/\varepsilon+\Phi^-}\check{J}^{-1}\}/(2\gamma_1), \end{aligned} \tag{2.7.16}$$

with

$$\begin{aligned} \Phi^+ &= -i\omega S^+/\varepsilon + \int_{\Gamma^+}[\triangle S^+/(2\gamma_1) - i(\omega/\varepsilon)\gamma_1\ \nu/2]ds \\ \Phi^- &= -i\omega S^-/\varepsilon + \int_{\Gamma^-}[\triangle S^-/(2\gamma_1) - i(\omega/\varepsilon)\gamma_1\ \nu/2]du, \end{aligned} \tag{2.7.17}$$

and s & u being the arc-length arguments along the characteristic rays associated with S^+ & S^- respectively. Note that the phase modification in (2.7.17) will be small by (2.6.20).

2.7.5 The approximate mode coupling equations.

In the purely layered case the bracketed terms on the right hand sides of (2.7.16) are asymptotically negligible. In Appendix D we show that they do not contribute to the leading order asymptotic approximation of the transmitted pressure in the locally layered case. Thus, retaining the notation for the amplitudes we arrive the following

approximate amplitude equations

$$\begin{aligned} d\alpha/ds &= i(\omega/2\varepsilon)\gamma_1\ \nu\ \hat{\beta}\ e^{(\Phi^+ - \hat{\Phi}^-)}\ J \\ d\beta/du &= i(\omega/2\varepsilon)\gamma_1\ \nu\ \check{\alpha}\ e^{(-\check{\Phi}^+ + \Phi^-)}\ \check{J}^{-1}. \end{aligned} \tag{2.7.18}$$

In a similar manner as in Section (2.6) we can now eliminate β from the first equation and obtain a stochastic integro-differential equation for the downgoing amplitude

$$\begin{aligned} d\alpha(\boldsymbol{x}, z, \boldsymbol{\kappa}, \omega)/ds = -(\omega/2\varepsilon)^2 \int_{\tilde{\Gamma}^-} [\gamma_1(\boldsymbol{x}, z)\ \gamma_1(\boldsymbol{x}(u), z(u))\ \nu(z/\varepsilon^2) \\ \times \nu(z(u)/\varepsilon^2) J(\boldsymbol{x}, z, \boldsymbol{\kappa})\ J^{-1}(\boldsymbol{x}(u), z(u), \tilde{\boldsymbol{\kappa}}(u))\ e^{\tilde{\Phi}(u)}] \alpha(\boldsymbol{x}(u), z(u), \tilde{\boldsymbol{\kappa}}(u), \omega)\ du, \end{aligned} \tag{2.7.19}$$

where $\tilde{\Gamma}^- = \tilde{\Gamma}^-(\boldsymbol{x}, z, \hat{\boldsymbol{\kappa}}(\boldsymbol{\kappa}; \boldsymbol{x}, z))$ is the semi-infinite characteristic ray-segment, among the rays associated with S^-, which terminates at $(\boldsymbol{x}, z)$. Thus Γ^- is the continuation of $\tilde{\Gamma}^-$, see Figure 2.7. Furthermore, for ease of notation, we define

$$\begin{aligned} \tilde{\boldsymbol{\kappa}}(u) &\equiv \hat{\boldsymbol{\kappa}}^{-1}(\hat{\boldsymbol{\kappa}}(\boldsymbol{\kappa}; \boldsymbol{x}, z); \boldsymbol{x}(u), z(u)) \\ \tilde{\Phi}(u) &\equiv \Phi^+(\boldsymbol{x}, z, \boldsymbol{\kappa}) - \Phi^+(\boldsymbol{x}(u), z(u), \tilde{\boldsymbol{\kappa}}(u)) \\ &\quad - \Phi^-(\boldsymbol{x}, z, \hat{\boldsymbol{\kappa}}(\boldsymbol{\kappa}; \boldsymbol{x}, z)) + \Phi^-(\boldsymbol{x}(u), z(u), \hat{\boldsymbol{\kappa}}(\boldsymbol{\kappa}; \boldsymbol{x}, z)). \end{aligned}$$

It follows from the definitions that $\tilde{\boldsymbol{\kappa}}(0) = \boldsymbol{\kappa}$ and $\tilde{\Phi}(0) = 0$ with $(\boldsymbol{x}(0), z(0)) = (\boldsymbol{x}, z)$. Note that (2.7.19) is a generalization of (2.6.10) in the purely layered case, where $J \equiv 1$.

2.7.6 Stabilization of the pulse.

The equation describing the evolution of the stochastic part of the amplitude is given by (2.7.19). In order to facilitate comparison with the corresponding expression in the layered case (2.6.10) we write this equation in the form

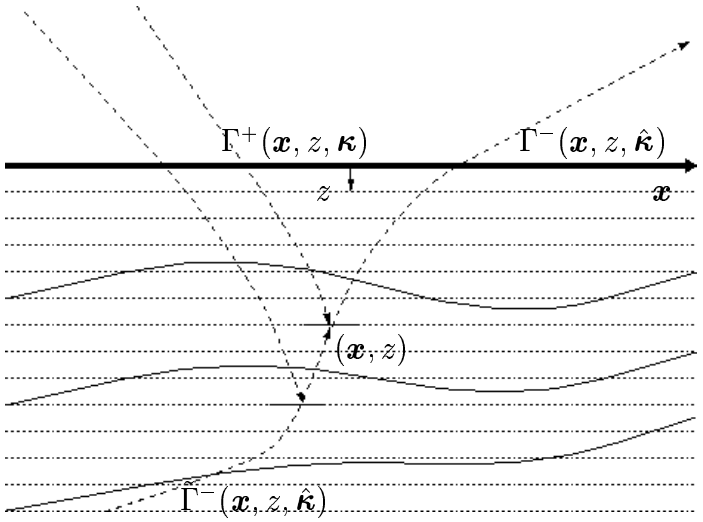

Figure 2.7: The rays involved in the integro differential equation (2.7.19).

$$d\alpha(\boldsymbol{y})/ds \;=\; \int_\Gamma K_\varepsilon(\boldsymbol{y}, \boldsymbol{y}(u))\; \alpha(\boldsymbol{y}(u))\; du,$$

with

$$\begin{aligned}
\boldsymbol{y} &\equiv (\boldsymbol{x}, z, \boldsymbol{\kappa}) \\
\boldsymbol{y}(u) &\equiv (\boldsymbol{x}(u), z(u), \tilde{\boldsymbol{\kappa}}(u)) \\
K_\varepsilon(\boldsymbol{y}, \boldsymbol{y}(u)) &= -(\omega/2\varepsilon)^2[\gamma_1(\boldsymbol{x}, z)\; \gamma_1(\boldsymbol{x}(u), z(u))\; \nu(z/\varepsilon^2)\; \nu(z(u)/\varepsilon^2) \\
&\quad \times J(\boldsymbol{x}, z, \boldsymbol{\kappa})\; J^{-1}(\boldsymbol{x}(u), z(u), \tilde{\boldsymbol{\kappa}}(u))\; e^{\tilde{\Phi}(u)}].
\end{aligned}$$

The quantities $\tilde{\boldsymbol{\kappa}}(u)$, J and $\tilde{\Phi}(u)$ are defined as in (2.7.19). Note that we suppressed the ω dependence. As before, s is the arc-length parameter along the path Γ^+. Furthermore, the path Γ is defined by requiring its projection on the subspace $(\boldsymbol{x}, z)$ to be $\tilde{\Gamma}^-$ and its projection on the subspace $\boldsymbol{\kappa}$ to be $\tilde{\boldsymbol{\kappa}}(u)$. The path Γ is parameterized by u, being again arc-length along $\tilde{\Gamma}^-$, that is $\Gamma(u) = \boldsymbol{y}(u)$. By a straightforward

calculation we obtain that $\forall\ \overline{\alpha}\ \in C$

$$\int_\Gamma E[K_\varepsilon(\boldsymbol{y}, \boldsymbol{y}(u))]\ \overline{\alpha}(\boldsymbol{y}(u))\ du \ \sim\ -\omega^2 D(\boldsymbol{y})\ \overline{\alpha}(\boldsymbol{y}) \qquad as\ \ \varepsilon \downarrow 0,$$

where

$$D \ = \ \gamma_1^2\ l/(4\cos(\theta)), \tag{2.7.20}$$

with θ being the angle between Γ^+ and the vertical direction at $(\boldsymbol{x}, z)$, see Figure 2.7. Assuming 'locality' as in the layered case we find $E[\alpha] \sim a\ \ as\ \ \varepsilon \downarrow 0$, with a solving

$$da/ds \ = \ -\omega^2 D\ a$$

The transmitted pressure can be approximated by the integral expression

$$p \ \sim\ (1/2\pi\varepsilon) \int\int\int A\ e^{i\omega(S^+ - t)/\varepsilon}\ d\boldsymbol{\kappa}\ d\omega \qquad as\ \ \varepsilon \downarrow 0,$$

To avoid having to deal with evanescent modes we confine the source to a neighborhood of the central ray slowness $\overline{\boldsymbol{\kappa}}$. From the assumption that the path $\Gamma^+(\boldsymbol{x}, z, \boldsymbol{\kappa})$ is nowhere horizontal it follows that $\cos(\theta) > 0$. Substituting the asymptotic approximation for A in this expression we arrive at a stochastic process given by

$$X \ = \ \int\int\int \overline{A}\ e^{-(\omega^2 \int_{\Gamma^+} D ds)}\ e^{i\omega(S^+ + \chi_\varepsilon - t)/\varepsilon}\ d\boldsymbol{\kappa}\ d\omega,$$

with $\overline{A}$ given in (2.6.18). Note that this expression is an exact analogue of (2.6.17), and differs only in that the phase S^+ and the associated rays Γ^+ are defined more generally. We therefore obtain an approximation for the transmitted pulse by analogy with the result in Section 2.6. In Appendix D we obtain the result by an invariant

imbedding argument. Thus, we finally arrive at the following approximation.

Consider problem (2.1.1). Then for $z > 0$ with probability one the transmitted pressure admits pathwise the asymptotic characterization

$$p(\boldsymbol{x}, z, \varphi + \chi_\varepsilon + \varepsilon s) \sim$$
$$(4\pi)^{-1} \varphi_z \sqrt{(d\Omega/da)(\gamma_0/\gamma_1)}\, [f' \star \mathcal{N}](s) \qquad as \quad \varepsilon \downarrow 0,$$

where $d\Omega$ is an element of solid angle of the initial direction of rays corresponding to Γ and da the associated element of area on the wavefront; see Figure 2.2 for an illustration. The function $\mathcal{N}$ is the centered Gaussian distribution of square width V, where

$$\chi_\varepsilon = \int_\Gamma \gamma_1 \, \nu/2 \, ds \tag{2.7.21}$$
$$V = (l/2) \int_\Gamma \gamma_1^2 \, \cos(\theta)^{-1} \, ds \tag{2.7.22}$$
$$l \equiv \int_0^\infty E[v(0)v(s)] \, ds \tag{2.7.23}$$
$$\gamma_1 = \sqrt{K_1^{-1}\rho}. \tag{2.7.24}$$

This is the result stated in Section 2.5.

2.8 Conclusions.

We have presented a theory for how fine scale structure in the medium parameters affects, over long propagation distances, a travelling acoustic pulse generated by a point source. The basic asumption in our theory is the separation of scales of variation of the medium properties: an essentially layered microscale structure modulating a smooth non-layered macroscopic background. We have analyzed the cases where the fluctuations are respectively, strong O(1) and where they go to zero with the square root of the ratio between the macroscopic and microscopic scales. In both cases we

obtain asymptotic approximations for the propagating pulse using averaging theory for stochastic equations. A main ingredient in our analysis is the decomposition of the wave-field into locally interacting up- and down-propagating generalized plane wave components. This enables us to capture the statistical coupling between the up- and down-propagating wave fields which causes the pulse modulation associated with the random layering.

The random fluctuations affect the pulse in two important ways. First, they cause a random travel-time correction on the order of the pulse duration. This correction can be expressed as a path integral over the medium parameters along the high frequency path from the source to the point of observation. The high frequency path is the one associated with the eiconal equation of the macro scale part of the medium and the point source. Second, they cause a smearing of the observed pulse shape through convolution with a Gaussian pulse, the heat kernel. Actually, the convolving pulse can be shown to satisfy the heat equation with the 'time'-variable replaced by the arc length parameter along the high frequency path. The shape of the Gaussian pulse depends only on the statistics of the medium, not the particular realization.

Further work will focus on extending the theory to more general hyperbolic systems, and to the case where the background is discontinuous, thus generating strong reflections. The assumption that the background medium is essentially layered is fundamental in the analysis, whether similar results can be derived for more general micro scale fluctuations is an open question.

We believe that our results contribute to the understanding of wave-propagation phenomena in heterogeneous media. Furthermore we expect that they will be useful in reflection seismology where a good understanding of the 'forward' problem, that is the propagation problem, is important.

Chapter 3

Pulse shaping & estimation of microstructure.

Density and velocity well log data can be used in many ways to construct stochastic models of the crustal structure. In this chapter we introduce a class of models based on well logs from the North Sea and explore their usefulness in understanding wave propagation phenomena. Only the microstructure in the lithology is modeled as random. The microstructure causes the traveling pulse to diffuse about its center. We examine this phenomenon for propagation (numerical simulation) in the model media and how well the O'Doherty-Anstey (OdA) approximation describes it. The approximation shows how the spreading of the pulse depends on the microstructure, and we illustrate how this can be used to validate the statistical estimation. For the model medium, we verify that the stabilization property predicted by the theory can be used to obtain precise estimates of important medium parameters by observing a *single* transmitted pulse. We also use the pulse shaping approximation to approximately remove the corruption of the transmitted pulse which is caused by the microstructure.

We consider propagation of acoustic plane waves in layered media. Thus, the problem involves only one space dimension. The O'Doherty-Anstey approximation is known to be valid in more general situations, and we regard this a first step toward understandig of realistic pulse shaping in more general media.

3.1 The acoustic equations.

We consider acoustic wave propagation with an impulsive plane wave source located in a homogeneous halfspace, initiating a pulse impinging on the heterogeneous halfspace $z > 0$. The governing equations are conservation of momentum and mass, for $z > 0$

$$\begin{aligned} \rho\ u_t + p_z &= 0 \\ K^{-1}\ p_t + u_z &= 0, \end{aligned} \tag{3.1.1}$$

where t is time and z is depth into the medium, defined so as to increase with depth, the downgoing direction. The density and compliance are denoted by ρ and K^{-1}. We assume that the medium parameters are *discretized* and vary only with depth

$$\begin{aligned} K^{-1} &= \begin{cases} K_0^{-1} & z \in (-\infty, 0] \\ K_k^{-1} & z \in ((k-1)\Delta z, k\Delta z] \end{cases} \\ \rho &= \begin{cases} \rho_0 & z \in (-\infty, 0] \\ \rho_k & z \in ((k-1)\Delta z, k\Delta z] \end{cases} . \end{aligned} \tag{3.1.2}$$

Thus for $z \neq n\Delta z,\ n = 0, 1, 2, \cdots$, p satisfies the scalar wave equation

$$p_{zz} - c_k^{-2} p_{tt} = 0 \tag{3.1.3}$$

with $c_k = \sqrt{K_k/\rho_k}$ being the local speed of sound. Since we consider one dimensional propagation we can decompose the wave into up- and down-going wave components in each section

$$\begin{aligned} p(z,t) &= (A_k(t - z/c_k) + B_k(t + z/c_k))\sqrt{\zeta}_k \\ u(z,t) &= (A_k(t - z/c_k) - B_k(t + z/c_k))/\sqrt{\zeta}_k \end{aligned} \tag{3.1.4}$$

for $z \in ((k-1)\Delta z, k\Delta z]$. The impedance, ζ_k, is given by $\zeta_k = \rho_k c_k$. These wave components interact only at the discontinuities where

$$\begin{bmatrix} A^+ \\ B^- \end{bmatrix} = G_k \begin{bmatrix} A^- \\ B^+ \end{bmatrix} \tag{3.1.5}$$

with superscripts $\pm$ indicating which side of interface k the function is evaluated. The matrix G_k is orthogonal, corresponding to a lossless interaction, and given by

$$G_k = \begin{bmatrix} \sqrt{1-r_k^2} & -r_k \\ r_k & \sqrt{1-r_k^2} \end{bmatrix}. \tag{3.1.6}$$

The interface reflection coefficient r_k is the fraction of the downpropagating wave A reflected back at interface k and is given by

$$r_k = (\xi_{k+1} - \xi_k)/(\xi_{k+1} + \xi_k). \tag{3.1.7}$$

In the wave propagation simulations we will probe the medium with a downpropagating pulse at the surface assuming that the halfspace $z > 0$ is initially at rest. The simulations in Section 3.4 are done with the medium realizations based on the stochastic model of Section 3.3.2.

3.2 Review of the pulse shaping approximation.

3.2.1 The medium model.

We use a generalization of the O'Doherty-Anstey approximation derived in [12], where the medium is discretized into equal travel-time sections, called a Goupillaud medium, essentially defined as in the previous section. We let the impedance in each section have the form

$$\zeta_k = \overline{\zeta}(1+\varepsilon e^{v_k}) \tag{3.2.1}$$

with ε being a small parameter and $\overline{\zeta}$ the background impedance level. The random variables v_k represent the fluctuations and are assumed to be stationary with a rapidly decaying correlation function. This model is similar to the one used in [12] where

$$\zeta_k = \overline{\zeta}e^{\varepsilon v_k}. \tag{3.2.2}$$

We found the model (3.2.1) to be an appropriate model for the well-logs we introduce in Section 3.3.1 in the context of pulse shaping. The parameter ε is small and the random variable v_k is assumed to have a rapidly decaying autocorrelation function, decaying on the scale ε^2 which is small compared to the macroscopic scale. In [3] such a medium was characterized as weakly heterogeneous. The data analysis that we carry out here confirms that such a model is appropriate for the medium corresponding to the well-logs. The O'Doherty-Anstey approximation has been generalized to strongly heterogeneous media in [15] and [11], but we will not use this here.

3.2.2 The pulse shaping approximation.

We review briefly the O'Doherty-Anstey approximation following [12].

Let a_k denote the autocovariance of the interface reflection coefficients r_k defined by (3.1.7)

$$a_{\Delta k} = E[r_k r_{k+\Delta k}]. \tag{3.2.3}$$

The medium is probed with a unit impulse impinging at the surface. After the pulse has traversed N sections of the discretized medium, its energy has spread out because of multiple reflections at the interfaces. Note that we think of the Goupillaud medium

as a discretization of a general medium. Hence, the correlation between the medium coefficients in the different sections depend on the choice of N for a given physical propagation distance. Denote this pulse train by $g = [g_1\ g_2\ g_3\ \cdots]$, where g_1 is the first arrival, the impulse being diminished in magnitude by reflections, g_2 is the pulse time lagged by $2\Delta t$ with Δt being the travel time for a section et cetera. It follows from the main result in [12] that

$$g \ \sim \ e^{-NA}e_1 \qquad as \ \ \varepsilon \downarrow 0, \tag{3.2.4}$$

where A is a lower triangular Toeplitz matrix whose first column is

$$A_1 \ = \ [a_0/2\ a_1\ a_2\ \cdots]',$$

and e_1 is the vector of zeros apart from the first entry which is one. Thus the pulse shaping is essentially defined by the autocorrelation of the interface reflection sequence.

To gain more insight into the character of the pulse shaping we write (3.2.4) as

$$g \ \sim \ e^{-a_0N/2}e^{a_0(N/2)\overline{A}}e_1 \qquad as \ \ \varepsilon \downarrow 0 \tag{3.2.5}$$

with the first column of the Toeplitz matrix $\overline{A}$ being

$$\overline{A}_1 \ = \ -2/a_0[0\ a_1\ a_2\ \cdots]' \equiv q.$$

We may think of $\overline{A}$ as a semi-infinite matrix and assume that the elements of $\overline{A}_1$ are non-negative. This will be the case for the model we consider in later sections. Moreover $\sum q_i \sim 1 \quad as \ \ \varepsilon \downarrow 0$, with q_i being the elements of q. Consequently we may think of q as the distribution of a random variable which we denote X. From the

representation (3.2.5) it follows that

$$g \sim \sum_{n=0}^{\infty} p_n \, q^{n*} \qquad as \;\; \varepsilon \downarrow 0 \tag{3.2.6}$$

with $p_n = e^{-a_0 N/2}(a_0 N/2)^n/n!$, and q^{n*} the n-fold convolution. The pulse can now be interpreted as the distribution of a random sum, with the number of terms Poisson distributed. Furthermore q^{n*} approaches weakly the Gaussian density by the central limit theorem, and from Theorem 4 page 265 [16] it actually follows that the pulse shape g itself converges weakly to the Gaussian density for large N. Hence, the pulse is essentially a Gaussian with increasing mean and standard deviation, corresponding to increasing delay and smearing of the pulse. The mean, $m(N)$, and variance, $V(N)$, of the distribution defined by (3.2.6) correspond, respectively, to the delay relative to the first arrival and to the square width of the pulse and are given by

$$\begin{aligned} m(N) &= a_0 \; N/2 \; E[X] = a_0 \; N/2 \; \sum_{i=1}^{\infty} i \; q_i = -N \sum_{i=1}^{\infty} i \; a_i \\ V(N) &= a_0 \; N/2 \; (Var[X] + E(X)^2) = -N \sum_{i=1}^{\infty} i^2 \; a_i, \end{aligned} \tag{3.2.7}$$

where X is a random variable with distribution q. These results correspond to (91) and (92) in [12].

It follows that the delay of the pulse relative to the first arrival is proportional to N times the first moment of the one-sided covariance function of the reflections. Moreover, the square width of the pulse is proportional to N times the second moment of the one-sided covariance function. These two moments are the most important aspects of the autocovariance of the reflections with respect to pulse shaping, and should be accurately represented in the modeling to come.

Note that we considered the transmitted pulse relative to the first arrival. Since the medium is random, the travel time to a certain depth will be a random quantity, which however can also be characterized by the central limit theorem. Moreover,

if we probe the medium with a pulse shape rather than an impulse as above, the O'Doherty-Anstey approximation of the transmitted pulse is found by convolution of the impulse response shown above with the source pulse.

These results can be generalized to the continuous case with the impedance being a general function of depth, (see [3, 11, 29, 49]). Note that the theory deals only with the front of the propagating pulse; see [3] for an analysis for the fluctuations.

In the next sections we carry out a statistical analysis of some well-logs that supports modeling as in (3.2.1) and obtain estimates of the parameters. By simulating numerically pulses propagating through realizations of this model we can characterize how well formula (3.2.4) predicts the pulse shaping for a realistic medium model. We then compare this simulation to one where the medium is given by the actual well-logs. Comparison of these two simulations provides a way of validating the estimated model for the medium.

3.3 The well-log data and its modeling.

3.3.1 The well-logs.

The data set comprises the well-logs from Block 31/2 of the Troll field in the North Sea. The data were kindly provided by Norsk-Hydro. The Troll field is located 80 km North-West of Bergen and has been the subject of extensive geostatistical and seismic modeling, see [20].

The water depth is about $200m$ and the maximum reservoir depth is about $1700m$, which makes it one of the shallowest reservoirs in the North Sea. The formation is assumed to represent a coastal deltaic environment comprising a series of stacked prograding delta lobes resulting in a layered structure dipping about 2-6 degrees.

We focus mainly on the data from well 10 in Block 31/2. *Figure* 3.1 shows the acoustic velocity and density logs for well 10 as a function of depth measured from sea level. We see that variations in the geology appear as shifts in level, trend and variability in the data. The large values in the bottom section of the log corresponds

to Calcite cemented sheets located in the oil zone. The logs show a lot of small scale fluctuations due to sedimentary cycles that produce fine scale layering.

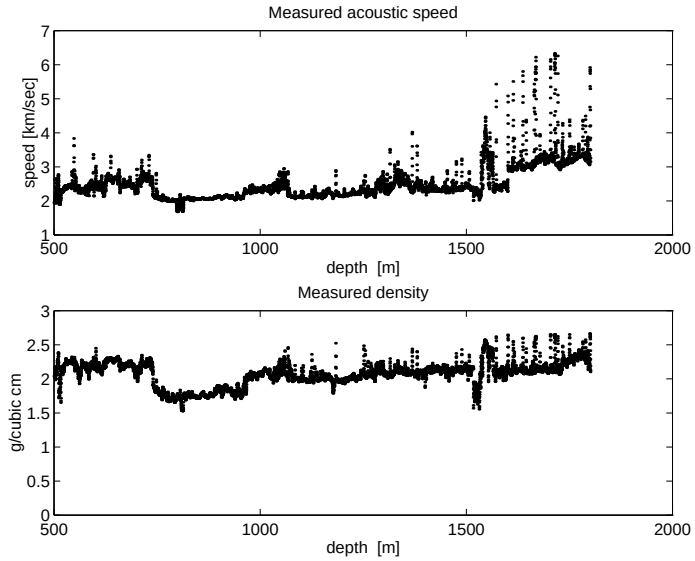

Figure 3.1: The sonic (top) and density logs from well 10. Each dot corresponds to an observation. Note the rapidly fluctuating micro scale heterogeneity.

Our primary interest is modeling of the fine scale structure of the medium and its role in pulse propagation. Since the well-logs are local averages of the 'true' medium parameters their fine scale structure does not correspond exactly to that of the medium. To remove the effect of the measurement tool we deconvolve the logs with a model transfer function for the tool. Details of this pre-processing are given in Appendix F.1.

In *Figure* 3.2, we show the actual well-logs for a subrange of the well in the top plot. The bottom plot is the deconvolved data. Henceforth, when we refer to the observations we mean the deconvolved data shown in the bottom plot.

In the stochastic model that we use the medium is perfectly layered. This is an idealization of the real physical medium that exaggerates somewhat the effect of the fine layering on the pulse shaping.

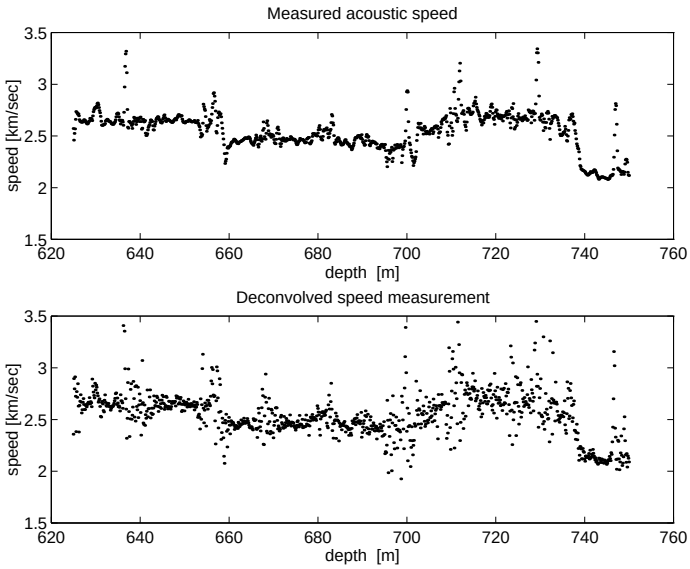

Figure 3.2: The sonic log plotted for a subrange of well 10. We show the the actual well-log in the top plot, and the deconvolved version in the bottom plot.

3.3.2 Statistical modeling.

In this section we define the stochastic models for the acoustic speed, c_k, and the density, ρ_k, in the k'th section of the discretized medium. Since our primary objective is to characterize acoustic pulse shaping in media of the kind defined by the well-logs, only those features that are actually 'seen' by the propagating pulse should be modeled explicitly. We assume therefore that the following model for the acoustic speed is appropriate

$$C_k \;=\; \overline{c}_k\,(1+\varepsilon e_k e^{X_k}). \tag{3.3.1}$$

The envelope function $\{\overline{c}_k\}$ models variations in the speed on the macroscale. The sequence $\{e_k\}$ defines together with $\{\overline{c}_k\}$ the macroscale variations in the strength of the random fluctuations which are modeled by the second term in 3.3.1. The normalization factor ε is chosen so that the mean square value of the sequence $\{e_k\}$ is

unity. Moreover X_k is chosen as a centered Gaussian random variable with standard deviation σ and spatial correlation defined in terms of the correlation range l as

$$E[X_k X_{k+\Delta k}]/\sigma^2 = e^{-\Delta k \Delta z/l}. \tag{3.3.2}$$

Pulse shaping is not sensitive to the specific form of the envelope functions e_k and $\overline{c}_k$, only to their average magnitude [12]. Thus we focus on the estimation of the parameters ε, σ and l. We now review briefly the main ingredients in the parameter estimation procedure, which is presented in Appendix F.2. The estimation is based mainly on the statistics of the interface reflection coefficients. This is because the interface reflection sequence is less sensitive to the heterogeneities seen in the underlying impedance sequence. Moreover, it follows from the description in Section 3 that the pulse shaping is largely governed by the statistics of the interface reflections which need to be accurately reflected in the model. Assuming a *constant density*, the expression for the interface reflections becomes

$$\begin{aligned} R_k &= (C_{k+1} - C_k)/(C_{k+1} + C_k) \\ &\approx (\varepsilon e_k/2)(e^{X_{k+1}} - e^{X_k}). \end{aligned} \tag{3.3.3}$$

We obtain this expression for ε small by making use of the approximations $\overline{c}_k \approx \overline{c}_{k+1}$ and $e_k \approx e_{k+1}$. We estimate the sequence e_k by a local average of the square of the sequence defined in (3.3.3). Based on this estimate of the sequence e_k, denoted by $\hat{e}_k$, we form the standardized reflections defined by

$$\tilde{r}_k = (c_{k+1} - c_k)/((c_{k+1} + c_k)\hat{e}_k), \tag{3.3.4}$$

with c_k being the observed velocities defined by the well-logs, a realization of the random variable C_k (represented by a capital letter). We compare the statistics of this sequence with that of a realization of the model (3.3.1) assuming $\overline{c}_k \equiv 1$ and

$e_k \equiv 1$. We choose the microscale parameters so as to obtain congruence between these statistics. This leads to the estimates $(\varepsilon, \sigma, l) = (.05, .8, .35m)$ associated with the sonic log observations in the depth range $500 - 1500m$ of well 10. The small value for ε implies that we can consider the medium as weakly heterogeneous. Note the small value for the correlation range, l, and that it is shorter than the averaging interval of the measurement tool.

We summarize the scaling we found for this particular data set from the Noth Sea. The relative magnitude of the fluctuations is small, on the order 7%. The spatial scale on which the fluctuations vary is very small, on the order $1m$, relative to the total travel distance for the pulse which might be on the order of several km.

3.4 Applications of the pulse shaping formula.

In this section we show how the pulse shaping formula can be used for prediction, estimation and validation. First we show how it can be used to compensate for the effect of the fine scale heterogeneity. We then use it to estimate scattering attenuation. Comparison with a pulse transmitted through the actual well-log provides validation for the estimated medium model. We also show how the formula can be used to explain the influence of the measurement tool on the pulse shaping properties of the underlying medium.

In the simulations we assume a *constant density*. The microscale parameters of the synthetic medium are *the ones obtained from the well-logs*, $(\varepsilon, \sigma, l) = (.05, .8, .35m)$. We choose $\{e_k \equiv 1\}$. At the surface, $z = 0$, we probe the medium with an impulsive down propagating pulse. We simulate the pulse propagation through a realization of the medium model down to a distance of $4km$, and plot it relative to the first arrival time. After $4km$, the pulse has opened up and its spatial spreading is determined by the microscale fluctuations. The up-propagating pulse is small because the macroscale variation in the bottom section of the medium is smooth.

We use an equal travel-time discretization in the simulations as in [12]. Pulse stabilization occurs relative to the first arrival time and *not* relative to the travel

distance. In the simulations we take the travel time to be the expected first arrival time at depth $4km$, hence the actual travel distance will vary somewhat with the medium realizations.

3.4.1 Feature identification and fine scale effect removal.

In seismic imaging we wish to identify the macroscopic features of the medium based on observations of the transmitted or reflected signals. These are in general blurred by the fine scale heterogeneities. We show in a very simple context how this blurring effect can be compensated by deconvolution based on the pulse shaping formula.

We choose the background profile so that the envelope function $\overline{c}_k$ equals 5 between $2000 - 2100m$ and 1 elsewhere. Thus, after the first arrival there will be multiples associated with the macroscopic medium variations. A section of the medium profile is shown in *Figure* 3.3.

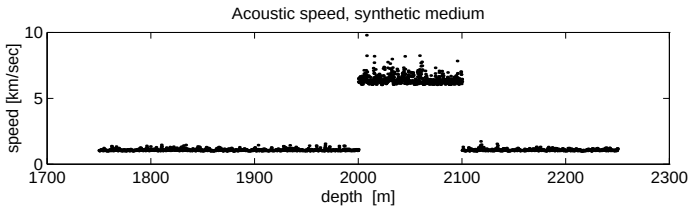

Figure 3.3: Medium with jumps in the background. The structure of the microscale fluctuations is as estimated in Section 3.3.2.

The transmitted signal from an impulsive source is shown by the solid line in *Figure* 3.4, top plot. The dashed line shows the corresponding O'Doherty-Anstey prediction. In [35] it was shown that the O'Doherty-Anstey theory extends to reflected signals and this example illustrates that indeed it accurately predicts the pulse shaping both for the front and for imbedded features, when we use a realistic model for the fine scale heterogeneities.

In the bottom plot, we show by solid and dashed lines the transmitted pulse shapes, simulated and predicted, when we probe the medium with a pulse which is the second derivative of the Gaussian. The dotted line corresponds to the transmitted

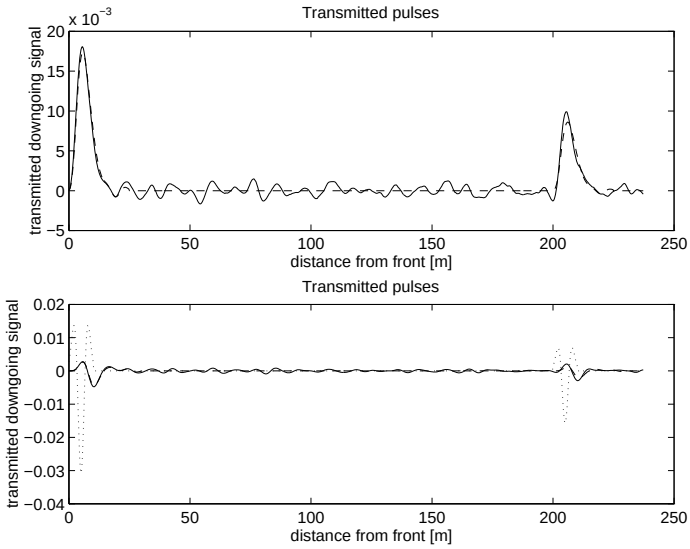

Figure 3.4: The figure illustrates that imbedded features also are being blurred according to the pulse shaping formula. The solid line in the top plot shows the transmitted features for a medium with strong macroscopic variations, the dashed line is the prediction of the transmitted signal based on the pulse shaping formula. The bottom plot is same except that the probing pulse is the second derivative of a Gaussian. The dotted line is the transmitted pulse for the background, without the fine scale structure.

pulse for the background medium, without fluctuations but with the same macroscale envelope and travel times. We see that the fluctuations have modified the pulse shape of the transmitted wave. The effect of the fine scale structure is not negligible.

Next, as shown in Figure 3.5, we attempt to compensate for the blurring effect by convolving the transmitted pulse with a filter which is an approximate inverse of the O'Doherty-Anstey pulse shaping effect. The solid line in the figure is the deconvolved trace and the dotted line is the transmitted pulse associated with the background medium. The choice of the deconvolution filter is described below. Compensating for the blurring is an ill-posted problem so we introduce a regularization in the deconvolution scheme, which means that some high frequency components of the coherent features of the pulse are lost.

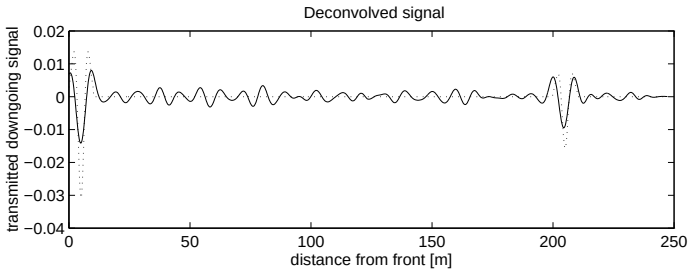

Figure 3.5: When we deconvolve the transmitted pulse of the previous figure with a filter that is approximately the inverse of the pulse shaping effect we get a pulse shape shown by the solid line in the figure. The dotted line is the transmitted pulse associated with the background medium.

For the purpose of the illustration we choose the deconvolution filter as the least-squares solution of the system obtained by requiring the convolution of the O'Doherty-Anstey pulse shaping filter with the deconvolution filter to be an impulse. The vector $\boldsymbol{v}$ of filter coefficients is the least-squares solution of '$\boldsymbol{A}\boldsymbol{v} = \boldsymbol{b}$', with $\boldsymbol{b}$ being a $2n \times 1$ vector, with coefficients equal to zero apart from the $n/2$'th entry which is 1. The top $n \times n$ part of $\boldsymbol{A}$ is a Toeplitz matrix whose rows contain the coefficients of the pulse shaping filter, that is the approximation for g given in (3.2.4). The bottom part, introduced for regularization, much as in [14] page 140, is defined as Δ times the identity matrix. We choose $\Delta = .1$, about the relative strength of the fluctuations in the transmitted trace, and a value for n corresponding to the support of the deconvolution filter being $25m$, roughly the spread of the features in the trace.

3.4.2 Estimation of scattering attenuation.

Estimation of spreading of the pulse.

Consider an impulse impinging on a heterogeneous halfspace as above. In this section we consider how the effect of the fluctuations can be estimated based on observing the transmitted pulse at a certain depth z. Recall that, at depth z, the pulse has been smeared out. Moreover, in the low frequency limit or in the limit of z large,

the pulse shape is close to a Gaussian. By observing the transmitted pulse we can estimate the smearing caused by the fluctuations.

In this section we do not restrict the discussion to the discretely layered case, but let K in (3.1.1) be

$$K^{-1} = K_0^{-1}(1+\nu(z)) \tag{3.4.1}$$

with $\nu(\cdot)$ a stationary random process with rapidly decaying correlation function and small variance. We know [49] that at depth z the second centered moment, that is, the variance or dispersion in time of the transmitted pulse, is given by

$$S(z) = z\ell/(2c_0^2) \equiv zs^2 \tag{3.4.2}$$

with $c_0 = \sqrt{K/\rho}$ being the speed of the background medium, the effective medium speed. The correlation length ℓ is $\ell = \int_0^\infty E[\nu(0)\nu(s)]ds$, and determines the influence of the microstructure or the pulse shaping. In the discrete case we find from (3.2.7) that $\ell = -8\Delta z \sum_{i=1}^{\infty} i^2\ a_i$. Above, the parameter s corresponds to the standard deviation, or temporal support, of the pulse shape at unit depth.

The key aspect of the O'Doherty-Anstey theory that enables us to obtain a robust estimate of $S(z)$ is the stabilization property. As the magnitude of the fluctuations becomes small, the transmitted pulse in the recorded time trace will have the spreading given by (3.4.2). The spreading does not depend on the particular realization or the specific formation except through its statistical properties represented by ℓ. This we illustrate in Figure 3.6 where we plot the pulses relative to the first arrival time. Because of the stabilization property they almost coincide with the O'Doherty-Anstey approximation shown by the solid line. For the medium at hand, $\sqrt{S(4km)} = 1.2 \times 10^{-3} sec.$ If we calculate the spreading of the transmitted pulses we obtain, for each trace, an associated estimate of s from (3.4.2). Doing this results in relative estimation errors on the order of 5%. For the estimated model we obtain by

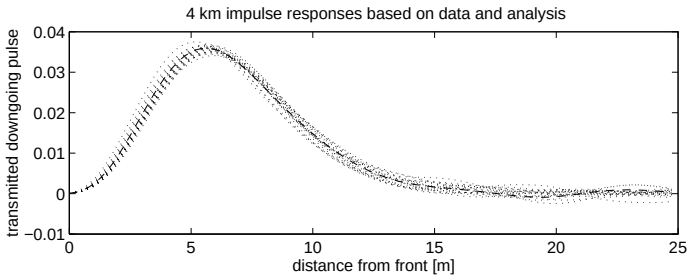

Figure 3.6: The dotted lines show transmitted pulses associated with 20 different realizations of the medium. They all agree well with the O'Doherty-Anstey approximation shown by the dashed line.

observing a *single* pulse at a *single* depth, corresponding to one medium realization, a very accurate estimate of strength of the blurring effect as defined by s.

In Figure 3.6 we have plotted the pulses relative to the first arrival time which is given by

$$\begin{aligned} T &= c_0^{-1} \int_0^z \sqrt{1+\nu(s)}ds \\ &\approx c_0^{-1} \int_0^z (1+\nu(s)/2)ds \\ &\equiv T_0 + X. \end{aligned}$$

By the central limit theorem the random variable X is approximately a centered Gaussian random variable with variance $S(z)$, where $S(z)$ is defined as in (3.4.2). Figure 3.7 shows the transmitted pulses of Figure 3.6, but now relative to a fixed time frame. We see that when we do not center the pulse with respect to the random arrival time, the pulses disperse. The average of the transmitted pulses is shown by the dashed line in the figure. Since the arrival time is essentially a Gaussian random variable, we get an estimate of the averaged pulse by convolving a Gaussian of variance $S(z)$ with the stabilized pulse shape, which actually is also close to a Gaussian with variance $S(z)$. Thus the averaged pulse is approximately a Gaussian with variance

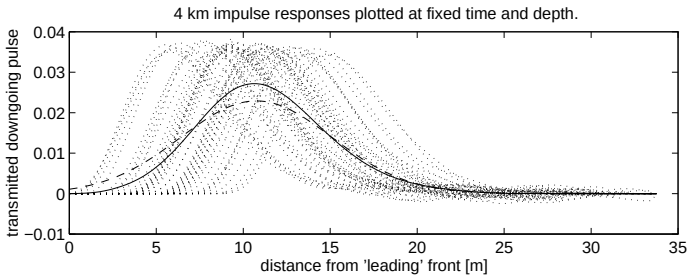

Figure 3.7: The dotted lines show transmitted pulses associated with 20 different realizations of the medium. The pulses are plotted relative to a fixed depth and time frame, in which case they do not stabilize. The solid line is the average of the transmitted traces and the dashed line a Gaussian with variance twice that of the individual transmitted pulses.

$2S(z)$. This pulse shape, centered at the effective medium arrival time, is shown by the dashed line in the figure.

We mentioned earlier that the O'Doherty-Anstey prediction generalizes to reflected pulses. If we have a perfect reflector at depth L, the reflected pulse emerges at the surface with a stabilized shape, but with random arrival time. Its spreading or variance is found as $S(2L) = 2S(L)$. Since however the arrival time is $2T$, its variance is 4, not 2, times the variance of T, the arrival time at depth L. Hence, when we average the pulses reflected to the surface in a fixed time frame, we obtain a pulse shape whose variance is $6S(L)$ rather than $4S(L)$.

Connection to localization.

Another consequence of the random layering is wave localization. If we Fourier transform the transmitted wave trace, we obtain the transmittivity at depth z and frequency f, which we denote $T_f(z)$. It is well known [2, 34, 48] that for almost all realizations

$$\frac{1}{z}\log|T_f(z)| \quad \sim \quad \frac{-1}{\mathcal{L}_f} = -c_\infty/(\pi f Q_f) \qquad as \quad z \uparrow \infty, \tag{3.4.3}$$

Well	10	12	14	15
$\sqrt{S(4)}[sec]$	1.2×10^{-3}	1.4×10^{-3}	$.7 \times 10^{-3}$	1.8×10^{-3}
$\mathcal{L}_f$ $[km]$	45	30	145	20

Table 3.1: Localization length estimates at $f = 40Hz$.

with $\mathcal{L}_f$ and Q_f the localization length and the quality Q factor, respectively, and c_∞ the mean speed in the high-frequency limit.

Localization and pulse smearing are both due to the effects of the layering on the propagating wave. In the low-frequency limit $f \ll 1$ [48],

$$\mathcal{L}_f \approx z/((2\pi f)^2 S(z)) = (2\pi f s)^{-2}. \tag{3.4.4}$$

Note that $s = \sqrt{S(z)/z}$ is the only parameter in this expression that depends on the medium and we have a robust estimate for it. If we use this estimate in (3.4.4) we get robust estimates also for the localization length.

In order to examine how the localization length varies for different wells we carried out a data analysis of several wells in Block 31/2, using the same medium model (3.3.1) as above. The associated localization length estimates, as defined by (3.4.4), are shown in Table 3.1. The large localization length estimates correspond to logs with very weak fluctuations, of relative magnitude .04. Note that we did not take the effect of density fluctuations into account. Doing this would lead to added variability in the fluctuations and shorter localization length. Moreover the magnitude of the fluctuations vary with respect to depth, so the above estimates will depend on the depth interval. In the case that the variability varies with depth S is found in terms of the *average* strength of the fluctuations in the considered depth interval [12].

In [24] an estimation of the localization length is carried out using the ARMA model for the synthetic reflection coefficients which was introduced in [51], whereas

[45] introduces a procedure for estimation of the correlation length of the medium velocity fluctuations. The authors base the estimation on the decay of plane wave modes, but they did not take into consideration the version of the O'Doherty-Anstey theory in [12] or [3] that emphasizes stabilization.

The relationship between the correlation of the lithology and localization length is also discussed in [53, 46]. White et al [53] report localization length estimates on the order of $16km$ at 40 Hz. The results of this paper support the model $\mathcal{L}_f = c_1 + c_2/f^2$ for the localization length with c_2 being inversely proportional to the correlation length ℓ as in (3.4.4).

Recall that the O'Doherty-Anstey theory describes the evolution of the *front* to a smooth Gaussian shape, hence provides information on the evolution in the low frequency regime of the harmonic spectrum in the transmitted trace. If we base the estimate of the localization length on (3.4.4) using the correlation length estimate based on pulse shaping we obtain, in the low frequency regime, an estimate with negligible fluctuations in the case that the correlation length is relatively small. However, the quantity $T_f(z)$ does not stabilize as the pulse shape itself does, and an estimate of the localization length based on it will have a wide relative confidence interval even though the fluctuations are small. Finally, note that if we actually have a probabilistic model for the medium as in (3.3.1), we can use the results of [47] to obtain the localization length in general, in particular in the high frequency limit determining c_1 in the above model for $\mathcal{L}_f$. In [27] these results are generalized to the elastic case. The O'Doherty-Anstey theory in the elastic case is discussed in [29, 43].

For the model (3.4.1), the center of mass of the pulse relative to the first arrival, the first moment of the pulse is given by $m(z) = zE[\nu^2]/(2c_0)$ [49]. If the fluctuations are exponentially correlated, $E[\nu(z)\nu(z+\Delta z)] \sim e^{-\Delta z/a}$, we thus find that

$$a \;=\; (c_0/2)(S(z)/m(z)). \tag{3.4.5}$$

This allows us to estimate the parameter a based on the transmitted pulse by estimating $m(z)$ and $S(z)$ from the trace and substitute these in (3.4.5). The top row of

Well	10	12	14	15
$\hat{a}[m]$	.31	.16	.15	.18
$a[m]$	.28	.14	.15	.14

Table 3.2: Comparison between estimates of the correlation range of the fluctuations and their 'actual' values.

Table 3.2 shows this estimate for four different wells based on a pulse having propagated through a realization of the associated medium model. The total propagation distance was as above $4km$. For the model (3.3.1) the correlation function of the fluctuations can be well approximated by an exponential. The bottom row of Table 3.2 shows the best fit value for a we obtained by comparing with the actual correlation function for the fluctuations of the synthetic medium. Note that by observing a *single* time trace at a *single* depth we have obtained a very accurate estimate of the parameter a, moreover the whole autocovariance function assuming an exponential model for this.

Whereas the parameter s, found in terms of the second moment of the pulse only, governs the localization in the low frequency regime, the parameter a determines the local character of the fluctuations which governs the localization of the high-frequency modes.

3.4.3 Validation of statistical estimation.

We now simulate wave propagation through a medium described by the actual well-logs, and compare the transmitted pulse with that propagating through the synthetic medium, and with the O'Doherty-Anstey prediction. A match of these pulses validates the assumed model for the medium as far as the effects of the fine scale structure on pulse spreading are concerned. Note that before we carry out the simulation we resample the log at equal travel times.

The solid line in *Figure* 3.8 shows a pulse having propagated through a medium

defined by the *tool corrected* speed measurement, the dashed line being the O'Doherty-Anstey approximation. In order to obtain a medium of total depth $4km$ with moderate variation in the macro scale components, that is the envelope functions e_k and $\overline{c}_k$, we take the c_k recordings in the depth interval $1000m$ – $1500m$ as our starting point and append to this the reverse of the same sequence, that is reflecting the sequence about its endpoint and then repeating it four times. The well is the one corresponding to the well-logs shown in Figure 3.1. A theoretical basis for using the pulse shaping formula in such a medium can be found in [35], where the approximation is derived in the presence of strong reflectors. The good match between the pulse shapes suggests that we have reasonable estimates for those aspects of the structure of the medium which are important for pulse shaping. Note that we did not include the effect of the envelope functions in the modeling. Since the background medium is smooth the transmitted pulse depends only marginally on the envelope $\overline{c}_k$. The O'Doherty-Anstey approximation depends on the envelope function e_k only through the 'effective magnitude' of the variability as defined by ε.

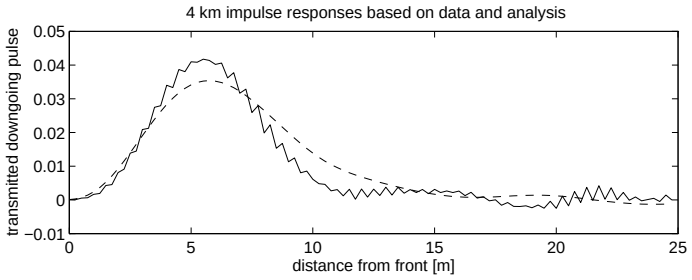

Figure 3.8: The solid line is the transmitted pulse shape obtained by propagating an initially impulsive-like signal through $4km$ of a medium defined by the well-log. The dashed line is the O'Doherty-Anstey approximation of the transmitted pulse corresponding to the estimated parameter values.

Note the ripples in the pulse that propagated through the medium defined by the log. This can be explained in terms of the description (3.2.6). The data analysis presented in Appendix F.2 shows that the process of deconvolving with respect to the model for the tool does not remove completely its effect and the autocorrelation of

the reflections, and also q in (3.2.6), has some anomalous values. The wave sees this 'mismatch', resulting in the ripples in the figure. If we use a slightly different model for the measurement tool, corresponding to $< a_1, \cdots, a_5 >=<$ 1 1.2 1.3 1.2 1. $>$ in (F.1.1), we obtain the result plotted in Figure 3.9. The figure is otherwise defined as the above Figure 3.8. We see that changing the model for the tool effectively removed the ripples. We do not pursue further the issue of estimating an 'optimal' model for the measurement tool.

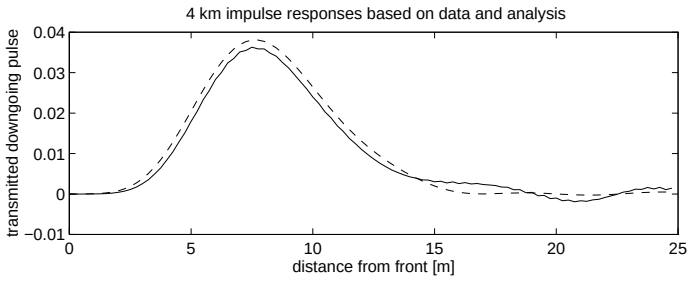

Figure 3.9: The figure is defined as the previous figure, except that we used a slightly different model for the tool.

The effect described above is more pronounced if we do not compensate for the tool at all. This we illustrate in the next figure. The medium through which the pulse shown by the solid line in *Figure* 3.10 has propagated differs from that in Figure 3.9 because the well-log has not been processed to eliminate tool effects. We see therefore the role of the tool in changing the pulse shaping properties of the medium. The dashed line is the O'Doherty-Anstey prediction for a medium whose stochastic structure contains tool effects. Even though the simulated medium does not have variations in $\overline{c}_k$ and e_k, the transmitted pulse shapes match very well. Furthermore, comparing with Figure 3.9 we see that the measurement filter changes substantially the microscale character of the fluctuations and the associated pulse shaping. From the analysis in Appendix F.2, see Figure F.6, it follows that the function q in (3.2.6) now has a set of relatively large negative values, and the result is therefore substantially different from the Gaussian case. Note the change of scale for the horizontal

axis. The tool has smoothed the medium which means that high frequency components propagate through.

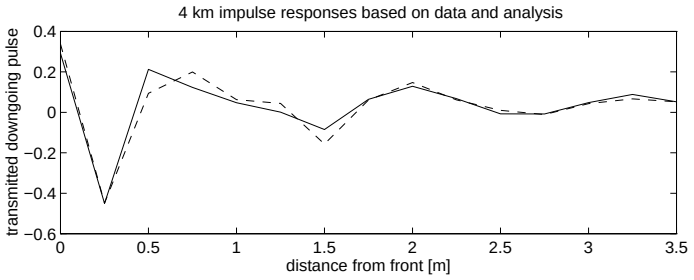

Figure 3.10: The transmitted pulse shape obtained by propagating an impulse through $4km$ of a medium defined by the actual sonic log without tool preprocessing compared with the associated O'Doherty-Anstey approximation, dashed line.

3.5 Effect of density fluctuations.

So far we have taken the density to be constant. Now assume that it can be represented by a stochastic model with the same form as in (3.3.1). The density, ρ_k, is thus a realization of the random variable

$$\Upsilon_k \;=\; \overline{\rho}_k\,(1+\varepsilon d_k e^{Y_k}). \tag{3.5.1}$$

We use exactly the same procedure for estimating the parameters as above, in this case assuming a constant velocity. We arrive at the estimates $(\varepsilon,\sigma,l)=(.02,.8,.2m)$, with σ being the standard deviation of the Gaussian random variable Y_k and l the correlation range. The fluctuations and correlation in the density sequence is somewhat smaller than the corresponding in the velocity sequence. The estimates in the case of the velocities were $(\varepsilon,\sigma,l)=(.05,.8,.35m)$. We model the covariance between the velocity and density by letting X_k and Y_k be correlated with correlation coefficient δ, and estimate this parameter to be .7. In estimating the microscale parameters

associated with the density and the acoustic speed we formed a set of standardized reflection coefficients based on each data set alone, the standardized reflections defined as in (3.3.4). We computed the correlation between these data sets and chose δ such that the corresponding modeled quantities had the same correlation.

Figure 3.11 shows the transmitted pulse through a realization of the synthetic medium defined by the estimated parameter set for well 10, using constant macroscale envelopes, but now including density modeling. That is we use both well-logs in the estimation. Note that the support of the transmitted pulse is about $15m$, whereas it was $10m$ when the model for the density not was included. The associated estimate of $\sqrt{S(4km)}$ has increased from $1.2 \times 10^{-3} sec$ to $1.6 \times 10^{-3} sec$. The added variability from variations in the density produces a larger correlation length and stronger pulse shaping, which is accurately described by the O'Doherty Anstey approximation shown by the dashed line.

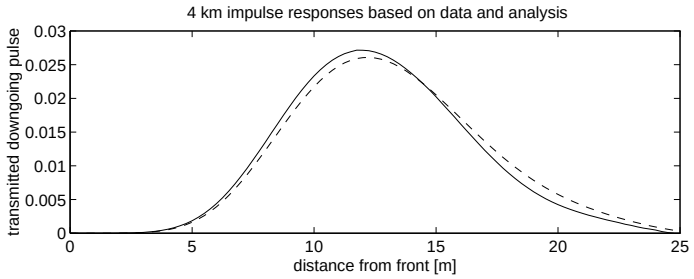

Figure 3.11: The transmitted pulse shape obtained by propagating an initially impulsive-like signal through $4km$ of the medium model. The pulse is plotted relative to the first arrival time. The dashed line is the OdA-approximation. Note that we included both the model for the density and the model for the speed heterogeneities when we simulated the medium.

3.6 Conclusions.

We have considered acoustic wave propagation in the earth's crust. Our primary objective was to explore the effect fine scale heterogeneities have on a propagating

pulse. In order to derive an appropriate stochastic model for the heterogeneities we took as our starting point a set of well-logs from a petroleum reservoir in the North Sea. Given this model we analyzed in detail the role of the fine scale heterogeneities by numerical simulation of wave propagation. Another objective was to explore how well the O'Doherty-Anstey formula, which asymptotically describes the effect of the heterogeneity, actually conforms with the simulation result for a realistic medium model. The results of our investigation suggest that the O'Doherty and Anstey approximation indeed characterizes the role of the heterogeneity very well. We found that the fine scale heterogeneity occurs on a surprisingly small scale, with an estimated correlation range of the fluctuations on the order of $.5m$. Note that we included a preprocessing step to remove the effects of the measurement tool. We also found that the magnitude of the fine scale heterogeneities is relatively small, which means that we have a weakly heterogeneous medium [3]. The well-log data support, moreover, the hypothesis that the medium can be represented well by a two-scale model, with a macro and a micro scale.

The O'Doherty-Anstey approximation determines pulse spreading by fine scale heterogeneities. For the medium model based on the well logs we found, for a total propagation distance of $4km$, that the spatial support of this pulse is about $15m$. Note that the relative strength of the fluctuations was small, on the order of 7%; in other cases with stronger fluctuations the pulse will be broader. As high resolution seismic imaging technology improves, we believe that the effect of the fine scale heterogeneities should be taken into account and that the O'Doherty-Anstey approximation is a powerful tool for doing so. We also showed how the pulse shaping formula can be used to *estimate* the localization length of the medium.

An important restriction is that the medium is purely layered. This is a first step in the analysis of pulse shaping in more general media. In [49] the O'Doherty-Anstey approximation is generalized to a class of non-layered, locally layered media, which are more appropriate for modeling sedimentary rock. The stochastic modeling done here applies also to such a medium. However, numerical simulation of wave propagation is much more complicated.

Finally, note that in the elastic wave propagation case the correlation between the

parameters associated with different modes of propagation becomes important. A high correlation between these will lead to stronger pulse shaping. Thus, estimating such correlations would be an interesting undertaking for further work. Moreover, it would be of interest to examine more closely how to design an 'optimal' scheme for deconvolution of the well logs so as to remove the effect of the tool.

Appendix A

Spherically symmetric medium.

Consider acoustic pulse propagation from a point source in spherically symmetric medium. The equation for the pressure field is

$$\triangle p - c(r)^{-2} p_{tt} \;=\; 0$$

away from the source, which is located at the origin. Here, r denotes the distance from the origin, p is the acoustic pressure and c the local speed of sound. As before we assume a constant density. In spherical coordinates this becomes

$$\begin{aligned} p_{rr} + (2/r)p_r + r^{-2}\sin(\theta)^{-1}\partial_\theta[\sin(\theta)p_\theta] + r^{-2}\sin(\theta)^{-2}p_{\phi\phi} - c(r)^{-2}p_{tt} \\ = \; p_{rr} + (2/r)p_r - c(r)^{-2}p_{tt} \;=\; 0 \end{aligned}$$

making use of spherical symmetry. We make the change of variables

$$w(r,t) \;=\; p(r,t)\; r$$

to obtain

$$w_{rr} - c(r)^{-2} w_{tt} \quad = \quad 0.$$

The above transformation corresponds to compensating for the geometrical effect described by the Greens function for the background medium. Note that this is exactly the governing equation (3.1.3). Hence, the one-dimensional analysis, corresponding to a purely layered model, generalizes to the spherically symmetric case. In the discrete case the propagation phenomenon is now described by (3.1.4) – (3.1.6). The only difference being that we in the layered case assumed $r_0 = 0$, whereas now $r_0 = -1$.

Appendix B

The slowness mapping.

In this appendix we construct the general slowness mapping used in Appendix D that concerns the transport equations. The rationale for constructing the mapping is to obtain a formulation for the transport equations where some laterally differentiated coupling terms can be controlled. In the case that the medium is layered the mapping we construct is the identity. On the ray paths going through the point of observation, the image of the slowness associated with the path is the one defined by the mapping introduced in section 2.7. That mapping we denoted $\hat{\kappa}(\kappa; x, z)$. For a function $g(x, z, \kappa)$ we used there the notation $\hat{g} = g(x, z, \hat{\kappa}(\kappa, x, z)$. Similarly, we will use the notation $\check{g} = g(x, z, \check{\kappa}(\kappa, x, z)$, with $\check{\kappa}$ being the corresponding inverse mapping. The slowness mapping introduced in this appendix will also be a function of location and be a generalization of the mapping introduced in Section 2.7. We will retain the above mentioned notation for this more general mapping.

For ease of notation we consider one horizontal spatial dimension. For $z \leq 0$ the coordinate transformation is the identity. First we show the existence of a mapping $\hat{\kappa}$ and then the inverse $\check{\kappa}$. The mapping is defined in terms of a certain function f. This function we choose only after having constructed the mapping, and choose it so that the mapping has the desired properties.

Let the phase functions $S^{\pm}$ solve the eiconal equation associated with the deterministic medium

$$
\begin{aligned}
(\nabla S^{\pm})^2 &= \gamma_1^2 \qquad \text{(B.0.1)}\\
S^{+}|_{z=z_s} &= \kappa\ x\\
S^{-}|_{z=z_s} &= \kappa(x+x_0)\\
S_z^{+}|_{z=z_s} &> 0\\
S_z^{-}|_{z=z_s} &< 0
\end{aligned}
$$

with $\gamma_1(x,z) = \sqrt{K_1^{-1}(x,z)\ \rho_0}$ being the slowness associated with the effective or deterministic medium. The parameter x_0 is introduced only to guarantee the existence of the mapping we are about to construct and has no further significance.

We seek to show that a certain invertible mapping $\hat{\kappa} \equiv \hat{\kappa}(\kappa, x, z)$ exists in a local neighborhood of the ray path from the source to the point of observation and for slownesses in a neighborhood of the slowness associated with this path. The mapping satisfies

$$
\begin{aligned}
\partial_x[S^{+}(x,z,\kappa) - S^{-}(x,z,\hat{\kappa}(\kappa;x,z))] &= 0 \qquad \text{(B.0.2)}\\
S_x^{+}(x,z,\kappa)|_{\kappa=k(x,z)} - S_x^{-}(x,z,\kappa)|_{\kappa=\hat{\kappa}(k(x,z);x,z)} &= 0 \qquad \text{(B.0.3)}\\
S_z^{+}(x,z,\kappa)|_{\kappa=k(x,z)} + S_z^{-}(x,z,\kappa)|_{\kappa=\hat{\kappa}(k(x,z);x,z)} &= 0 \qquad \text{(B.0.4)}\\
\check{\kappa}_x(\kappa;x,z)|_{\kappa=\hat{\kappa}(k(x,z);x,z)} &= 0. \qquad \text{(B.0.5)}
\end{aligned}
$$

Here $k(x,z)$ is the slowness that at the point (x,z) is associated with a ray going through the point of observation. In this appendix we will use the notation

$$
g_x(x, z_0(x), \kappa_0(x)) \equiv \partial_x g(x,z,\kappa)|_{(z=z_0(x),\kappa=\kappa_0(x))}
$$

and similarily for differentiation with respect to z and κ. To denote partial differentiation of a composite function we use ∂_x.

In order to show the existence we define a mapping $\Re^4 \mapsto \Re$

$$H_f(x,z,\kappa,\hat{\kappa}) = S^+(x,z,\kappa) - S^-(x,z,\hat{\kappa}) - \{S^+(x(z),z,\kappa) - S^-(x(z),z,\hat{\kappa}(\kappa;x(z),z) + f(z,\kappa))\}. \quad \text{(B.0.6)}$$

The function $f \in C^1$ is the one referred to above and will be chosen so that the mapping satisfies (B.0.5). The path $\{(x(z),z); z_s \leq z \leq \bar{z}\}$ is the ray path in between the source and the point of observation, we will refer to this ray as the 'central ray'. The slowness associated with this path and S^+ we denote $\bar{\kappa}$. We constrain f such that

$$f(z,\bar{\kappa}) = 0. \quad \text{(B.0.7)}$$

The mapping $\hat{\kappa} \in C^1$ is chosen so that

$$S_x^+(x,z,\kappa) = S_x^-(x,z,\hat{\kappa}(\kappa;x,z)). \quad \text{(B.0.8)}$$

Its existence follows by construction or a simple application of the implicit function theorem. Observe that we restrict κ to be in a neighborhood of the central ray slowness. For κ in this neighborhood and (x,z) in a neighborhood of the central path we assume that $S^{\pm} \in C^1$. Let the mapping, $\hat{\kappa}$ be defined by

$$H_f(x,z,\kappa,\hat{\kappa}(\kappa;x,z)) = 0. \quad \text{(B.0.9)}$$

We use the implicit function theorem to show existence of such a mapping.

Note that $\exists\ \bar{z}^+ > 0$ & $\Delta > 0$ such that

$$H_f|_{\Gamma(\bar{z}^+)} = 0 \quad \text{(B.0.10)}$$

$$|\partial_{\hat{\kappa}} H_f|_{\Gamma(\bar{z}^+)}| \;>\; \Delta \tag{B.0.11}$$

with $\Gamma(\bar{z}^+)$ being the path $\{(x,z,\kappa,\hat{\kappa}) \equiv (x(z),z,\bar{\kappa},\hat{\kappa}(\bar{\kappa};x(z),z)); z_s \leq z \leq \bar{z}^+\}$. The relation (B.0.10) follows by construction, and (B.0.11) from

$$\begin{aligned} \partial_{\hat{\kappa}} H_f &= -S^-_{\kappa} \\ \partial_{\kappa} S^-|_{z=0} &= (x+x_0) + \kappa\ z_s/\sqrt{\gamma_1^2-\kappa^2}. \end{aligned}$$

We assume x_0 has been chosen large enough such that S^-_{κ} is bounded away from zero in the domain of interest. Since, $H_f \in C^1$, it then follows by the implicit function theorem [32] $p\,67$ that there exists a unique mapping $\hat{\kappa}(\kappa;x,z) \in C^1$ in a neighborhood of the path $\Upsilon^+ \;:\; \{(x,z,\kappa) \equiv (x(z),z,\bar{\kappa}); z_s \leq z \leq \bar{z}^+\}$, denote this neighborhood B^+_f, such that

$$\begin{aligned} \hat{\kappa}|_{\Upsilon^+} &= \hat{\kappa}|_{\Upsilon^+} \\ H_f(x,z,\kappa,\hat{\kappa}(\kappa;x,z))|_{B^+_f} &= 0. \end{aligned} \tag{B.0.12}$$

Note that $\bar{z}^+$ does not depend on f.

That the mapping is invertible follows by a similar argument. If $\exists\ \bar{z}^- > 0\ \&\ \Delta > 0$ such that

$$|\partial_{\kappa} H_f|_{\Gamma(\bar{z}^-)}| \;>\; \Delta, \tag{B.0.13}$$

then by a similar argument as above the inverse mapping $\check{\kappa} = \check{\kappa}(\kappa;x,z) \in C^1$ exists in a neighborhood of the path $\Upsilon^- \;:\; \{(x,z,\hat{\kappa}) \equiv (x(z),z,\hat{\kappa}(\bar{\kappa};x(z),z)); z_s \leq z \leq \bar{z}^-\}$. Denote the associated neighborhood $\check{B}^-_f$ and its range under the mapping $(x,z,\kappa) \mapsto (x,z,\check{\kappa}(\kappa,x,z))\ B^-_f$. Then

$$\check{\kappa}|_{\Upsilon^-} = \bar{\kappa} \tag{B.0.14}$$

$$H_f(x,z,\check{\kappa}(\hat{\kappa};x,z),\hat{\kappa})|_{\check{B}_f^-} = 0, \tag{B.0.15}$$

and the slowness mapping, $\hat{\kappa}$, exits and is invertible in $B_f^+ \cap B_f^-$. Observe that

$$\begin{aligned}&\partial_\kappa H_f|_{x(z)}\\ &= S_\kappa^-(x(z),z,\hat{\kappa}(\kappa;x(z),z)+f(z,\kappa))[\hat{\kappa}_\kappa(\kappa;x(z),z))+f(z,\kappa)_\kappa].\end{aligned}$$

Note that $\hat{\kappa} \in C^1$ and that $\partial_\kappa \hat{\kappa}|_{z=0} \equiv 1$. Hence, if (B.0.7) is satisfied and

$$|f(z,\bar{\kappa})_\kappa| < \delta \tag{B.0.16}$$

for $z \leq \bar{z}^*$ with $\bar{z}^* > 0$ and δ sufficiently small, then the relation (B.0.13) is satisfied for some $\bar{z}^- > 0$ & $\Delta > 0$. Note also that $\bar{z}^-$ does not depend on f.

Next we choose the function f so that the conditions (B.0.7,B.0.16) are satisfied. To this effect define the function

$$\begin{aligned}F(z,\kappa,f) = {} & S^+(\bar{x}(z,\kappa),z,\kappa) - S^-(\bar{x}(z,\kappa),z,h(z,\kappa)) \\ & - \{S^+(x(z),z,\kappa) - S^-(x(z),z,\hat{\kappa}(\kappa;x(z),z)+f)\}.\end{aligned} \tag{B.0.17}$$

Here $\bar{x}(z,\kappa)$ is the value of the horizontal argument defined such that the ray that is associated with the slowness κ and S^+ and goes through $(\bar{x}(z,\kappa),z)$ also goes through the point of observation, moreover

$$h(z,\kappa) \equiv \hat{\kappa}(\kappa;\bar{x}(z,\kappa),z). \tag{B.0.18}$$

We let

$$F(z, \kappa, f(z, \kappa)) \;=\; 0 \tag{B.0.19}$$

define f, and need to show existence of the implicit function f. Note that

$$\begin{aligned} F(z, \bar{\kappa}, 0) &= 0 \\ \partial_f F(z, \kappa, f)|_{f=0} &= S_\kappa^-(x(z), z, \hat{\kappa}(\kappa; x(z), z)). \end{aligned}$$

The partial with respect to the implicit function is again defined in terms of S_κ^-. Therefore, a similar argument as above can be used to show that $\exists\ \bar{z}^* > 0$ so that there is a unique mapping $f = f(z, \kappa) \in C^1$ for $z \leq \bar{z}^*$ and κ in a neighborhood of $\bar{\kappa}$. Denote this neighborhood in the (x, z, κ) space B_f.

Observe that (B.0.7) follows by construction. However, we need to verify that (B.0.16) is satisfied for small δ. The depth at the point of observation $\bar{z}$ must satisfy $\bar{z} \leq min\{\bar{z}^*, \bar{z}^{\pm}\}$. By making $\bar{z}$ small enough we show that (B.0.16) will be satisfied with $\bar{z} \leq min\{\bar{z}^*, \bar{z}\pm\}$. Note that

$$\begin{aligned} \partial_\kappa f|_{z=0} &\equiv 0 \\ \partial_\kappa f|_{z=\bar{z}} &\equiv 0. \end{aligned}$$

That we can choose $\bar{z}^*$ and $\bar{z}$ such that $min\{\bar{z}^*, \bar{z}^{\pm}\} > \bar{z} > 0$ so that (B.0.16) is satisfied follows by observing that on the central path and for $\kappa = \bar{\kappa}$ we have $|S_\kappa^-| > \Delta > 0$.

Making use of this we find from (B.0.18,B.0.19) that when evaluated at $\kappa = \bar{\kappa}$

$$f(z, \kappa)_\kappa \;=\; \partial_\kappa[h(z, \kappa) - \hat{\kappa}(\kappa; x(z), z)]$$

$$= \quad \hat{\kappa}_\kappa(\kappa; x(z), z)\bar{x}_\kappa(z, \kappa).$$

Note that $\hat{\kappa}_\kappa|_{z=0} = 0$, moreover, that to first order the rays emanate radially from the point of observation. In the constant medium case

$$|\partial_\kappa \bar{x}(z, \kappa)| \quad \leq \quad (z - \bar{z})const$$

in a neighborhood of $\kappa = \bar{\kappa}$. In the general case we can bound $|\partial_\kappa \bar{x}(z, \kappa)|_{\kappa=\bar{\kappa}}$ in terms of the ray expansion ratio along the central path with the point of observation regarded as the source point. Since our basic assumption is that the ray picture along the central path is non-degenerate this quantity will be bounded. Hence, we can choose $\bar{z}^*$ and $\bar{z}$ such that $min\{\bar{z}^*, \bar{z}^\pm\} > \bar{z} > 0$ and (B.0.16) being satisfied for any $\delta > 0$.

Thus we have shown existence of the invertible mapping, $\hat{\kappa}$, in the neighborhood $B = B_f^+ \cap B_f^- \cap B_f$.

We now show that the slowness mapping constructed above, $\hat{\kappa}$, satisfies (B.0.2 – B.0.5) in the neighborhood $(x, z, \kappa) \in B$.

From (B.0.9) it follows that

$$\partial_x H_f(x, z, \kappa, \hat{\kappa}(\kappa; x, z)) \quad = \quad \partial_x[S^+(x, z; \kappa) - S^-(x, z, \hat{\kappa}(\kappa; x, z))] \quad = \quad 0,$$

which is (B.0.2).

Also from $H_f = 0$

$$\begin{aligned} & S^+(\bar{x}(z, \kappa), z, \kappa) - S^-(\bar{x}(z, \kappa), z, \hat{\kappa}(\kappa; \bar{x}(z, \kappa), z)) \\ & \quad = \quad S^+(x(z), z, \kappa) - S^-(x(z), z, \hat{\kappa}(\kappa; x(z), z) + f(z, \kappa)). \end{aligned} \tag{B.0.20}$$

Then, in view of (B.0.18,B.0.19) and the fact that $\bar{x}(z, k(x,z)) = x$, the unique solution $\hat{\kappa} = \hat{\kappa}(k(x,z); x, z)$ of (B.0.20) is given by

$$\hat{\kappa}(k(x,z); x, z) \;=\; \hat{\kappa}(k(x,z); x, z). \tag{B.0.21}$$

It follows from (B.0.8) that (B.0.3) is satisfied.

Consider next (B.0.4). Recall that the phase functions $S^{\pm}$ solve the eiconal equation. In view of (B.0.3) and the assumption on the ray geometry, that $S^{\pm}$ corresponds to upward/downward going rays, we can conclude that for $\kappa = k(x,z)$

$$S_z^+(x,z,\kappa) \;=\; -S_z^-(x,z,\hat{\kappa}(\kappa;x,z))$$

and have shown (B.0.4).

Finally, consider (B.0.5). It follows from (B.0.9) that

$$\begin{aligned}&\partial_x H_f(x,z,\kappa,\hat{\kappa}(\kappa;x,z))\\ &\quad= \; S_x^+(x,z;\kappa) - S_x^-(x,z,\hat{\kappa}(\kappa;x,z)) - S_\kappa^-(x,z,\hat{\kappa}(\kappa;x,z))\hat{\kappa}_x(\kappa;x,z) \;=\; 0.\end{aligned}$$

From (B.0.3) it then follows

$$\hat{\kappa}_x(k(x,z); x, z) \;=\; 0.$$

Note that we again used the fact that S_κ^- is bounded away from zero. From

$$\hat{\kappa}_\kappa(\check{\kappa}(\kappa;x,z);x,z)\check{\kappa}_x(\kappa;x,z) + \hat{\kappa}_x(\check{\kappa}(\kappa;x,z);x,z) \;=\; 0,$$

it moreover follows that

$$\check{\kappa}_x(\hat{\kappa}(k(x,z);x,z);x,z) \quad = \quad 0,$$

which finally is (B.0.5).

Appendix C

Microstructure relative to level curves.

C.0.1 The generalized medium model.

In Chapter 2 the random medium modulations are defined in terms of depth z only. Here we consider the case when they are defined in terms of level curves, as in (2.1.2). The seemingly more general model can be transformed into one with a layered medium modulation by a change of variables argument. As we show, the resulting modified transport equations agree to leading order with those we considered in Chapter 2. For brevity of notation we consider only one horizontal space dimension. The model then reads

$$\begin{aligned} \rho\ u_t + \nabla p &= F_\varepsilon(x,z,t) \\ K_\varepsilon^{-1}(x,z)\ p_t + \nabla \cdot u &= 0, \end{aligned} \tag{C.0.1}$$

with $u(x,z,t)$ and $p(x,z,t)$ being the acoustic velocity and pressure as before. The geometry of the problem is shown in Figure 2.1. In a *locally layered strongly heterogeneous* random medium, the material properties, density and compliance are modeled by

$$\begin{aligned} \rho(x,z) &\equiv \rho_0 \\ K_\varepsilon^{-1}(x,z) &= \begin{cases} K_0^{-1} & z \in (-\infty, 0] \\ K_1^{-1}(x,z)(1+\nu(\Phi(x,z)/\varepsilon^2)) & z \in (0,\infty) \end{cases}, \end{aligned} \tag{C.0.2}$$

where the mean K_1^{-1} is a smooth and positive function. The random medium fluctuations are denoted ν. The random modulation includes the smooth function Φ, that define a family of level curves. We carry out a change of variables with respect to this function. The modulation ν is not involved in the change of variables and we let $\nu \equiv 0$ for simplicity of notation.
Denote

$$\hat{p}(z,\omega) = \int p(z,s) e^{i\omega s/\varepsilon} ds,$$

then for $z > 0$

$$\triangle \hat{p} + (\gamma_1 \omega/\varepsilon)^2 \, \hat{p} = 0, \tag{C.0.3}$$

with $\gamma_1(x,z) = \sqrt{K_1^{-1}(x,z)\ \rho_0}$ being the slowness associated with the deterministic medium.

We assume that the levelcurves Φ are defined such that there exits a mapping

$$u(x,z) = \Phi^{\perp}(x,z) \tag{C.0.4}$$

$$v(x,z) = \Phi(x,z) \tag{C.0.5}$$

with $\nabla u \perp \nabla v$ in the domain of interest. In the (u,v) coordinate system ν in (C.0.2) becomes a function of one variable only.

C.0.2 Modification of ansatz and transport equations.

Let $u = u(x,z)$ and $v = v(x,z)$ be the coordinate mapping determined by the level curves associated with the random modulation. In this appendix we define

$$\begin{aligned} S^+ &= S^+(u,v,\kappa) \equiv S^+(x(u,v),z(u,v),\kappa) \\ S^- &= S^-(u,v,\kappa) \equiv S^-(x(u,v),z(u,v),\kappa) \\ A &= A(u,v,\kappa) \equiv A(x(u,v),z(u,v),\kappa) \\ B &= B(u,v,\kappa) \equiv B(x(u,v),z(u,v),\kappa). \end{aligned}$$

The phase functions $S^{\pm}$ solve the Eiconal equations associated with γ_1, as in (2.7.4,2.7.5). The modified ansatz is

$$\hat{p} = \int [A\ e^{i\omega S^+/\varepsilon} + B\ e^{i\omega S^-/\varepsilon}] d\kappa \tag{C.0.6}$$

$$0 = \int [A_v\ e^{i\omega S^+/\varepsilon} + B_v\ e^{i\omega S^-/\varepsilon}] d\kappa \tag{C.0.7}$$

Subscript v indicates partial differentiation with respect to v. Based on this modified ansatz we shall show that the transport equations (2.7.12,2.7.13) become

$$\begin{aligned} & 2\ v_A \cdot \nabla_t A + \triangle S^+ A \\ &= i(\varepsilon/\omega)[(\nabla\Phi^\perp)^2 A_{uu} + \triangle\Phi^\perp A_u] - \hat{R}^-\ e^{i\omega(\hat{S}^- - S^+)/\varepsilon}\ J \\ & 2\ v_B \cdot \nabla_t B + \triangle S^- B \\ &= i(\varepsilon/\omega)[(\nabla\Phi^\perp)^2 B_{uu} + \triangle\Phi^\perp B_u] - \check{R}^+\ e^{i\omega(\check{S}^+ - S^-)/\varepsilon}\ \check{J}^{-1}, \end{aligned} \tag{C.0.8}$$

$$\begin{aligned} R^+ &= w_A\ A_u + \triangle S^+ A - i(\varepsilon/\omega)[(\nabla\Phi^\perp)^2 A_{uu} + \triangle\Phi^\perp A_u] \\ R^- &= w_B\ B_u + \triangle S^- B - i(\varepsilon/\omega)[(\nabla\Phi^\perp)^2 B_{uu} + \triangle\Phi^\perp B_u]. \end{aligned}$$

We denote $\nabla_t \equiv (\partial_u, \partial_v)$ and $\nabla \equiv (\partial_x, \partial_z)$, moreover, J is the Jacobian of the slowness mapping. With $\hat{f}\&\check{f}$ we mean the function f evaluated at the slowness/inverse slowness mapping. The mapping is the one defined in Appendix B.

The equations have changed essentially only in that the terms involving $\triangle\Phi^{\perp}$ have been added, and in that the path directions v_A and v_B have been modified. These vectors define the directions of propagation. However, along the relevant ray paths, the ones going through the point of observation,

$$v_A \cdot \nabla_t A = \nabla S^+ \cdot \nabla A \tag{C.0.9}$$

$$\hat{v}_B \cdot \nabla_t \hat{B} = \nabla \hat{S}^+ \cdot \nabla \hat{B}. \tag{C.0.10}$$

C.0.3 The resulting pulse shaping approximation.

The modification of the transport equations involve only lower order terms. hence, the pulse shaping approximation as stated in Chapter 1 are valid when expressed relative to the (u, v) coordinate system. In the (x, z) coordinate system the approximation concerning the strongly heterogeneous case is still given by (2.5.1), but now the pulse shaping function $\mathcal{N}$ solves

$$\begin{aligned} \mathcal{N}_u &= D\,\mathcal{N}_{ss} \\ \mathcal{N}|_{z=0} &= \delta(s), \end{aligned}$$

where $\mathcal{N}_u = [\gamma_1^{-1}\nabla\varphi] \cdot \nabla\mathcal{N}$ with u being arc length along the ray path associated with the phase. Here the phase φ is the one associated with the deterministic point source problem. The 'diffusion coefficient' is

$$D(\boldsymbol{x}, z) = l\ \gamma_1^2(\boldsymbol{x}, z)/(4\cos(\theta(\boldsymbol{x}, z))|\nabla\Phi|).$$

with now θ being the angle *in between* $\nabla\Phi$ *and the ray direction*, rather than the

angle in between the vertical and the ray direction.

C.0.4 Generalization of the slowness mapping.

In the next section we derive the modified transport equations. There we use a phase mapping $\hat{\kappa}$ that is defined relative to the level curves Φ of the microstructure. We introduce here this phase mapping. Define

$$k \equiv k(u,v) = k(x(u,v), z(u,v)) \tag{C.0.11}$$

with $k(x,z)$ being the slowness that at the point (x,z) is associated with a ray going through the point of observation.

Now the relations (B.0.2) – (B.0.5) become

$$\begin{aligned}
\partial_u[S^+(u,v,\kappa) - S^-(u,v,\hat{\kappa}(\kappa;u,v))] &= 0 && \text{(C.0.12)}\\
[S_u^+(u,v,\kappa)|_{\kappa=k(u,v)} - S_u^-(u,v,\kappa)|_{\kappa=\hat{\kappa}(k(u,v);u,v)}] &= 0 && \text{(C.0.13)}\\
[S_v^+(u,v,\kappa)|_{\kappa=k(u,v)} + S_v^-(u,v,\kappa)|_{\kappa=\hat{\kappa}(k(u,v);u,v)}] &= 0 && \text{(C.0.14)}\\
\check{\kappa}_u(\kappa;u,v)|_{\kappa=\hat{\kappa}(k(u,v);u,v)} &= 0. && \text{(C.0.15)}
\end{aligned}$$

The existence of such a mapping can be shown just as in Appendix B. We point out the minor modifications in the argument.

The mapping $\hat{\kappa}$ is now defined so that

$$S_u^+(u,v,\kappa) = S_u^-(u,v,\hat{\kappa}(\kappa;u,v)). \tag{C.0.16}$$

As before (C.0.14) follows from (C.0.13). This is seen by decomposing as

$$\nabla S^+ = S_u^+ \nabla\Phi^\perp + S_v^+ \nabla\Phi$$

$$\nabla S^- = S^-_u \nabla\Phi^\perp + S^-_v \nabla\Phi.$$

with $\nabla \equiv (\partial_x, \partial_z)$. Since the phase functions $S^\pm$ solve the eiconal equation we find

$$(S^+_u)^2(\nabla\Phi^\perp)^2 + (S^+_v)^2(\nabla\Phi)^2 = (S^-_u)^2(\nabla\Phi^\perp)^2 + (S^-_v)^2(\nabla\Phi)^2.$$

In view of (C.0.13) and the assumption on the ray geometry, that $S^\pm$ corresponds to upward/downward going rays, we can conclude that for $\kappa = k(u,v)$

$$S^+_v(u,v,\kappa) = -S^-_v(u,v,\hat{\kappa}(\kappa;u,v)),$$

which is (C.0.14).

C.0.5 Derivation of the modified transport equations.

We start the derivation by substituting (C.0.6) in (C.0.3) to obtain

$$\begin{aligned} &\int [\{2\nabla S^+ \cdot \nabla A + \triangle S^+ A - i(\varepsilon/\omega)\triangle A\} e^{i\omega S^+/\varepsilon} \\ &+\{2\nabla S^- \cdot \nabla B + \triangle S^- B - i(\varepsilon/\omega)\triangle B\} e^{i\omega S^-/\varepsilon} d\kappa = 0. \end{aligned} \tag{C.0.17}$$

We next evaluate the expression, H, involving the laplace differentiated terms

$$\begin{aligned} H &\equiv \int [\triangle A e^{i\omega S^+/\varepsilon} + \triangle B e^{i\omega S^-/\varepsilon}] d\kappa \\ &= \int [(\nabla\Phi)^2 A_{vv} + (\nabla\Phi^\perp)^2 A_{uu} + 2\nabla\Phi\cdot\nabla\Phi^\perp A_{uv} + \triangle\Phi A_v + \triangle\Phi^\perp A_u] e^{i\omega S^+/\varepsilon} \\ &\quad + [(\nabla\Phi)^2 B_{vv} + (\nabla\Phi^\perp)^2 B_{uu} + 2\nabla\Phi\cdot\nabla\Phi^\perp B_{uv} + \triangle\Phi B_v + \triangle\Phi^\perp B_u] e^{i\omega S^-/\varepsilon}\, d\kappa. \end{aligned} \tag{C.0.18}$$

The terms involving A_v and B_v cancel due to (C.0.7). From (C.0.7) it also follows that

$$\begin{aligned}
\int [i\omega/\varepsilon [S_v^+ A_v \ e^{i\omega S^+/\varepsilon} + S_v^- B_v \ e^{i\omega S^-/\varepsilon}] \\
+ [A_{vv} \ e^{i\omega S^+/\varepsilon} + B_{vv} \ e^{i\omega S^-/\varepsilon}]] d\kappa &= 0 \\
\int [i\omega/\varepsilon [S_u^+ A_v \ e^{i\omega S^+/\varepsilon} + S_u^- B_v \ e^{i\omega S^-/\varepsilon}] \\
+ [A_{uv} \ e^{i\omega S^+/\varepsilon} + B_{uv} \ e^{i\omega S^-/\varepsilon}]] d\kappa &= 0.
\end{aligned} \tag{C.0.19}$$

Hence

$$\begin{aligned}
H &= \int [i\omega/\varepsilon \ c_1 A_v + (\nabla\Phi^\perp)^2 A_{uu} + \triangle\Phi^\perp A_u] e^{i\omega S^+/\varepsilon} \\
&+ [i\omega/\varepsilon \ c_2 B_v + (\nabla\Phi^\perp)^2 B_{uu} + \triangle\Phi^\perp B_u] e^{i\omega S^-/\varepsilon} \ d\kappa
\end{aligned} \tag{C.0.20}$$

with

$$\begin{aligned}
c_1 &= -(\nabla\Phi)^2 S_v^+ - 2\nabla\Phi \cdot \nabla\Phi^\perp S_u^+ \ = \ -(\nabla\Phi)^2 S_v^+ \\
c_2 &= -(\nabla\Phi)^2 S_v^- - 2\nabla\Phi \cdot \nabla\Phi^\perp S_u^-. \ = \ -(\nabla\Phi)^2 S_v^-
\end{aligned} \tag{C.0.21}$$

Next we obtain the transport equations in a manner analogous to the way we obtained them in Chapter 2. We substitute (C.0.20) in (C.0.17), evaluate the terms involving the B amplitude at $\hat{\kappa} = \hat{\kappa}(\kappa; x, z)$ and enforce the equation pointwise. Then we obtain

$$\begin{aligned}
&\{v_1 \cdot \nabla_t A + \triangle S^+ A - i(\varepsilon/\omega)[(\nabla\Phi^\perp)^2 A_{uu} + \triangle\Phi^\perp A_u]\} e^{i\omega S^+/\varepsilon} \\
&= \ -[\{v_2 \cdot \nabla_t B + + \triangle S^- B - i(\varepsilon/\omega)[(\nabla\Phi^\perp)^2 B_{uu} + \triangle\Phi^\perp B_u]\} e^{i\omega S^-/\varepsilon} \ ]_{\hat{\kappa}} J
\end{aligned} \tag{C.0.22}$$

with

$$v_1 \cdot \nabla_t A \ \equiv \ 2\nabla S^+ \cdot \nabla A + c_1 A_v \tag{C.0.23}$$

$$v_2 \cdot \nabla_t B \equiv 2\nabla S^- \cdot \nabla B + c_2 B_v. \tag{C.0.24}$$

Similarly, from (C.0.7) we get

$$A_v e^{i\omega S^+/\varepsilon} + [B_v e^{i\omega S^-/\varepsilon}]_{\hat{\kappa}} J = 0. \tag{C.0.25}$$

By combining (C.0.22) and (C.0.25), eliminating respectively the A_v / B_v terms, we arrive at the transport equations

$$\begin{aligned} 2v_A \cdot \nabla_t A + \triangle S^+ A = i(\varepsilon/\omega)[(\nabla\Phi^\perp)^2 A_{uu} + \triangle\Phi^\perp A_u] \\ - \hat{R}^- \; e^{i\omega(\hat{S}^- - S^+)/\varepsilon} \; J \\ 2v_B \cdot \nabla_t B + \triangle S^- B = i(\varepsilon/\omega)[(\nabla\Phi^\perp)^2 B_{uu} + \triangle\Phi^\perp B_u] \\ - \check{R}^+ \; e^{i\omega(\check{S}^+ - S^-)/\varepsilon} \; \check{J}^{-1}, \end{aligned}$$

$$\begin{aligned} R^+ &= w_A \; A_u + \triangle S^+ A - i(\varepsilon/\omega)[(\nabla\Phi^\perp)^2 A_{uu} + \triangle\Phi^\perp A_u] \\ R^- &= w_B \; B_u + \triangle S^- B - i(\varepsilon/\omega)[(\nabla\Phi^\perp)^2 B_{uu} + \triangle\Phi^\perp B_u]. \end{aligned}$$

which is (C.0.8), with v_A & v_B being vectors and w_B & w_A scalars. We comment on their definition below.

We now verify (C.0.9) and (C.0.10). Define $k = k(u, v)$ as that slowness which at location (u, v) is associated with a ray going through the point of observation. We want to show that (C.0.9) and (C.0.10) are valid when evaluated at $\kappa = k(u, v)$. The slowness mapping as defined in Appendix B is defined relative to the (u, v) coordinates. There we show that for $\kappa = k(u, v)$

$$S_v^+ = -\hat{S}_v^-. \tag{C.0.26}$$

Define

$$\begin{aligned} G(A,B) &= v_1 \cdot \nabla_t A e^{i\omega S^+/\varepsilon} + [v_2 \cdot \nabla_t B e^{i\omega S^-/\varepsilon}]_{\hat{\kappa}} J \\ &= 2v_A \cdot \nabla_t A e^{i\omega S^+/\varepsilon} + [w_B B_u e^{i\omega S^-/\varepsilon}]_{\hat{\kappa}} J \\ &= \{2\nabla S^+ \cdot \nabla A - (\nabla\Phi)^2 S_v^+ A_v\} e^{i\omega S^+/\varepsilon} \\ &\quad + [\{2\nabla S^- \cdot \nabla B - (\nabla\Phi)^2 S_v^- B_v\} e^{i\omega S^-/\varepsilon}]_{\hat{\kappa}} J. \end{aligned} \tag{C.0.27}$$

Using (C.0.25) and (C.0.26) we find that for $\kappa = k(u,v)$

$$\begin{aligned} G(A,B) &= 2\nabla S^+ \cdot \nabla A e^{i\omega S^+/\varepsilon} \\ &\quad + [\{2\nabla S^- \cdot \nabla B - 2(\nabla\Phi)^2 S_v^- B_v\} e^{i\omega S^-/\varepsilon}]_{\hat{\kappa}} J \\ &= [2\nabla S^- \cdot \nabla B e^{i\omega S^-/\varepsilon}]_{\hat{\kappa}} J \\ &\quad + [\{2\nabla S^+ \cdot \nabla A - 2(\nabla\Phi)^2 S_v^+ A_v\} e^{i\omega S^+/\varepsilon}]. \end{aligned} \tag{C.0.28}$$

Making use of the identities

$$\begin{aligned} \nabla S^+ \cdot \nabla A - (\nabla\Phi)^2 \; S_v^+ A_v &= (\nabla\Phi^\perp)^2 S_u^+ A_u \\ \nabla S^- \cdot \nabla B - (\nabla\Phi)^2 \; S_v^- B_v &= (\nabla\Phi^\perp)^2 S_u^- B_u, \end{aligned}$$

we find from (C.0.28) that for $\kappa = k(u,v)$

$$\begin{aligned} G(A,B) &= 2\nabla S^+ \cdot \nabla A e^{i\omega S^+/\varepsilon}] \\ &\quad + 2(\nabla\Phi^\perp)^2 [S_u^- B_u e^{i\omega S^-/\varepsilon}]_{\hat{\kappa}} J. \end{aligned}$$

Hence, in view of (C.0.27) we can conclude that for $\kappa = k(u,v)$

$$\begin{aligned} v_A \cdot \nabla_t A &= \nabla S^+ \cdot \nabla A \\ \hat{w}_B &= 2(\nabla \Phi^\perp)^2 \hat{S}_u^- \end{aligned}$$

and similarly that for $\kappa = \hat{\kappa}(k(u,v);u,v)$

$$\begin{aligned} v_B \cdot \nabla_t B &= \nabla S^- \cdot \nabla B \\ \check{w}_A &= 2(\nabla \Phi^\perp)^2 \check{S}_u^+, \end{aligned}$$

which is (C.0.9) and (C.0.10). From,

$$\nabla A = A_u \nabla \Phi^\perp + A_v \nabla \Phi$$

we find that

$$\begin{aligned} v_{A,1} &= \nabla S^+ \nabla \Phi^\perp \\ v_{A,2} &= \nabla S^+ \nabla \Phi. \end{aligned}$$

Finally, note that if $v(x,z) = z$ then for $\kappa = k(u,v)$

$$\begin{aligned} v_A &= \nabla S^+ \\ \hat{v}_B &= \widehat{\nabla S^-}. \end{aligned} \tag{C.0.29}$$

Appendix D

Transport equations and stabilization.

D.1 The transport equations for the amplitudes.

In formulating the transport equations of Chapter 2 we sought to eliminate terms with fast lateral variation such that lateral coupling terms that are formally small are indeed higher order corrections terms. In this section we show that, to the extent possible, fast laterally varying terms have been eliminated and how the reduced transport equations introduced in Section 2.7.5 follows from our formulation.

In the purely layered case we showed, in Appendix E.3, the pulse stabilization result by an invariant imbedding argument. In Section D.2 we generalize this analysis to the locally layered case as described by the unreduced transport equations.

D.1.1 Integral expression for the pressure.

For brevity of notation we consider the case with one horizontal spatial dimension and consider the model

$$\rho\, u_t + \nabla p \;=\; F_\varepsilon(x,z,t) \tag{D.1.1}$$

$$K_\varepsilon^{-1}(x,z)\ p_t + \nabla \cdot u \ = \ 0,$$

with $u(x,z,t)$ and $p(x,z,t)$ being the acoustic velocity and pressure. The density and compliance are modeled by

$$\begin{aligned} \rho(x,z) &\equiv \rho_0 \\ K_\varepsilon^{-1}(x,z) &= \begin{cases} K_0^{-1} & z \in (-\infty, 0] \\ K_1^{-1}(x,z)(1+\nu(z/\varepsilon^2)) & z \in (0,\infty) \end{cases}, \end{aligned} \tag{D.1.2}$$

where the mean K_1^{-1} is a smooth and positive function. The random medium fluctuations are denoted ν. Here we assume that they are a function of depth only. In Appendix C we show that the more general case where the fluctuations are functions of level curves Φ can be transformed to the above model type by a change of variables.

Recall the expression for the pressure

$$p(x,z,t) \ = \ \int_{-\infty}^{\infty} h(\omega) \int_{-\infty}^{\infty} [A\ e^{i\omega S^+/\varepsilon} + B\ e^{i\omega S^-/\varepsilon}] d\kappa e^{-i\omega t/\varepsilon} d\omega \tag{D.1.3}$$

with $h(\omega)$ being defined by the source pulse and where $S^\pm$ solves the Eiconal equation associated with the deterministic medium, see (B.0.1). We assume that in the region of interest

$$\begin{aligned} \partial_z S^+ &> \Delta > 0 \\ \partial_z S^- &< \Delta, \end{aligned} \tag{D.1.4}$$

hence, the rays are bounded away from the horizontal direction and there are no turning points. We seek an asymptotic approximation for the down-propagating part of the pressure

$$p_d(x,z,t) \;=\; \int_{-\infty}^{\infty} h(\omega) \int_{-\infty}^{\infty} A\; e^{i\omega S^+/\varepsilon} d\kappa e^{-i\omega t/\varepsilon} d\omega, \tag{D.1.5}$$

at *the point of observation* $(x,z) = (\bar{x},\bar{z})$.

D.1.2 Transformation of the transport equations.

In (D.1.3) we express the pressure as an integral over generalized plane waves parameterized by their horizontal slowness in the homogeneous halfspace; the plane waves are decomposed in terms of locally up- and down-traveling modes. Recall that the transport equations, describing how the modes interact, were obtained in Section 2.7 using a slowness mapping. In Appendix B we introduce a slowness mapping $\hat{\kappa}$ that is a slight generalization of the mapping used in Section 2.7. The main property of the generalized mapping is

$$\partial_x[S^+(x,z,\kappa) - S^-(x,z,\hat{\kappa}(\kappa;x,z))] \;=\; 0, \tag{D.1.6}$$

that is, there is no lateral variation in the phase discrepancy between the interacting up- and down-traveling modes. Recall that $\hat{f}$ and $\check{f}$ denotes respectively the function f evaluated at the slowness/inverse slowness mapping; we also use the shorthand notation $\hat{\kappa} = \hat{\kappa}(\kappa;x,z)$ and $\check{\kappa} = \check{\kappa}(\kappa;x,z) \equiv \hat{\kappa}^{-1}(\kappa;x,z)$. Using this more general slowness-mapping the transport equations can be derived as in Section 2.7, this we did explicitly in Appendix C. The transport equations then read

$$\begin{aligned} 2v_A \cdot \nabla A + \triangle S^+ A - i(\varepsilon/\omega) A_{xx} \;&=\; i\omega\gamma_1^2\nu/\varepsilon[A + \hat{B}e^{i\omega\phi/\varepsilon} J] \\ &- [w_B B_x + \triangle S^- B - i\varepsilon/\omega B_{xx}]_{\hat{\kappa}} e^{i\omega\phi/\varepsilon} J \qquad \text{(D.1.7)} \\ 2v_B \cdot \nabla B + \triangle S^- B - i(\varepsilon/\omega) B_{xx} \;&=\; i\omega\gamma_1^2\nu/\varepsilon[[\; A e^{-i\omega\phi/\varepsilon}/J]_{\check{\kappa}} + B] \\ &- [(w_A A_x + \triangle S^- A - i\varepsilon/\omega A_{xx}) e^{-i\omega\phi/\varepsilon}/J]_{\check{\kappa}} \qquad \text{(D.1.8)} \end{aligned}$$

where J is the Jacobian of the slowness mapping, $\nabla = (\partial_x, \partial_z)$ and

$$\phi \equiv \hat{S}^- - S^+. \tag{D.1.9}$$

The transport equations (D.1.7) and (D.1.8) differ from those in (2.7.12) and (2.7.13) in that the characteristic directions v_A and v_B are more generally defined. Moreover, in that the coefficients of the lateral coupling terms w_A and w_B are modified. As in Appendix B let $k(x,z)$ be the slowness that at location (x,z) is associated with a ray going through also the point of observation, then from (C.0.29)

$$v_A|_{\kappa=k(x,z)} = \nabla S^+ \tag{D.1.10}$$

$$\hat{v}_B|_{\kappa=k(x,z)} = \nabla S^-|_{\hat{\kappa}}. \tag{D.1.11}$$

Next we define

$$b(x,z,\kappa) \equiv B(x,z,\hat{\kappa}(\kappa;x,z)) = \hat{B} \tag{D.1.12}$$

and apply the slowness mapping to (D.1.8) to obtain the modified transport equations

$$\begin{aligned} &2\ v_A \cdot \nabla A + \triangle S^+ A - i(\varepsilon/\omega) A_{xx} \\ &\quad = \ i\omega\gamma_1^2 \nu/\varepsilon [A + be^{i\omega\phi/\varepsilon} J] + \mathcal{L}_b(b) e^{i\omega\phi/\varepsilon} \end{aligned} \tag{D.1.13}$$

$$\begin{aligned} &2\ v_b \cdot \bar{\nabla} b + \triangle \hat{S}^- b - i(\varepsilon/\omega)[b_{xx} + q_2 b_\kappa + 2q b_{\kappa x} + q^2 b_{\kappa\kappa}] \\ &\quad = \ i\omega\gamma_1^2 \nu/\varepsilon [Ae^{-i\omega\phi/\varepsilon}/J + b] + \mathcal{L}_A(A) e^{-i\omega\phi/\varepsilon} \end{aligned} \tag{D.1.14}$$

with $\bar{\nabla} \equiv (\partial_x, \partial_z, \partial_\kappa)$ and $\check{\kappa} = \check{\kappa}(\kappa;x,z)$. Here

$$q \equiv \check{\kappa}_x(\kappa_0;x,z)|_{\kappa_0=\hat{\kappa}(\kappa;x,z)}$$

$$
\begin{aligned}
q_2 &\equiv \check{\kappa}_{xx}(\kappa_0; x, z)|_{\kappa_0=\hat{\kappa}(\kappa;x,z)} \\
q_3 &\equiv \check{\kappa}_z(\kappa_0; x, z)|_{\kappa_0=\hat{\kappa}(\kappa;x,z)} \\
v_b &= < \hat{v}_B, q\hat{v}_{B,1} + q_3\hat{v}_{B,2} > \\
\mathcal{L}_A(A) &= -[w_A A_x + \triangle S^- A - i\varepsilon/\omega A_{xx}]/J \\
\mathcal{L}_b(b) &= -[\hat{w}_B b_x + q\hat{w}_B b_\kappa + \triangle \hat{S}^- b - i(\varepsilon/\omega)\{b_{xx} + q_2 b_\kappa + 2qb_{\kappa x} + q^2 b_{\kappa\kappa}\}]J
\end{aligned}
$$

with $v_{B,i}$ being the i'th component of v_B. The amplitude A, the locally down-propagating field, is given at the surface $z = 0$, see Appendix E.1. There is no source in the halfspace $z > 0$ and the medium is at rest initially so we obtain the boundary conditions

$$
A|_{z=0} = 1 \tag{D.1.15}
$$

$$
\lim_{z\to\infty} b = 0, \tag{D.1.16}
$$

corresponding to (2.6.11). We point out two important aspects of the above formulation.

First, from (B.0.2) it follows that

$$
\phi = \phi(z, \kappa).
$$

Hence, there is nothing in the above problem formulation which is rapidly varying with respect to x, and the amplitudes A & b do not carry any rapid deterministic lateral phase modulation. The phase modulation with respect to x caused by the random term on the right hand side in (D.1.13,D.1.14) will be small since ν is zero-mean and rapidly varying in depth only.

Second, for $\kappa = k(x, z)$

$$q = 0 \tag{D.1.17}$$

$$v_A = \nabla S^+, \tag{D.1.18}$$

see (B.0.5, C.0.29). Consider the ray from the surface to the point of observation that is defined by ∇S^+ for $\kappa \equiv \kappa^*$. On this ray $k(x,z) \equiv \kappa^*$. In view of (D.1.17) and (D.1.18) we find that the governing equation for the amplitude A at $\kappa = \kappa^*$ essentially decouples and becomes autonomous in the deterministic case. The resulting governing equation coincides with the first order transport equation of geometrical optics, the high frequency approximation. Note also that the random coupling terms are defined similarly as in the layered case discussed in Chapter 2.

D.1.3 Comments on the model and the analysis.

We now turn to comment on how to properly deal with the transport equations. We begin by observing that the expression (D.1.3) is formal because the integrals with respect to the slowness is not well defined. For large values of κ the phase S^+ becomes complex and the slowness mapping is not defined. Physically this corresponds to evanescent or rapidly decaying modes. To avoid having to deal with these modes we shall assume that the source is supported in a neighborhood of the central ray slowness, $\bar{\kappa}$. That is h in (D.1.3) is given by

$$h = h(\omega, \kappa)$$

with h smooth and supported in a neighborhood of $\kappa = \bar{\kappa}$. In Appendix B we showed the existence of a smooth slowness mapping in a neighborhood of the central ray. However, in the transport equations we use the mapping as if it where globally defined in x and z. To do this we need to assume that the deterministic medium can be imbedded, *vertically* and *horizontally*, in a smooth medium such that the mapping is globally defined. Thus making use of hyperbolicity of the original problem. Let

$\tilde{\gamma}_1$ be the slowness of the imbedded problem, then $\tilde{\gamma}_1 \equiv \gamma_1$ in a neighborhood of the central ray.

Note that in the layered case the stabilization of the pulse shape was only shown using an invariant imbedding argument. That is, the boundary value problem defined by the transport equations is converted to an initial value problem. In Appendix D.2 we generalize this analysis to the locally layered case by introducing reflection and transmission operators. In the analysis presented there we do not derive higher order correction terms. For the simpler problems defined by the deterministic high frequency approximation and averaging of stochastic ordinary differential equations higher order correction terms are complicated to derive and rarely used in practise. We consider higher order correction terms of the more complicated wave propagation problem at hand to be of limited interest and do not pursue them.

The argument in Appendix D.2 requires the above mentioned assumptions on the existence of a globally defined slowness mapping. To carry out a complete analysis of the problem we need to introduce a class of smooth test functions that localize the problem to a neighborhood of the central ray. Such a weak analysis is carried out for instance in [37]. We shall not pursue this analysis here.

D.1.4 Reduced transport equations and pulse shaping.

Before we go to the invariant imbedding argument in the next section we show how the approximate transport equations we introduced in Section 2.7.5 follows from (D.1.13) and (D.1.14).

As mentioned above nothing in the problem formulation (D.1.13) and (D.1.14) is rapidly varying with respect to the lateral dimension x. This we obtained by the particular choice of ansatz and phase mapping. Hence, we can consider the x differentiated terms to be $O(1)$ terms.

Recall first that in the deterministic case the transmitted pressure is found as an integral over the generalized plane wave modes, the modes being evaluated at the point of observation. To leading order the amplitudes of the modes are found in

terms of ordinary differential equations evolving along the rays going into the point of observation. Along these rays $k(x,z)$ is constant and equal to the horizontal slowness associated with this ray for $z \leq 0$.

For the purpose of this illustration we ignore some lower order terms and consider

$$\begin{aligned} 2\ v_A \cdot \nabla A + \triangle S^+ A &= i\omega\gamma_1^2\nu/\varepsilon[A + be^{i\omega\phi/\varepsilon}J] \\ &\quad + [qc_1 b_\kappa + \varepsilon q^2 c_2 b_{\kappa\kappa}]e^{i\omega\phi/\varepsilon} \\ 2\ v_b \cdot \bar{\nabla} b + \triangle \hat{S}^- b - i(\varepsilon/\omega)q^2 b_{\kappa\kappa} &= i\omega\gamma_1^2\nu/\varepsilon[Ae^{-i\omega\phi/\varepsilon}/J + b], \end{aligned}$$

using c_i as a generic symbol for a smooth, ε independent, function. Let s denote the arc length parameter along the characteristic path defined by the direction ∇S^+ and call the path segment starting at the surface for Γ^+. We write the transport equations as

$$\begin{aligned} A_s &= g_1 A + i\omega\gamma_1\nu/(2\varepsilon)be^{i\omega\phi/\varepsilon}J \\ &\quad + [qc_3 b_\kappa + \varepsilon q^2 c_4 b_{\kappa\kappa}]e^{i\omega\phi/\varepsilon} \\ \mathcal{L}(b) &= i\omega\gamma_1\nu e^{-i\omega\phi/\varepsilon}/(2J\varepsilon)A \end{aligned}$$

with

$$g_1 = -(\triangle S^+/2\gamma_1) + i\omega\gamma_1\nu/(2\varepsilon).$$

Next we evaluate this expression at $\kappa = k(x,z)$. Consider the geometrical optics paths, defined by the directions ∇S^+, that go through the point of observation. On these paths the value of $k(x,z)$ is constant. Then we get, since $q|_{\kappa=k} = 0$,

$$A_s = g_1 A + i\omega\gamma_1\nu/(2\varepsilon)be^{i\omega\phi/\varepsilon}J$$

$$\mathcal{L}(b) \;=\; i\omega\gamma_1\nu e^{-i\omega\phi/\varepsilon}/(2J\varepsilon)A$$

and

$$A \;=\; 1+\int_{\Gamma_+}[g_1A+i\omega\gamma_1\nu/(2\varepsilon)e^{i\omega\phi/\varepsilon}J\mathcal{L}^{-1}[i\omega\gamma_1\nu e^{-i\omega\phi/\varepsilon}/(2J\varepsilon)A]]ds.$$

The operator $\mathcal{L}$ is essentially the Schrödinger operator with a small coupling term. Recall that the statistical interaction is a local phenomenon. If we 'freeze' the parameters of the operator $\mathcal{L}$ at $\kappa = k(x,z)$ it is easily inverted since it then simply becomes a directional derivative. Using this local approximation for $\mathcal{L}$ we find

$$A \;=\; 1+\int_{\Gamma_+}[g_1A+i\omega\gamma_1\nu/(2\varepsilon)e^{i\omega\phi/\varepsilon}J\int_{\Gamma_-}g_2[i\omega\gamma_1\nu e^{-i\omega\phi/\varepsilon}/(2J\varepsilon)A]]duds$$

with g_2 being unity at the 'source-point' and u & s being arc length parameters along the integration paths. Note that this expression for the amplitude A corresponds to the one that derives from (2.7.18). The tangent of the path Γ^- at the terminal point is moreover the direction ∇S^-. This is the only aspect of the path Γ^- which is important for pulse shaping.

Thus the reduced equations are associated with the right leading order expression for the *pulse front*. It follows that the equations (2.7.18) should be interpreted as representing the unreduced amplitude equations in the weak sense; they are associated with the same pulse shaping. Next, in the following section, we confirm this explicitly by a multiple scales analysis of reflection and transmission operators.

D.2 Invariant imbedding in locally layered case.

By a multiple scales argument using invariant imbedding we derive the pulse stabilization result in the locally layered strongly heterogeneous case.

To this effect define the stochastic process

$$X(t) \;=\; \int_{-\infty}^{\infty} h(\omega) \int_{-\infty}^{\infty} \bar{A}\; e^{-\omega^2 D}\; e^{i\omega S^+/\varepsilon} e^{i\omega\chi_\varepsilon/\varepsilon} d\kappa e^{-i\omega t/\varepsilon} d\omega \qquad \text{(D.2.1)}$$

with $\bar{A}$ being the amplitude term in the deterministic case. The right hand side of (D.2.1) is evaluated at the point of observation. Moreover

$$\begin{aligned} D \;&=\; D(\bar{x},\bar{z},\kappa) \;=\; (l/4)\int_{\Gamma(\bar{x},\bar{z},\kappa)} \gamma_1^2\; \cos(\theta)^{-1}\; du \\ \chi_\varepsilon \;&=\; \chi_\varepsilon(\bar{x},\bar{z},\kappa) \;=\; \int_{\Gamma(\bar{x},\bar{z},\kappa)} \gamma_1 \nu/2\; du \\ l \;&\equiv\; \int_0^\infty E[\nu(0)\nu(s)]\; ds, \\ \gamma_1 \;&=\; \gamma_1(x,z) \;=\; \sqrt{K_1^{-1}(x,z)\rho} \end{aligned} \qquad \text{(D.2.2)}$$

with u being arc-length along the path Γ and $\cos(\theta(x,z))$ the angle between the tangent of Γ and the vertical direction. The parameter γ_1 is the slowness of the deterministic or 'effective' medium. The path $\Gamma = \Gamma(x,z,\kappa)$ is the ray path from the surface $z = 0$ to the point (x,z) that is associated with the slowness κ. Upon applying a stationary phase argument, as in Chapter 2, the stabilization of the pulse shape to the O'Doherty-Anstey limiting pulse shape follows if we can show

$$p_d \;\sim\; X \qquad as \;\; \varepsilon \downarrow 0 \qquad \text{(D.2.3)}$$

with p_d given in (D.1.5). Define for $t_1 < t_2 < \cdots < t_N$

$$I \;=\; \sum_{n=1}^{N} [X(t_n) - p_d(\bar{x},\bar{z},t_n)]^2. \qquad \text{(D.2.4)}$$

Then

$$
\begin{aligned}
E[I] &= \int_{-\infty}^{\infty}\int_{-\infty}^{\infty}\sum_{n=1}^{N} e^{-i(\omega_1+\omega_2)t_n/\varepsilon} h(\omega_1)h(\omega_2) \\
&\quad \int_{-\infty}^{\infty}\int_{-\infty}^{\infty} e^{i(\omega_1 S_1^+ + \omega_2 S_2^+)/\varepsilon} E[(\bar{A}_1\ e^{-\omega_1^2 D_1}\ e^{i\omega_1\chi_{\varepsilon,1}/\varepsilon} - A_1) \\
&\quad (\bar{A}_2\ e^{-\omega_2^2 D_2}\ e^{i\omega_2\chi_{\varepsilon,2}/\varepsilon} - A_2)] d\kappa_1 d\kappa_2 d\omega_1 d\omega_2
\end{aligned} \tag{D.2.5}
$$

with subscript i indicating that the function is evaluated at (κ_i, ω_i). We seek to show that $E[I] \sim 0$, this follows from

$$
\begin{aligned}
E[A_1 e^{i\omega_2\chi_{\varepsilon,2}/\varepsilon}] &\sim \bar{A}_1\ e^{-\omega_1^2 D_1}\ E[e^{i(\omega_1\chi_{\varepsilon,1}+\omega_2\chi_{\varepsilon,2})/\varepsilon}] \\
E[A_1 A_2] &\sim \bar{A}_1\ e^{-\omega_1^2 D_1}\ \bar{A}_2\ e^{-\omega_2^2 D_2}\ E[e^{i(\omega_1\chi_{\varepsilon,1}+\omega_2\chi_{\varepsilon,2})/\varepsilon}] \quad as\ \ \varepsilon \downarrow 0,
\end{aligned}
$$

where

$$
\begin{aligned}
D_i &= D(\bar{x}, \bar{z}, \kappa_i) \\
\chi_{\varepsilon,i} &= \chi_\varepsilon(\bar{x}, \bar{z}, \kappa_i).
\end{aligned}
$$

By applying the limit result (D.3.13) of Appendix D.3 we find that

$$
E[e^{i(\omega_1\chi_{\varepsilon,1}+\omega_2\chi_{\varepsilon,2})/\varepsilon}] \sim e^{-l\int_0^{\bar{z}}(\omega_1[\gamma_1/(2cos(\theta))]_{\Gamma_1(u)}+\omega_2[\gamma_1/(2cos(\theta))]_{\Gamma_2(u)})^2 du} \quad as\ \ \varepsilon \downarrow 0
$$

with $\Gamma_i = \Gamma(\bar{x}, \bar{z}, \kappa_i)$. We therefore need to show

$$
\begin{aligned}
E[A_1 e^{i\omega_2\chi_{\varepsilon,2}}] &\sim e^{-\int_{\Gamma_1}\triangle S^+/(2\gamma_1)\ du}\ e^{-l\omega_1^2/4\int_{\Gamma_1}\gamma_1^2/\cos(\theta)\ du} \\
&\quad \times e^{-l\int_0^{\bar{z}}(\omega_1[\gamma_1/(2cos(\theta))]_{\Gamma_1(u)}+\omega_2[\gamma_1/(2cos(\theta))]_{\Gamma_2(u)})^2 du} \\
E[A_1 A_2] &\sim e^{-\int_{\Gamma_1}\triangle S^+/(2\gamma_1)\ du}\ e^{-\int_{\Gamma_2}\triangle S^+/(2\gamma_1)\ du} \\
&\quad \times e^{-l\omega_1^2/4\int_{\Gamma_1}\gamma_1^2/\cos(\theta)\ du}\ e^{-l\omega_2^2/4\int_{\Gamma_2}\gamma_1^2/\cos(\theta)\ du}
\end{aligned} \tag{D.2.6}
$$

$$\times e^{-l\int_0^{\bar{z}}(\omega_1[\gamma_1/(2cos(\theta))]_{\Gamma_1(u)}+\omega_2[\gamma_1/(2cos(\theta))]_{\Gamma_2(u)})^2 du} \quad as \quad \varepsilon \downarrow 0. \tag{D.2.7}$$

In doing this we will make use of the slowness mapping derived in Appendix B, which is a generalization of the slowness mapping introduced in Section 2.7.3. Above and in the sequel we will most often suppress the ω dependence of the involved functions.

D.2.1 The transmission and reflection operators.

The transport equations (D.1.13) and (D.1.14) define a complicated boundary value problem. In order to apply limit results pertaining to Markov processes and initial value problems we now introduce transmission and reflection operators. The appropriate limit result for these is found in Section D.3. Let them be defined by

$$A(\bar{z},x,\kappa) = \int\int t(z,x,\kappa,s,v)A(z,s,v)dsdv \tag{D.2.8}$$

$$b(z,x,\kappa) = \int\int r(z,x,\kappa,s,v)A(z,s,v)dsdv. \tag{D.2.9}$$

Write (D.1.13,D.1.14) as

$$\begin{aligned} A_z &= w_1A_x + h_1A + \varepsilon^{-1}i\omega\nu[h_2A + h_3be^{i\omega\phi/\varepsilon}] + i\varepsilon/\omega h_4A_{xx} + \mathcal{L}_1(b)e^{i\omega\phi/\varepsilon} \\ b_z &= w_2b_x + w_3b_\kappa + h_5b + \varepsilon^{-1}i\omega\nu[h_6Ae^{-i\omega\phi/\varepsilon} + h_7b] + i\varepsilon/\omega\mathcal{L}_2(b) + \mathcal{L}_3(A)e^{-i\omega\phi/\varepsilon} \end{aligned}$$

with

$$\begin{aligned} \mathcal{L}_1(b) &= -[\hat{w}_Bb_x + q\hat{w}_Bb_\kappa + \triangle\hat{S}^-b - i(\varepsilon/\omega)\{b_{xx} + q_2b_\kappa + 2qb_{\kappa x} + q^2b_{\kappa\kappa}\}]J/(2v_{A,2}) \\ \mathcal{L}_2(b) &= [b_{xx} + q_2b_\kappa + 2qb_{\kappa x} + q^2b_{\kappa\kappa}]/(2v_{b,2}) \\ \mathcal{L}_3(A) &= -[w_AA_x + \triangle S^-A - i\varepsilon/\omega A_{xx}]/(2v_{b,2}J). \end{aligned}$$

It follows that

$$
\begin{aligned}
t_z(z,x,\kappa,s,v) \;&=\; \partial_s[w_1(z,s,v)t(z,x,\kappa,s,v)] - [h_1(z,s,v) \qquad \text{(D.2.10)}\\
&\quad + \varepsilon^{-1}i\omega\nu h_2(z,s,v)]t(z,x,\kappa,s,v) - i\varepsilon/\omega\partial_s^2[h_4(z,s,v)t(z,x,\kappa,s,v)]\\
&\quad - \int\int [\varepsilon^{-1}i\omega\nu h_3(z,s_1,v_1)t(z,x,\kappa,s_1,v_1)r(z,s_1,v_1,s,v)\\
&\quad + t(z,x,\kappa,s_1,v_1)\mathcal{L}_1(z,s_1,v_1)(r(z,s_1,v_1,s,v))]e^{i\omega\phi(z,v_1)/\varepsilon}ds_1dv_1\\
r_z(z,x,\kappa,s,v) \;&=\; \partial_s[w_1(z,s,v)r(z,x,\kappa,s,v)]\\
&\quad + [w_2(z,x,\kappa)\partial_x + w_3(z,x,\kappa)\partial_\kappa]r(z,x,\kappa,s,v)\\
&\quad - [h_1(z,s,v) - h_5(z,x,\kappa) + \varepsilon^{-1}i\omega\nu(h_2(z,s,v) - h_7(z,x,\kappa))]r(z,x,\kappa,s,v)\\
&\quad - i\varepsilon/\omega\partial_s^2[h_4(z,s,v)r(z,x,\kappa,s,v)] + i\varepsilon/\omega\mathcal{L}_2(z,x,\kappa)(r(z,x,\kappa,s,v))\\
&\quad + [\varepsilon^{-1}i\omega\nu h_6 + \mathcal{L}_3](z,x,\kappa)(\delta(x-s)\delta(\kappa-v))e^{-i\omega\phi(z,v)/\varepsilon}\\
&\quad - \int\int [\varepsilon^{-1}i\omega\nu h_3(z,s_1,v_1)r(z,x,\kappa,s_1,v_1)r(z,s_1,v_1,s,v)\\
&\quad + r(z,x,\kappa,s_1,v_1)\mathcal{L}_1(z,s_1,v_1)(r(z,s_1,v_1,s,v))]e^{i\omega\phi(z,v_1)/\varepsilon}ds_1dv_1.
\end{aligned}
$$

We modified slightly the notation for the operators $\mathcal{L}_i$ so as to explicitly indicate with respect to which variables they are acting. To apply the limit result of Appendix D.3 we need a formulation with deterministic initial values. From hyperbolicity of the original problem we can use imbedding and let the medium be deterministic for $z > L$ say and seek a formulation with deterministic initial values evaluated at depth $z = L$. We obtain this by equating to zero the source terms in the t equation for $z > \bar{z}$. That is $\mathcal{L}_\infty \mapsto \mathcal{L}_\infty{}^* \equiv \mathcal{L}_\infty I_{z<\bar{z}}$ and $\nu \mapsto \nu^* \equiv \nu I_{z<\bar{z}}$, with I_S being the indicator function on the set S (in the sequel we suppress the $*$). Observe that the equation for r is *autonomous*. Thus, we have arrived at a formulation with deterministic initial values at depth $z = L >> \bar{z}$ that derive from the 'natural initial condition' at depth $z = \bar{z}$ for t and the radiation condition for r. We shall not need explicit expressions for these initial values. The initial condition, evaluated at $z = \bar{z}$, for the transmission operator is

$$
t(\bar{z},x,\kappa,s,v) \;=\; \delta(x-s)\delta(\kappa-v). \qquad \text{(D.2.11)}
$$

Next we derive equations for the moments needed in order to verify (D.2.6) and (D.2.7).

D.2.2 The pulse shape.

From (D.2.10) we find the governing equation for $\tau^0(z,x,\kappa,s,v) = E[t(z,x,\kappa,s,v)]$ using the limit result (D.3.13) of Appendix D.3.

$$\begin{aligned}
\tau^0_z(z,x,\kappa,s,v) &= \partial_s[w_1(z,s,v)\tau^0(z,x,\kappa,s,v)] \qquad \text{(D.2.12)}\\
&\quad - h_1(z,s,v)\tau^0(z,x,\kappa,s,v) - i\varepsilon/\omega\partial_s^2[h_4(z,s,v)\tau^0(z,x,\kappa,s,v)]\\
&\quad + \int\int \mathcal{L}_1(z,s_1,v_1;2)\tau^1(z,x,\kappa,s_1,v_1;s_1,v_1,s,v)e^{i\omega\phi(z,v_1)/\varepsilon}ds_1dv_1\\
&\quad + \omega^2 l[h_2^2(z,s,v) - h_3(z,s,v)h_6(z,s,v)]\tau^0(z,x,\kappa,s,v)\\
&\quad + \omega^2 l\int\int h_3(z,s_1,v_1)(2h_2(z,s,v) + h_2(z,s_1,v_1) - h_7(z,s_1,v_1))\\
&\quad \times \tau^1(z,x,\kappa,s_1,v_1;s_1,v_1,s,v)e^{i\omega\phi(z,v_1)/\varepsilon}ds_1dv_1\\
&\quad + 2\omega^2 l\int\int\int\int h_3(z,s_1,v_1)h_3(z,s_2,v_2)\\
&\quad \times \tau^2(z,x,\kappa,s_1,v_1;s_1,v_1,s_2,v_2;s_2,v_2,s,v)e^{i\omega(\phi(z,v_1)+\phi(z,v_2))/\varepsilon}ds_1dv_1ds_2dv_2\\
\tau^0(\bar{z},x,\kappa,s,v) &= \delta(x-s)\delta(\kappa-v)
\end{aligned}$$

where we used the notation

$$\begin{aligned}
&\tau^n(z,x,\kappa,s,v;x_1,\kappa_1,s_1,v_1;\cdots;x_n,\kappa_n,s_n,v_n) = \qquad \text{(D.2.13)}\\
&\quad E[t(z,x,\kappa,s,v)r(z,x_1,\kappa_1,s_1,v_1)\cdots r(z,x_n,\kappa_n,s_n,v_n)].
\end{aligned}$$

Also the notation $\mathcal{L}_1(z,s,v;n)$ indicates that the operator $\mathcal{L}_1$ acts on the n'th set of variables only. In the deterministic case it follows from the high frequency (geometrical optics) approximation that

$$t(z,x,\kappa,s,v) = \tilde{t}(z,x,\kappa,s,v)\delta(s-\bar{s}(z,x,\kappa))\delta(v-\kappa) + O(\varepsilon)$$

$$r(z, x, \kappa, s, v) \;=\; O(\varepsilon).$$

The quantity $\bar{s}(z, x, \kappa)$ is defined as follows: Consider the geometrical optics ray going through the point $(\bar{z}, x)$ that is associated with the slowness κ. Then $\bar{s}(z, x, \kappa)$ is the lateral location for this ray at depth z. As before, with geometrical optics rays we refer to the rays associated with the solution of the Eiconal of the deterministic problem with plane-waves, parameterized by the horizontal slowness κ, impinging from the halfspace $z < 0$. The interpretation of the above is that the first order transport equations determine the amplitude in terms of ordinary differential equations evolving along the characteristic rays. There is no coupling between different generalized plane waves or 'slowness-modes'. Finally, the reflected field will be small since the background medium is smooth. We thus make an ansatz regarding the higher order moments in $(D.2.13)$. For $n \geq 1$

$$\tau^n \;=\; O(\varepsilon) \tag{D.2.14}$$

and, moreover, τ^n contains no rapid phase modulation in $\{\kappa_j, v_j\}$ for $j \geq 1$. We verify this in Appendix D.2.4. Therefore, to leading order, the governing equation for τ^0 decouples and becomes (retaining the notation)

$$\begin{aligned} \tau^0_z(z, x, \kappa, s, v) \;&=\; \partial_s[w_1(z, s, v)\tau^0(z, x, \kappa, s, v) \\ &+\{-h_1(z, s, v) + \omega^2 l[h_2^2(z, s, v) - h_3(z, s, v)h_6(z, s, v)]\}\tau^0(z, x, \kappa, s, v)]. \end{aligned} \tag{D.2.15}$$

In the layered case, with the lateral derivatives vanishing, (D.2.15) corresponds to (E.3.8). Note that in (E.3.8) $h_2 = 0$ since there we carried out a random time centering. For (x, κ, v) fixed, $(z, s) = (z, \bar{s}(z, x, v)$ are characteristic paths associated with (D.2.15). The equation (D.2.15) entails the following governing equation for the leading order part of the mean amplitude $a = E[A]$

$$a_z - w_1 a_x = h_1 a - \omega^2 l[h_2^2 - h_3 h_6]a. \qquad \text{(D.2.16)}$$

This can be shown by deriving the governing equation for the transmission operator associated with (D.2.16). It follows from (D.2.16) that

$$\begin{aligned} E[[A_1](\bar{x},\bar{z},\kappa_1,\omega_1)] \sim\ & e^{-\int_{\Gamma_1} \triangle S^+/(2\gamma_1)\ du}\ e^{-l\omega_1^2/4 \int_{\Gamma_1} \gamma_1^2/\cos(\theta)\ du} \\ & \times e^{-l\int_0^{\bar{z}} (\omega_1[\gamma_1/(2cos(\theta))]_{\Gamma_1(s)})^2 ds}. \end{aligned}$$

with u being arc length along the path of integration and θ the angle between the tangent to this path and the vertical. The path Γ_1 is the geometrical optics ray associated with κ_1 that goes through the point of observation $(\bar{x},\bar{z})$. In order to obtain this expression we made use of the fact that the geometrical optics paths going through $(\bar{x},\bar{z})$ are characteristic paths of (D.2.16) and also of (B.0.4) and (C.0.29). The criterion (D.2.6) concerns $E[A_1 e^{i\omega_2 \chi_{\varepsilon,2}/\varepsilon}]$ rather than $E[A_1]$. To obtain an estimate of the former quantity we introduce $\tilde{A} = Ay$ and $\tilde{b} = by$ as the new states of interest, with

$$\begin{aligned} y &= y(z) = e^{i\omega_2 \chi_\varepsilon(\bar{s},z,\kappa_2)/\varepsilon} \\ \chi_\varepsilon(\bar{s},z,\kappa_2) &= \int_{\Gamma(\bar{s},z,\kappa_2)} \gamma_1 \nu/2\ du \end{aligned}$$

with $\bar{s} = \bar{s}(z,\bar{x},\kappa_2)$ and with the operators now being defined by

$$\begin{aligned} \tilde{A}(\bar{z},x,\kappa) &= \int\int t(z,x,\kappa,s,v)\tilde{A}(z,s,v)dsdv \\ \tilde{b}(z,x,\kappa) &= \int\int r(z,x,\kappa,s,v)\tilde{A}(z,s,v)dsdv. \end{aligned}$$

note that the initial conditions for these are unchanged. The operator equations are

changed only in that

$$\omega h_2(z,x,\kappa) \mapsto \omega h_2(z,x,\kappa) + \omega_2 h_2(z,\bar{s}(z,\bar{x},\kappa_2),\kappa_2)$$
$$\omega h_7(z,x,\kappa) \mapsto \omega h_7(z,x,\kappa) + \omega_2 h_2(z,\bar{s}(z,\bar{x},\kappa_2),\kappa_2).$$

We then find

$$\begin{aligned} E[[A_1 e^{i\omega_2 \chi_{\varepsilon,2}}](\bar{x},\bar{z},\kappa_1,\omega_1)] \quad &\sim \quad e^{-\int_{\Gamma_1} \triangle S^+/(2\gamma_1)\ du}\ e^{-l\omega_1^2/4 \int_{\Gamma_1} \gamma_1^2/\cos(\theta)\ du} \\ &\quad \times e^{-\int_0^{\bar{z}} (\omega_1 [\gamma_1/(2cos(\theta))]_{\Gamma_1(s)} + \omega_2 [\gamma_1/(2cos(\theta))]_{\Gamma_2(s)})^2 ds} \qquad as \ \ \varepsilon \downarrow 0 \end{aligned}$$

which is (D.2.6).

D.2.3 Stabilization to the pulse shape.

Consider now the criterion (D.2.7). This will be verified by a procedure similar to the one above. We need to approximate

$$\begin{aligned} &E[A(\bar{z},\bar{x},\kappa_1,\omega_1)A(\bar{z},\bar{x},\kappa_2,\omega_2)] \\ &= E[\int\int t(z,\bar{x},\kappa_1,s_1,v_1,\omega_1)A(z,s_1,v_1,\omega_1)ds_1 dv_1 \\ &\quad \times \int\int t(z,\bar{x},\kappa_2,s_2,v_2,\omega_2)A(z,s_2,v_2,\omega_2)ds_2 dv_2] \\ &= \int\int\int\int E[t(0,\bar{x},\kappa_1,s_1,v_1,\omega_1)t(0,\bar{x},\kappa_2,s_2,v_2,\omega_2)]ds_1 dv_1 ds_2 dv_2. \end{aligned}$$

making the ω dependence explicit since in (D.2.7) we evaluate the amplitudes at two different frequencies. For brevity of notation though, we will partly suppress the ω dependence. We seek an equation for

$$\tau^0(z,x_1,\kappa_1,s_1,v_1;x_2,\kappa_2,s_2,v_2) \quad \equiv \quad E[t(z,x_1,\kappa_1,s_1,v_1)t(z,x_2,\kappa_2,s_2,v_2)].$$

By another application of the limit result (D.3.13) it follows that

$$
\begin{aligned}
&\tau_z^0(z,x_1,\kappa_1,s_1,v_1;x_2,\kappa_2,s_2,v_2) \qquad\qquad (D.2.17)\\
&= \sum_{j=1}^{2}\{\partial_{s_j}[w_1(z,s_j,v_j)\tau^0(z,x_1,\kappa_1,s_1,v_1;x_2,\kappa_2,s_2,v_2)]\\
&\quad - h_1(z,s_j,v_j)\tau^0(z,x_1,\kappa_1,s_1,v_1;x_2,\kappa_2,s_2,v_2)\\
&\quad - i\varepsilon/\omega_j\partial_{s_j}^2[h_4(z,s_j,v_j)\tau^0(z,x_1,\kappa_1,s_1,v_1;x_2,\kappa_2,s_2,v_2)]\\
&\quad - \int\int \mathcal{L}_1(z,s,v;3,\omega_j)\\
&\quad \times \tau^1(z,x_J,\kappa_J,s_J,v_J;x_j,\kappa_j,s,v;z,s,v,s_j,v_j)e^{i\omega_j\phi(z,v)/\varepsilon}dsdv\}\\
&\quad + l(\sum_{j=1}^{2}\omega_j h_2(z,s_j,v_j))^2\tau^0(z,x_1,\kappa_1,s_1,v_1;x_2,\kappa_2,s_2,v_2)\\
&\quad - l\sum_{j=1}^{2}\{\omega_j^2 h_3(z,s_j,v_j)h_6(z,s_j,v_j)\tau^0(z,x_1,\kappa_1,s_1,v_1;x_2,\kappa_2,s_2,v_2)\\
&\quad - \int\int h_3(z,s,v)[2\omega_j^2 h_2(z,s_j,v_j)+\omega_j^2 h_2(z,s,v)-\omega_j^2 h_7(z,s,v)\\
&\quad -2\omega_j\omega_J h_2(z,s_J,v_J)]\\
&\quad \times\tau^1(z,x_J,\kappa_J,s_J,v_J;x_j,\kappa_j,s,v;s,v,s_j,v_j)e^{i\omega_j\phi(z,v)/\varepsilon}dsdv\\
&\quad - \int\int\int\int \omega_j h_3(z,s,v)[\ 2\omega_j^2 h_3(z,\tilde{s},\tilde{v})\\
&\quad \times\tau^2(z,x_J,\kappa_J,s_J,v_J;x_j,\kappa_j,s,v;s,v,\tilde{s},\tilde{v};\tilde{s},\tilde{v},s_j,v_j)e^{i\omega_j(\phi(z,v)+\phi(z,\tilde{v}))/\varepsilon}\\
&\quad +\omega_J h_3(z,\tilde{s},\tilde{v})\tau^2(z,x_j,\kappa_j,s,v;x_J,\kappa_J,\tilde{s},\tilde{v};s,v,s_j,v_j;\tilde{s},\tilde{v},s_J,v_J)\\
&\quad e^{i(\omega_j\phi(z,v)+\omega_J\phi(z,\tilde{v}))/\varepsilon}\ ]dsdvd\tilde{s}d\tilde{v}\ \}
\end{aligned}
$$

with $J=3-j$ and

$$
\begin{aligned}
&\tau^n(z,x,\kappa,s,v;x_0,\kappa_0,s_0,v_0;x_1,\kappa_1,s_1,v_1;\cdots;x_n,\kappa_n,s_n,v_n) \qquad (D.2.18)\\
&= E[t(z,x,\kappa,s,v)t(z,x_0,\kappa_0,s_0,v_0)r(z,x_1,\kappa_1,s_1,v_1)\cdots t(z,x_n,\kappa_n,s_n,v_n)].
\end{aligned}
$$

We make an ansatz corresponding to (D.2.14), but now regarding the moments of the operators defined in (D.2.18). For $n\geq 1$

$$\tau^n \;=\; O(\varepsilon) \tag{D.2.19}$$

and, moreover, τ^n contains no rapid phase modulation in $\{\kappa_j, v_j\}$ for $j \geq 1$. As we point out in Section D.2.4 the ansatz (D.2.19) is valid upto a set of measure zero with respect to the ω_j. Retaining the notation for the leading order part we get by a similar argument as in the first moment case that

$$\begin{aligned}
&\tau_z^0(z, x_1, \kappa_1, s_1, v_1; x_2, \kappa_2, s_2, v_2) \qquad\qquad (D.2.20)\\
&= \sum_{j=1}^{2}\{\partial_{s_j}[w_1(z, s_j, v_j)\tau^0(z, x_1, \kappa_1, s_1, v_1; x_2, \kappa_2, s_2, v_2)]\\
&\quad - (h_1(z, s_j, v_j) + \omega_j^2 l h_3(z, s_j, v_j)h_6(z, s_j, v_j))\tau^0(z, x_1, \kappa_1, s_1, v_1; x_2, \kappa_2, s_2, v_2)\}\\
&\quad + l(\sum_{j=1}^{2}\omega_j h_2(z, s_j, v_j))^2\tau^0(z, x_1, \kappa_1, s_1, v_1; x_2, \kappa_2, s_2, v_2).
\end{aligned}$$

Recall that our objective is to estimate

$$\alpha(z, x_1, \kappa_1; x_2, \kappa_2) \;\equiv\; E[A(z, x_1, \kappa_1)A(z, x_2, \kappa_2)] \tag{D.2.21}$$

at $(z, x_1, x_2) = (\bar{z}, \bar{x}, \bar{x})$. The result (D.2.20) entails the following equation for the leading order part of α

$$\begin{aligned}
&\alpha_z - w_1(z, x_1, \kappa_1)\;\alpha_{x_1} - w_1(z, x_2, \kappa_2)\;\alpha_{x_2} \qquad\qquad (D.2.22)\\
&\quad = \; [h_1(z, x_1, \kappa_1) + h_1(z, x_2, \kappa_2)]\;\alpha\\
&\qquad - l[(\omega_1 h_2(z, x_1, \kappa_1) + \omega_2 h_2(z, x_2, \kappa_2))^2 - \omega_1^2 h_3(z, x_1, \kappa_1)h_6(z, x_1, \kappa_1)\\
&\qquad -\omega_2^2 h_3(z, x_2, \kappa_2)h_6(z, x_2, \kappa_2)]\;\alpha\\
&\alpha_{z=0} \;=\; 1.
\end{aligned}$$

Consider the paths in the 'space' (z, x_1, x_2) that go through $(\bar{z}, \bar{x}, \bar{x})$ and whose procjection on the (z, x_1) and (z, x_2) subspaces are geometrical optics rays. These are also characteristic paths associated with $D.2.22$ and on these $-w_i = S_x^+/S_z^+$, see (B.0.4). We thus finally obtain

$$\begin{aligned}\alpha(\bar{z}, \bar{x}, \kappa_1; \bar{x}, \kappa_2) \;\sim\; & e^{-\int_{\Gamma_1} \triangle S^+/(2\gamma_1)\ du}\ e^{-\int_{\Gamma_2} \triangle S^+/(2\gamma_1)\ du} \\ & \times e^{-l\omega_1^2/4 \int_{\Gamma_1} \gamma_1^2/\cos(\theta)\ du}\ e^{-l\omega_2^2/4 \int_{\Gamma_2} \gamma_1^2/\cos(\theta)\ du} \\ & \times e^{-\int_0^{\bar{z}} (\omega_1[\gamma_1/(2cos(\theta))]_{\Gamma_1(s)} + \omega_2[\gamma_1/(2cos(\theta))]_{\Gamma_2(s)})^2 ds} \qquad as \;\; \varepsilon \downarrow 0\end{aligned}$$

which is (D.2.7). As above Γ_i denotes geometrical optics rays going through the point of observation and θ the angle between the tangent to these and the vertical.

D.2.4 On the higher order moments.

In this subsection we state the governing equations for the higher order moments and show that these moments constitute higher order terms. The argument is based on the method of stationary phase. We use here the notation

$$\begin{aligned} t^n &\equiv t(z, X_1) r(z, X_2) \cdots r(z, X_{n+1}) e^{i\Phi(z)/\varepsilon} \\ \tau^n &\equiv E[t^n] \end{aligned}$$

with $X_j \equiv \{x_j, \kappa_j, s_j, v_j, \omega_j\}$ and $\Phi(z) \equiv \sum_{j=1}^{n+1} \omega_j \phi(z, v_j)$. The phase ϕ is defined in (D.1.9). It follows from (D.2.10) that

$$\begin{aligned} t_z^n \;=\; & \sum_{j=1}^{m} \{\ \partial_{s_j}[w_1(z, s_j, v_j) t^n] + I_j[w_2(z, x_j, \kappa_j)\partial_{x_j} + w_3(z, x_j, \kappa_j)\partial_{\kappa_j}] t^n \\ & + [I_j h_5(z, x_j, \kappa_j) - h_1(z, s_j, v_j)] t^n - i\varepsilon/\omega_j \partial_{s_j}^2 [h_4(z, s_j, v_j) t^n] \\ & + i\varepsilon/\omega_j I_j [\mathcal{L}_2(z, x_j, \kappa_j)](t^n) + I_j \mathcal{L}_3(z, x_j, \kappa_j)(\delta(x_j - s_j)\delta(\kappa_j - v_j)) t^{n/j} \\ & - \int\int t^{n/j} \tilde{r}_j(z, x_j, \kappa_j, s, v) \mathcal{L}_1(z, s, v)(r(z, s, v, s_j, v_j)) ds dv \end{aligned}$$

$$
\begin{aligned}
&- \varepsilon^{-1} i\omega_j \nu (h_2(z, s_j, v_j) - I_j h_7(z, x_j, \kappa_j)) t^n \\
&+ I_j \varepsilon^{-1} i\omega_j \nu h_6(z, x_j, \kappa_j)(\delta(x_j - s_j)\delta(\kappa_j - v_j)) t^{n/j} \\
&- \varepsilon^{-1} i\omega_j \nu \int\int h_3(z, s, v) t^{n/j} \tilde{r}_j(z, x_j, \kappa_j, s, v) r(z, s, v, s_j, v_j)) ds dv \ \} \\
&+ \varepsilon^{-1} i\Phi_z(z) t^n
\end{aligned}
$$

with $m = n + 1$, $I_j = 0$ for $j = 1$ and 1 otherwise, $\tilde{r}_j(\cdots) = t(\cdots)$ for $j = 1$ and $\tilde{r}_j(\cdots) = r(\cdots)$ otherwise, finally, where $t^{n/j}(\cdots) \equiv t^n(\cdots)/\tilde{r}(z, X_j)$. We again apply the limit result (D.3.13) to get the governing equation for the moments and write it as

$$
\begin{aligned}
\tau_z^n \ = \ & \sum_{j=1}^{m} \{ \ \partial_{s_j}[w_1(z, s_j, v_j)\tau^n] + I_j[w_2(z, x_j, \kappa_j)\partial_{x_j} + w_3(z, x_j, \kappa_j)\partial_{\kappa_j}]\tau^n \qquad \text{(D.2.23)} \\
& + [I_j h_5(z, x_j, \kappa_j) - h_1(z, s_j, v_j)]\tau^n - i\varepsilon/\omega_j \partial_{s_j}^2 [h_4(z, s_j, v_j)\tau^n] \\
& + i\varepsilon/\omega_j I_j [\mathcal{L}_2(z, x_j, \kappa_j)](\tau^n) + I_j \mathcal{L}_3(z, x_j, \kappa_j)(\delta(x_j - s_j)\delta(\kappa_j - v_j))\tau^{n/j} \\
& - \int\int \mathcal{L}_1(z, \omega_j, s, v; m)(\tau^{n \cdot j}) ds dv \ \} \\
& + l\{ \ [\sum_{j=1}^{m} \omega_j (I_j h_7(z, x_j, \kappa_j) - h_2(z, s_j, v_j))]^2 \tau^n \\
& - [\sum_{j=1}^{m} \omega_j^2 (h_3(z, s_j, v_j) h_6(z, s_j, v_j) + I_j h_3(z, x_j, \kappa_j) h_6(z, x_j, \kappa_j))]\tau^n \\
& + [\sum_{k=1}^{m} \omega_k I_k h_6(z, x_k, \kappa_k)\delta(x_k - s_k)\delta(\kappa_k - v_k) \\
& \times \sum_{j=1}^{m} (2 - I_{\{j=k\}}) \omega_j (I_j h_7(z, x_j, \kappa_j) - h_2(z, s_j, v_j))]\tau^{n/k} \\
& + [\sum_{j=1}^{m} \sum_{k=1 \neq j}^{m} \omega_j \omega_k I_j I_k h_6(z, x_j, \kappa_j) h_6(z, x_k, \kappa_k) \\
& \times \delta(x_j - s_j)\delta(\kappa_j - v_j)\delta(x_k - s_k)\delta(\kappa_k - v_k)]\tau^{n/\{j,k\}} \\
& - \sum_{j=1}^{m} \omega_j \int\int h_3(z, s, v)(\sum_{k=1}^{m-1} \tau^{n \cdot j/k} I_k \omega_{a(k)} h_6(z, x_{a(k)}, \kappa_{a(k)}) \\
& \times \delta(x_{a(k)} - s_{a(k)})\delta(\kappa_{a(k)} - v_{a(k)})) \ ds dv
\end{aligned}
$$

$$
\begin{aligned}
&- \sum_{j=I}^{m} \omega_j h_6(z, x_j, \kappa_j)\delta(x_j - s_j)\delta(\kappa_j - v_j)(\sum_{k=1\neq j}^{m} \omega_k \int\int h_3(z, s, v)\tau^{(n/j)\cdot k} ds dv) \\
&- (\sum_{j=1}^{m} \omega_j (I_j h_7(z, x_j, \kappa_j) - h_2(z, s_j, v_j)))(\sum_{k=1}^{m} \omega_k \int\int h_3(z, s, v)\tau^{n\cdot k} ds dv) \\
&- \sum_{j=1}^{m} \omega_j \int\int h_3(z, s, v)\tau^{n\cdot j} ds dv (\sum_{k=1}^{m+1} \omega_k (I_k h_7(z, x_{b(k)}, \kappa_{b(k)}) - h_2(z, s_{b(k)}, v_{b(k)}))) \\
&+ \sum_{j=1}^{m} \omega_j \int\int h_3(z, s, v)(\sum_{k=1}^{m+1} \omega_{b(k)} \int\int h_3(z, \tilde{s}, \tilde{v})\tau^{n\cdot j\cdot k} d\tilde{s} d\tilde{v}) ds dv\} \\
&+ \varepsilon^{-1} i \Phi_z(z)\tau^n
\end{aligned}
$$

using the notation

$$
\begin{aligned}
\tau^{n\cdot j} &= E[t^{n\cdot j}] \equiv E[t^{n/j}\tilde{r}(z, x_j, \kappa_j, s, v) r(z, s, v, s_j, v_j)] \\
&\equiv \tau^{n+1}(\cdots; X_{b(j)}; \cdots) \\
\tau^{n\cdot j/k} &= E[t^{n\cdot j}/\tilde{r}(z, x_k, \kappa_k, s_k, v_k)] \\
&\equiv \tau^{n+1}(\cdots; X_{a(j)}; \cdots) \\
\tau^{n\cdot j\cdot k} &= E[t^{(n\cdot j)\cdot k}].
\end{aligned}
$$

We rewrite (D.2.23) as

$$
\frac{d}{d\eta_n}\tau^n = \mathcal{H} + \varepsilon^{-1} i \Phi_z \tau^n \tag{D.2.24}
$$

with $\mathcal{H}$ being defined in terms of the various moments and η_n being the characteristic direction. Note that, according to the ansatz, the operator $\mathcal{L}_1$ does not generate higher order terms, moreover, that τ^n satisfies the radiation condition $\tau^n|_{z=\infty} = 0$. It follows from our assumptions that the geometrical optics rays are bounded away from the horizontal. The phase, Φ, is defined by $\Phi(z) = \sum_{i=1}^{n+1} \omega_i \phi(z, v_i)$. In view of (D.2.12) we need only consider $\omega_i = \omega$. There are therefore no stationary points associated with the integration in (D.2.24), apart from a set of measure zero with

respect to ω. Specifically, at the surface $\Phi_z|_{z=0} = -2\omega \sum_{i=1}^{n+1} \sqrt{\gamma_1^2 - v_i^2}$, and according to our assumptions the square root is bounded away from zero. From the ansatz (D.2.14) it follows that $\mathcal{H}$ contains no phase factor in $\{v_j, \kappa_j\}$ for $j > 1$. This is consistent with (D.2.24); since Φ has no stationary points τ^n, as defined by (D.2.24), involve only exponentially small terms with such phase modulation.

Consider now the ansatz (D.2.19). The same argument as above can be used to show that this is consistent with (D.2.24), appropriately modified. We now need the governing equations for the moments

$$\tau^n \equiv E[t(z, X_1)t(z, X_2)r(z, X_3) \cdots r(z, X_{n+2})]e^{i\Phi(z)/\varepsilon}.$$

These are still given by (D.2.23), only that now $m = n + 2$, $I_j = 0$ for $j = 1$ & 2 and 1 otherwise, moreover, $\tilde{r}_j(\cdots) = t(\cdots)$ for $j = 1$ & 2 and $\tilde{r}_j(\cdots) = r(\cdots)$ else. In this case we need to consider two different values of ω_i, thus there might be resonance effects associated with the integration in (D.2.24). However, we need only consider slownesses in an $O(\sqrt{\varepsilon})$ neighborhood of the central ray slowness, $\bar{\kappa}$, to derive the expression for the coherent pulse front. The leading order phase is thus defined by $\Phi(z) = \sum_{i=1}^{n+2} \omega_i \phi(z, \bar{\kappa})$. Hence, as above, the set on which there are stationary points with respect to the phase Φ is of measure zero with respect to the ω_i.

D.3 Limit result for the operator equations.

We present a multiple scales derivation for the governing equations of the asymptotic means of the operators introduced in Appendix D. Recall that the small parameter in the problem is ε, defined so that the random modulation ν vary on the spatial scale z/ε^2.

Let Γ satisfy

$$\Gamma_z = \varepsilon^{-1}\nu F(z, \Gamma) + G(z, \Gamma) \tag{D.3.1}$$

$$\Gamma|_{z=0} \;=\; \Gamma_0.$$

with $\Gamma^0 \in S$ and deterministic. Here S denotes the space of complex valued sequences of rapidly decaying functions on $\Re^n$ indexed by z. We assume that ν is a zero mean stationary ergodic Markov process starting from ν_0 at $z = 0$. Let Q be its infintesimal generator and P^* its invariant measure. We assume that νF is zero mean with respect to P^*. The correlation length of ν is defined by

$$l \;=\; \int_0^\infty E[\nu(0)\nu(s)]ds. \tag{D.3.2}$$

Consider the augmented Markov process $Y =< \nu, \Gamma >$, with state-space $\Re \times S$. Let

$$V \;=\; V(z;\Gamma_0,\nu_0) \;=\; E_{[\Gamma_0,\nu_0]}[f(\Gamma(z),\nu(z))] \tag{D.3.3}$$

with f being a mapping $\Re \times S \mapsto \Re$. The infinitesimal generator for the augmented process is

$$\mathcal{L} \;=\; \varepsilon^{-2}Q + \varepsilon^{-1}\nu F \cdot \nabla_\Gamma + G \cdot \nabla_\Gamma. \tag{D.3.4}$$

The backward Kolomogorov equation for the extended process is

$$(\partial_z + \mathcal{L})V \;=\; 0. \tag{D.3.5}$$

Decompose V as

$$V \;=\; \sum_{i=0}^{\infty} \varepsilon^i V_i(z;\nu,\Gamma). \tag{D.3.6}$$

Note that we allow V_i to depend on ε in general. Using (D.3.1) we obtain a hierarchy

of equations for the different scales, the first three which are

$$\begin{aligned} QV_0 &= 0 && \text{(D.3.7)} \\ QV_1 + \nu F \cdot \nabla_\Gamma V_0 &= 0 && \text{(D.3.8)} \\ QV_2 + \nu F \cdot \nabla_\Gamma V_1 + G \cdot \nabla_\Gamma V_0 + \partial_z V_0 &= 0 && \text{(D.3.9)} \\ &\vdots \end{aligned}$$

The solution in the deterministic case, $\nu \equiv 0$, is determined by (D.3.9) and then $V_i = 0$ for $i > 0$. We seek a leading order expression for the mean of Γ, $\bar{\Gamma}$, from the solvability condition of (D.3.9).

First, from (D.3.7) we find $V_0 = V_0(z, \Gamma)$.

Second, using the zero mean property of νF and assuming the Fredholm alternative to hold for the process ν, we get from (D.3.8)

$$V_1 = -Q^{-1}\nu F \cdot \nabla_\Gamma V_0 + V_{1,0} \qquad \text{(D.3.10)}$$

with Q^{-1} chosen so that $V_{1,0}$ has vanishing mean. Since $V_{1,0}$ does not depend on ν it is actually zero.

Third, from $(D.3.9)$ it follows, upon integration with respect to P^*,

$$\int dP^*[\nu F \cdot \nabla_\Gamma(-Q^{-1})\nu F \cdot \nabla_\Gamma]V_0 + G \cdot \nabla_\Gamma V_0 + \partial_z V_0 = 0. \qquad \text{(D.3.11)}$$

Write this as

$$\partial_z V_0 + \mathcal{L}^* V_0 = 0,$$

where

$$\mathcal{L}^*\Phi(\Gamma) = 1/2A(z,\Gamma)\cdot\nabla^2_\Gamma\Phi(\Gamma) + B(z,\Gamma)\cdot\nabla_\Gamma\Phi(\Gamma). \tag{D.3.12}$$

From (D.3.12) we can obtain an expression for the drift term $B(z,\Gamma)$ using the probabilistic interpretation for the construction of Q^{-1}. In the case that B is a linear operator on S, $B(z,\Gamma) = \mathcal{L}_B(z,\Gamma)$, it follows

$$\begin{aligned} \bar{\Gamma}_z &= \mathcal{L}_B(z,\bar{\Gamma}) \\ &= lF(z,\bar{\Gamma})\cdot\nabla_\Gamma F(z,\bar{\Gamma}) + G(z,\bar{\Gamma}) \end{aligned} \tag{D.3.13}$$

Hence, we have arrived at the sought after characterization of $\bar{\Gamma}$ in the linear case.

Appendix E

Results used in Chapter 2.

E.1 Plane wave decomposition of impinging pulse.

We show how the downpropagating pressure pulse at the surface, z=0, can be expressed in terms of plane waves. In the halfspace $z < 0$ we find, upon elimination of $\boldsymbol{u}$, that the pressure satisfies

$$\triangle \hat{p} + (\omega/\varepsilon)^2 \gamma_0^2 \ \hat{p} \ = \ \varepsilon^2 \hat{f}(\omega)\delta(\boldsymbol{x})\delta'(z - z_s).$$

Consider the standard point source problem

$$\mathcal{L}g \ \equiv \ \triangle g + (\omega/\varepsilon)^2 \gamma_0^2 \ g = -\delta(\boldsymbol{x})\delta(z - z_s)$$

associated with the reduced wave equation. The solution, the free space Green's function, can be written in terms of the Weyl integral [1] as

$$g \ = \ i\omega/(8\pi^2\varepsilon) \int\int e^{i\omega\phi/\varepsilon}/\phi_z \ d\boldsymbol{\kappa}.$$

Here the phase ϕ is given by

$$\phi \;=\; \boldsymbol{\kappa}\cdot\boldsymbol{x} + \sqrt{\gamma_0^2 - \boldsymbol{\kappa}^2}\;|z - z_s|$$

with $\boldsymbol{x} = (x_1, x_2)$, $\boldsymbol{\kappa} = (\kappa_1, \kappa_2)$ and $Im[\omega\sqrt{\gamma_0^2 - \boldsymbol{\kappa}^2}] > 0$. Hence,

$$\mathcal{L}[-\varepsilon^2 \hat{f}\;\partial_z g] \;=\; \varepsilon^2 \hat{f}(\omega)\delta(\boldsymbol{x})\delta'(z - z_s)$$

Thus we find that at the surface

$$\begin{aligned}\hat{p} \;&=\; -i\omega\varepsilon\hat{f}(\omega)/(8\pi^2)\int\int \partial_z[e^{i\omega\phi/\varepsilon}/\phi_z]\;d\boldsymbol{\kappa} + \hat{p}_{refl}\\ &\sim\; \omega^2\hat{f}(\omega)/(8\pi^2)\int\int e^{i\omega\phi/\varepsilon}\;d\boldsymbol{\kappa} + \hat{p}_{refl} \qquad as\;\; \varepsilon \downarrow 0,\end{aligned}$$

with $\hat{p}_{refl}$ denoting the the up-going pressure pulse, being reflected from the heterogeneous half-space $z > 0$. Recall the expression (2.6.18) for the time transformed pressure. The amplitude of the down-propagating pulse at the surface as defined therein follows from the above expression for $\hat{p}$

$$\mathcal{A} \;\sim\; \omega^2\hat{f}(\omega)/(8\pi^2) \qquad as\;\; \varepsilon \downarrow 0.$$

E.2 Pulse approximation for plane wave source.

We seek the high frequency approximation of p for $z > 0$ given a decomposition of the impinging pulse as in (2.7.6). Note that we are solving the same problem as we did in Section 2.2. Our motivation for doing so is to be able to relate the approximation for p we obtain based on the parameterization (2.7.6) to the standard high frequency approximation given in Section 2.2.

Thus we state the ansatz

$$\hat{p} \;\sim\; \int\int A\, e^{i\omega S^+}\, d\boldsymbol{\kappa} \qquad as \;\; \varepsilon \downarrow 0,$$

and seek the associated representation of the high frequency approximation. The phase solves the eiconal equation with the initial condition

$$S(\boldsymbol{x}, 0, \boldsymbol{\kappa}) \;=\; \boldsymbol{\kappa}\cdot\boldsymbol{x} + \sqrt{\gamma_0^2 - \kappa^2}\; z_s$$

and the outgoing condition being that $S_z > 0$ at the surface, which reflects the fact that the wave-component we are considering enters the positive half-space $z > 0$. In Appendix E.1 we show that

$$A(0, \boldsymbol{\kappa}, \omega) \;\sim\; \omega^2\, \hat{f}(\omega)/(8\pi^2) \;\equiv\; \mathcal{A} \qquad as \;\; \varepsilon \downarrow 0. \tag{E.2.1}$$

Furthermore, the leading order amplitude term solves the first transport equation given in (2.2.7). The associated leading order approximation for p is

$$p(\boldsymbol{x}, z, t) \;\sim\; (1/(2\pi\varepsilon)) \int\int\int \mathcal{A}(\boldsymbol{\kappa}, \omega)\; e^{-\int_{\Gamma^+} \triangle S/(2\gamma_1) ds}\; e^{i\omega(S-t)/\varepsilon}\; d\boldsymbol{\kappa}\; d\omega \tag{E.2.2}$$

By an application of Gauss theorem we find, see [23] for details of the calculation, that

$$e^{-\int_{\Gamma^+} \triangle S/(2\gamma_1) ds} \;=\; \sqrt{\gamma_0/(\gamma_1(\boldsymbol{x}, z)\zeta(\boldsymbol{x}, z, \boldsymbol{\kappa}))}$$

with $\zeta(\boldsymbol{x}, z, \boldsymbol{\kappa})$ being the expansion ratio for a ray-tube along the ray-segment Γ^+ emanating from the surface $z = 0$ and terminating at $(\boldsymbol{x}, z)$. The ray path $\Gamma^+ =$

$\Gamma^+(\boldsymbol{x}, z, \boldsymbol{\kappa})$, parameterized in terms of arc length, corresponds to the characteristic ray segment between the surface $z = 0$ and $(\boldsymbol{x}, z)$.

By a straight forward application of the method of stationary phase the representations (2.2.8) and (E.2.2) can be connected. Applying the method of stationary phase to (E.2.2) we find

$$p(\boldsymbol{x}, z, t) \quad \sim \quad -(2\pi i\varepsilon/(\sqrt{\triangle}\omega) \int \mathcal{A}\; e^{-\int_{\Gamma^+} \triangle S/(2\gamma_1) ds}\; e^{i\omega(S-t)/\varepsilon}\; d\omega$$

with the integral kernel being evaluated at the stationary phase point, $\overline{\boldsymbol{\kappa}}$, satisfying

$$\nabla S(\boldsymbol{x}, z, \overline{\boldsymbol{\kappa}}) \quad = \quad 0. \tag{E.2.3}$$

The quantity $\triangle = \triangle(\boldsymbol{x}, z, \boldsymbol{\kappa})$ is the determinant of the Hessian of S with respect to $\boldsymbol{\kappa}$. We assume that the solution of the eiconal equation is unique. In this case $\overline{\boldsymbol{\kappa}}$ is uniquely defined. As explained in Appendix E.4 the stationary slowness corresponds to the slowness which is associated with a ray going through the source point and the point of observation. The path $\Gamma^+(\boldsymbol{x}, z, \overline{\boldsymbol{\kappa}})$ is showed with a solid line in Figure 2.2. Now making use of the identity

$$[\varphi_z\; \sqrt{(d\Omega/da)}](\boldsymbol{x}, z) \quad = \quad 1/\sqrt{\Delta(\boldsymbol{x}, z, \overline{\boldsymbol{\kappa}})\; \xi(\boldsymbol{x}, z, \overline{\boldsymbol{\kappa}})}, \tag{E.2.4}$$

and the fact that

$$\varphi(\boldsymbol{x}, z) \quad = \quad S(\boldsymbol{x}, z, \overline{\boldsymbol{\kappa}})$$

we obtain from (E.2.2) the approximation

$$p(\boldsymbol{x}, z, \varphi + \varepsilon s) \sim (4\pi)^{-1} \varphi_z \sqrt{(d\Omega/da)(\gamma_0/\gamma_1)}\, f'(s) \qquad as \quad \varepsilon \downarrow 0$$

for p, which is (2.2.8).

We briefly turn to the special case of a uniform background medium, that is $\gamma_1(\boldsymbol{x}, z) = \gamma_1$, and easily find

$$\begin{aligned} \overline{\boldsymbol{\kappa}} &= \gamma_1\, \boldsymbol{x}/r \\ S^+ &= \gamma_1\, r \end{aligned}$$

with $r = \sqrt{\boldsymbol{x} \cdot \boldsymbol{x} + (z - z_s)^2}$. The value of the geometric factor in this case is

$$[\varphi_z \sqrt{(d\Omega/da)}](\boldsymbol{x}, z) = 1/\sqrt{\Delta(\boldsymbol{x}, z, \overline{\boldsymbol{\kappa}})\, \xi(\boldsymbol{x}, z, \overline{\boldsymbol{\kappa}})} = \gamma_1\, z/r^2,$$

which corresponds to geometrical spreading in three spatial dimensions.

E.3 Limit result, layered case.

We verify (2.6.19). This follows from

$$E[\alpha_1(z)] \sim e^{-\omega_1^2 V_1(z)} \tag{E.3.1}$$

$$E[\alpha_1(z) e^{i\Phi(z)/\varepsilon}] \sim E[\alpha_1(z)]\; E[e^{i\Phi(z)/\varepsilon}] \tag{E.3.2}$$

$$E[\alpha_1(z)\alpha_2(z) e^{i\Phi(z)/\varepsilon}] \sim E[\alpha_1(z)]\; E[\alpha_2(z)]\; E[e^{i\Phi(z)/\varepsilon}] \qquad as \quad \varepsilon \downarrow 0 \tag{E.3.3}$$

Here $\alpha_i(z) \equiv \alpha(z, \boldsymbol{\kappa}_i, \omega_i)$, $V_i(z) \equiv \int_0^z \cos(\theta)^{-1} D(\boldsymbol{\kappa}_i, s) ds$ with θ and D being defined respectively by (2.6.7) (2.6.13). Also $\Phi \equiv \omega_1 \chi_\varepsilon(z, \boldsymbol{\kappa}_1) + \omega_2 \chi_\varepsilon(z, \boldsymbol{\kappa}_2)$, with χ_ε being

defined in (2.6.18). We show only (E.3.1) and (E.3.3), (E.3.2) follows by a similar argument.

We will make us of the following result, see [11]. Let X^ε be a finite dimensional state vector satisfying

$$\frac{dX^\varepsilon}{dz} = \varepsilon^{-1}F(z,\nu(z/\varepsilon^2),\tau(z)/\varepsilon,X^\varepsilon)+G(z,\nu(z/\varepsilon^2),\tau(z)/\varepsilon,X^\varepsilon) \quad \text{(E.3.4)}$$

with ν a random, mean zero, stationary process with rapidly decaying correlation function. The dependence on τ is through a periodic function and $\partial_z\tau \neq 0$. Also $E[F(z,\nu(s),\tau,X)]=0$ for all z,s,τ,X.

Define the operator

$$B(z,X)^j = \lim_{Y\to\infty} Y^{-1}\int_0^Y\int_0^\infty E[F(z,\nu(0),y,X)\cdot\nabla_X F^j(z,\nu(r),y,X)]\,drdy + \lim_{Y\to\infty} Y^{-1}\int_0^Y E[G^j(z,\nu(0),y,X)]\,dy \quad \text{(E.3.5)}$$

If it is linear, $B^j(z,X)=b^j(z)\cdot X$, then

$$d\frac{<X>}{dz} = B(z)<X> \quad \text{(E.3.6)}$$

with the columns of B being b^j and $<X>=E[X]$.

In order to apply the above result we use an invariant imbedding approach; we assume that the medium parameters are constant for $z>L$. Due to a finite speed of propagation we can do this without affecting the solution over a finite time frame.

Recall the amplitude equations (2.6.6). We make the change of variables

$$\alpha = A\, e^{\int_0^z[\tau_{1,zz}/(2\gamma_1)-i(\omega/\varepsilon)\gamma_1\ \nu/2]\cos(\theta)^{-1}\ ds}$$
$$\beta = B\, e^{\int_0^z[\tau_{1,zz}/(2\gamma_1)+i(\omega/\varepsilon)\gamma_1\ \nu/2]\cos(\theta)^{-1}\ ds}\ e^{2i\omega\tau/\varepsilon+iT}$$

with

$$\begin{aligned} \tau &= \int_z^L \sqrt{\gamma_1(s)^2 - \boldsymbol{\kappa}^2}\, ds \\ T &= \varepsilon^{-1} \int_z^L \gamma_1(s)\nu(s/\varepsilon^2)\cos(\theta(s))^{-1}\, ds. \end{aligned}$$

Observe that β differs from the one defined in (2.6.8) by a phase factor. The resulting amplitude equations are

$$\begin{aligned} d\alpha/dz &= \zeta\beta \\ d\beta/dz &= \overline{\zeta}\alpha, \end{aligned} \tag{E.3.7}$$

with now

$$\begin{aligned} \zeta(z) &= \cos(\theta)^{-1}[i\omega\gamma_1(z)\nu(z/\varepsilon^2)/(2\varepsilon) + \tau_{1,zz}/(2\ \gamma_1(z))]\ e^{2i(\tau/\varepsilon+T)} \\ &\equiv (i\nu f/\varepsilon + g)e(\omega), \end{aligned}$$

where we defined

$$e(\omega) = e^{2i\omega(\tau/\varepsilon+T)}.$$

We first show (E.3.1). Define

$$\begin{aligned} \Gamma(z,\boldsymbol{\kappa},\omega) &= \beta(z,\boldsymbol{\kappa},\omega)/\alpha(z,\boldsymbol{\kappa},\omega) \\ \Theta(z,\boldsymbol{\kappa},\omega) &= \alpha(L,\boldsymbol{\kappa},\omega)/\alpha(z,\boldsymbol{\kappa},\omega) \end{aligned}$$

and let the state vector be $X = [\Gamma, \Theta, T]$. Then

$$\begin{aligned}
\frac{d\Gamma}{dz} &= \overline{\zeta} - \zeta\Gamma^2 \\
&= -i\nu f/\varepsilon[e(-\omega) + e(\omega)\Gamma^2] + g\ [e(-\omega) - e(\omega)\Gamma^2] \\
\frac{d\Theta}{dz} &= -\zeta\Theta\Gamma \\
&= -i\nu f/\varepsilon e(\omega)\Theta\Gamma - g\ e(\omega)\Theta\Gamma \\
\frac{dT}{dz} &= -2f\ \nu/\varepsilon
\end{aligned}$$

In view of (E.3.5) we find that the drift operator B associated with the above system is linear, moreover it is *diagonal*. In particular

$$\frac{d < \Theta >}{dz} = -f^2 l < \Theta > \tag{E.3.8}$$

from which (E.3.1) follows.

Next we show (E.3.3). Define

$$J(z, \boldsymbol{\kappa}_1, \boldsymbol{\kappa}_2, \omega_1, \omega_2) = \Theta(z, \boldsymbol{\kappa}_1, \omega_1)\ \Theta(z, \boldsymbol{\kappa}_2, \omega_2)\ \Psi(z, \boldsymbol{\kappa}_1, \boldsymbol{\kappa}_2, \omega_1, \omega_2)$$

with

$$\Psi(z, \boldsymbol{\kappa}_1, \boldsymbol{\kappa}_2, \omega_1, \omega_2) = e^{i(\Phi(L)-\Phi(z))/\varepsilon} = e^{i\int_z^L \nu(f_1+f_2)/\varepsilon ds}$$

and subscript j indicating that the function is evaluated at $(\boldsymbol{\kappa}_j, \omega_j)$. Let the state vector be $X = [J, \Psi, \Theta_1, \Theta_2, \Gamma_1, \Gamma_2, T_1, T_2]$. Then

$$\frac{dJ}{dz} = -i\nu/\varepsilon \sum_{j=1}^{2}[f_j e(\omega_j)\Gamma_j + f_j]J - \sum_{j=1}^{2}[g_j e(\omega_j)\Gamma_j]J$$

$$\begin{aligned}
\frac{d\Psi}{dz} &= -i\nu(f_1+f_2)/\varepsilon\ \Psi \\
\frac{d\Gamma_j}{dz} &= -i\nu f_j/\varepsilon[e(-\omega_j)+e(\omega_j)\Gamma_j^2]+g_j\ [e(-\omega_j)-e(\omega_j)\Gamma_j^2] \\
\frac{d\Theta_j}{dz} &= -i\nu f_j/\varepsilon e(\omega_j)\Theta_j\Gamma_j - g_j\ e(\omega_j)\Theta_j\Gamma_j \\
\frac{dT_j}{dz} &= -2f_j\ \nu/\varepsilon.
\end{aligned}$$

In view of (E.3.5) we find, for $\omega_1 \neq \omega_2$, that the drift operator B is *diagonal* and that

$$\begin{aligned}
\frac{d<J>}{dz} &= -[f_1^2+f_2^2+(f_1+f_2)^2]\ l<J> \\
\frac{d<\Psi>}{dz} &= -(f_1+f_2)^2 l<\Psi>,
\end{aligned}$$

from which we can conclude (E.3.3). Finally, note that the above gives the transmitted pulse at depth $z=L$. We obtain the pulse at depth $z=\bar{z}$, the depth at the point of observation, by equating to zero the source terms in the governing equation for Θ in the interval $(\bar{z}, L)$. See also Appendix D.2.

E.4 Stationary phase point.

We show that the stationary phase slowness $\overline{\boldsymbol{\kappa}}$ is uniquely defined. Furthermore, how it relates to the rays of the high frequency approximation associated with a point source, that is the characteristic rays associated with solving for the phase φ defined in (2.2.5).

Recall that $\overline{\boldsymbol{\kappa}}$ is defined by

$$\nabla_{\boldsymbol{\kappa}} S(\overline{\boldsymbol{x}}, \overline{z}, \overline{\boldsymbol{\kappa}}) = 0,$$

with $(\overline{\boldsymbol{x}}, \overline{z})$ being the point of observation and S the phase defined in (5.7). By construction the phase front $\varphi(\boldsymbol{x}, z) = \varphi(\overline{\boldsymbol{x}}, \overline{z})$ is an envelope for the family phase

fronts of S parameterized by the slowness vector $\boldsymbol{\kappa}$. These phase fronts are defined by the two parameter family of surfaces

$$F(\boldsymbol{x}, z; \boldsymbol{\kappa}) \;=\; S(\boldsymbol{x}, z, \boldsymbol{\kappa}) - \varphi(\overline{\boldsymbol{x}}, \overline{z}) = 0.$$

From this representation we find that the envelope is determined as the solution of

$$\begin{aligned} \nabla_{\boldsymbol{\kappa}} S(\overline{\boldsymbol{x}}, \overline{z}, \overline{\boldsymbol{\kappa}}) &= 0 \\ S(\boldsymbol{x}, z, \boldsymbol{\kappa}) &= \varphi(\overline{\boldsymbol{x}}, \overline{z}). \end{aligned} \tag{E.4.1}$$

In particular consider the slowness $\tilde{\boldsymbol{\kappa}}$ associated with a ray going through the source point and also the point of observation, $(\overline{\boldsymbol{x}}, \overline{z})$. Then $(\overline{\boldsymbol{x}}, \overline{z}, \tilde{\boldsymbol{\kappa}})$ is a solution of (E.4.1) and $\nabla_{\boldsymbol{\kappa}} S(\overline{\boldsymbol{x}}, \overline{z}, \tilde{\boldsymbol{\kappa}}) = 0$. Hence the slowness corresponding to a phase S which is associated with a characteristic ray going through both the source and the the point of observation is a stationary point. This is also a characteristic ray of the point source high frequency phase φ. Below we show that $\tilde{\boldsymbol{\kappa}}$ is uniquely defined. The path is thus the one labelled, Γ^+ in Figure 2.4, witch goes through both the source point and the point of observation.

Uniqueness follows from the assumption that $(\overline{\boldsymbol{x}}, \overline{z})$ is associated with a single point on the phase front φ. Because, assume otherwise, that is there is a $\hat{\boldsymbol{\kappa}}$ such that

$$\begin{aligned} \nabla_{\boldsymbol{\kappa}} S(\overline{\boldsymbol{x}}, \overline{z}, \hat{\boldsymbol{\kappa}}) &= 0 \\ \hat{\boldsymbol{\kappa}} &\neq \tilde{\boldsymbol{\kappa}}. \end{aligned} \tag{E.4.2}$$

Now let

$$\hat{S} \;=\; S - \boldsymbol{\kappa} \cdot \hat{\boldsymbol{x}},$$

with $(\hat{\boldsymbol{x}}, z_s)$ being the point from which the ray going through $(\overline{\boldsymbol{x}}, \overline{z})$ and being associated with the slowness $\hat{\boldsymbol{\kappa}}$ emerges. By the assumption on φ, $\hat{\boldsymbol{\kappa}}$ must be a stationary point of $\hat{S}$

$$\nabla_{\boldsymbol{\kappa}} \hat{S}(\overline{\boldsymbol{x}}, \overline{z}, \hat{\boldsymbol{\kappa}}) \;=\; 0,$$

but this contradicts (E.4.2), hence $\overline{\boldsymbol{\kappa}}$ is uniquely defined.

E.5 Pulse approximation by stationary phase.

An asymptotic expression for the transmitted pulse was given in (2.6.17)

$$p \;\sim\; X \;=\; \int\int\int \overline{A}\; e^{-(\omega^2 \int_{\Gamma+} D ds)}\; e^{i\omega(S^+ + \chi_\varepsilon - t)/\varepsilon}\; d\boldsymbol{\kappa}\; d\omega.$$

In this appendix, we show how we can relate this expression to the geometrical optics approximation associated with the deterministic medium.

We are interested in the pulse front and want to observe this on the time scale of the source pulse. Thus we 'open a window' on this scale around the arrival time of the coherent pulse. We take the arrival time of the pulse to be $S^+(\mathbf{x}, z, \overline{\boldsymbol{\kappa}}) + \chi_\varepsilon(\mathbf{x}, z, \overline{\boldsymbol{\kappa}})$, with $\overline{\boldsymbol{\kappa}}$ denoting the slowness associated with the ray going through both the source point and the point of observation. As in the purely layered case a random travel time correction has been introduced, the one associated with the high frequency path from the source to the point of observation. In this appendix we use the notation

$$\begin{aligned} S(\mathbf{x}, z, \boldsymbol{\kappa}) &= S^+(\mathbf{x}, z, \boldsymbol{\kappa}) - S^+(\mathbf{x}, z, \overline{\boldsymbol{\kappa}}) \\ \chi(\mathbf{x}, z, \boldsymbol{\kappa}) &= \chi_\varepsilon(\mathbf{x}, z, \boldsymbol{\kappa}) - \chi_\varepsilon(\mathbf{x}, z, \overline{\boldsymbol{\kappa}}). \end{aligned}$$

Note that for large values of $\boldsymbol{\kappa}$ the phase S^+ becomes complex corresponding to

evanescent modes. To avoid having to deal with these we assume the source is compactly supported in the slowness domain. Thus we want a more convenient expression for

$$\begin{aligned} Y &= \int\int\int \psi\overline{A}\; e^{-(\omega^2 \int_{\Gamma^+} Dds)}\; e^{i\omega(S+\chi)/\varepsilon}\; d\boldsymbol{\kappa}\; e^{-i\omega s} d\omega \\ &\equiv \int I\; e^{-i\omega s} d\omega \end{aligned}$$

with $\psi = \psi(\boldsymbol{\kappa})$ being a smooth neutralizer compactly supported and being unity in a neighborhood of $\boldsymbol{\kappa}_0$. The 'time' variable is

$$s = (t - S^+(\mathbf{x}, z, \boldsymbol{\kappa}_0) - \chi_\varepsilon(\mathbf{x}, z, \boldsymbol{\kappa}_0))/\varepsilon.$$

Write

$$\begin{aligned} I &= \int\int \psi\overline{A}\; e^{-(\omega^2 \int_{\Gamma^+} Dds)}\; e^{i\omega(S+\chi)/\varepsilon}\; d\boldsymbol{\kappa} \\ &\equiv \int\int \psi g\; e^{i\omega(S+\chi)/\varepsilon}\; d\boldsymbol{\kappa} \end{aligned}$$

The smooth function g is independent of ε. Let $\psi = \psi_1 + \psi_2$ with the neutralizer ψ_1 being unity in a suitably small neighborhood of $\boldsymbol{\kappa}_0$ and define

$$\begin{aligned} I &= \int\int (\psi_1 + \psi_2) g\; e^{i\omega(S+\chi)/\varepsilon}\; d\boldsymbol{\kappa} \\ &\equiv I_1 + I_2. \end{aligned}$$

The leading order contribution to the integral will be associated with I_1 since S has no stationary points in the support of ψ_2. Note that the random phase factor χ makes this a non-standard stationary phase problem. Making use of the bound (2.6.20) we show that this phase component can be ignored when computing the stationary phase

point in the method of stationary phase.

Consider first the integral I_1 and rewrite this as

$$\begin{aligned} I_1 &= \int\int \psi_1 g\ e^{i\omega S/\varepsilon}(1 + i\omega/\varepsilon\ \nabla_{\boldsymbol{\kappa}}\chi\ e^{i\omega\chi/\varepsilon}(\boldsymbol{\kappa} - \boldsymbol{\kappa}_0))\ d\boldsymbol{\kappa} \\ &\equiv I_{1a} + I_{1b}. \end{aligned}$$

In the above expression χ is evaluated at $\hat{\boldsymbol{\kappa}}(\boldsymbol{\kappa})$ as determined by the mean value theorem. By a standard stationary phase argument, see (3.18) [56] we find that

$$I_{1a} = \int\int \psi_1 g\ e^{i\omega S/\varepsilon}\ d\boldsymbol{\kappa} \tag{E.5.1}$$

$$\sim (-i2\pi\varepsilon/\omega)(g/\sqrt{\triangle})|_{\boldsymbol{\kappa}_0} \tag{E.5.2}$$

with $\triangle$ being the determinant of the Hessian of S with respect to $\boldsymbol{\kappa}$. If we transform the expression in (E.5.1) with respect to the time variable we find, in view of (E.2.4), that this is the approximation stated in (2.6.21). We next show that this is indeed the leading order contribution.

Consider

$$I_{1b} = \int\int \psi_1 g\ e^{i\omega S/\varepsilon} i\omega/\varepsilon\ \nabla_{\boldsymbol{\kappa}}[\chi]\ e^{i\omega\chi/\varepsilon}(\boldsymbol{\kappa} - \boldsymbol{\kappa}_0)\ d\boldsymbol{\kappa}.$$

Since $\boldsymbol{\kappa}_0$ is a strict maximum for S we can define the change of variables

$$\begin{aligned} r &= S(\boldsymbol{\kappa}) \\ \theta &= arg(\boldsymbol{\kappa} - \boldsymbol{\kappa}_0) \end{aligned}$$

We assume that the support of ψ_1 has been chosen small enough such that, $\frac{\partial(\kappa_1,\kappa_2)}{\partial(r,\theta)}$, the determinant of the Jacobian of the mapping, is strictly positive in this domain.

Hence we can write

$$I_{1b} \;=\; \int\int \psi_1 g\; i\omega/\varepsilon\; \nabla_{\boldsymbol{\kappa}}[\chi]\; e^{i\omega\chi/\varepsilon}(\boldsymbol{\kappa}-\boldsymbol{\kappa}_0)\frac{\partial(\kappa_1,\kappa_2)}{\partial(r,\theta)}\; d\theta e^{i\omega r/\varepsilon}\; dr.$$

Recall that χ is evaluated at an argument according to the mean value theorem. We write this as

$$I_{1b} \;=\; \varepsilon^{-1}\int_{-L}^{0} h(r;\varepsilon)\; e^{i\omega r/\varepsilon}\; dr$$

with $h(-L,\varepsilon)=h(0,\varepsilon)=0$. Hence with probability one we find

$$\begin{aligned} I_{1b} &= (i/\omega)\int_{-L}^{0} h_r(t;\varepsilon)\; e^{i\omega r/\varepsilon}\; dr \\ &= O(\varepsilon \log\log \varepsilon^{-1}), \end{aligned}$$

making use of the bound (2.6.20) on the random phase component.

Consider next

$$I_2 \;=\; \int\int \psi_2 g\; e^{i\omega(S+\chi)/\varepsilon}\; d\boldsymbol{\kappa}.$$

Since S has no stationary points in the support of ψ_2 we can define

$$u \;=\; \nabla_{\boldsymbol{\kappa}} S/|\nabla_{\boldsymbol{\kappa}} S|^2\; \psi_2 g\; e^{i\omega\chi/\varepsilon}.$$

Observe that

$$\nabla_{\boldsymbol{\kappa}}\cdot(u\; e^{i\omega S/\varepsilon}) \;=\; (\nabla_{\boldsymbol{\kappa}}\cdot u)e^{i\omega S/\varepsilon} + i\omega/\varepsilon\; \psi_2 g\; e^{i\omega(S+\chi)/\varepsilon}.$$

Consequently, we obtain from the divergence theorem

$$I_2 \;=\; i\varepsilon/\omega \int\int (\nabla_{\boldsymbol{\kappa}} \cdot u) e^{i\omega S/\varepsilon}\, d\boldsymbol{\kappa}.$$

This expression is of the same form as I_{1b} and we may repeat the argument concerning that term to show that the above integral is with probability one $O(\varepsilon \log\log \varepsilon^{-1})$. Hence the leading order approximation for the transmitted pressure is as stated in (2.6.21).

Appendix F

The well-logs and their estimation.

F.1 The measurement model.

The well-logs represent certain physical parameters associated with the medium. However, the recording procedure introduces errors and the logs represent the actual parameters only indirectly. Recall that the medium is described by a discrete model (3.1.2). In this appendix we relate the well-logs to the underlying parameters of the medium by approximately removing the influence of the measurement tool with deconvolution.

The measured acoustic speed is obtained as shown schematically in *Figure* F.1. A tool is lowered into the bore hole and for each evenly spaced location z_k down the well, an acoustic signal is emitted from one endpoint of the tool and recorded at the two receivers at the other end. The discrepancy in the first-arrival times for the two receivers, normalized by the separation distance, defines the local estimate of the acoustic speed. This time difference corresponds roughly to the integral of the material slowness between the two receivers. We model the measured acoustic speed $\hat{c}_k$ by

$$\hat{c}_k^{-1} \;=\; \sum_{i=1}^{n} a_i \; c_{k+i}^{-1} / (\sum_{i=1}^{n} a_i) + v_k \qquad \text{(F.1.1)}$$

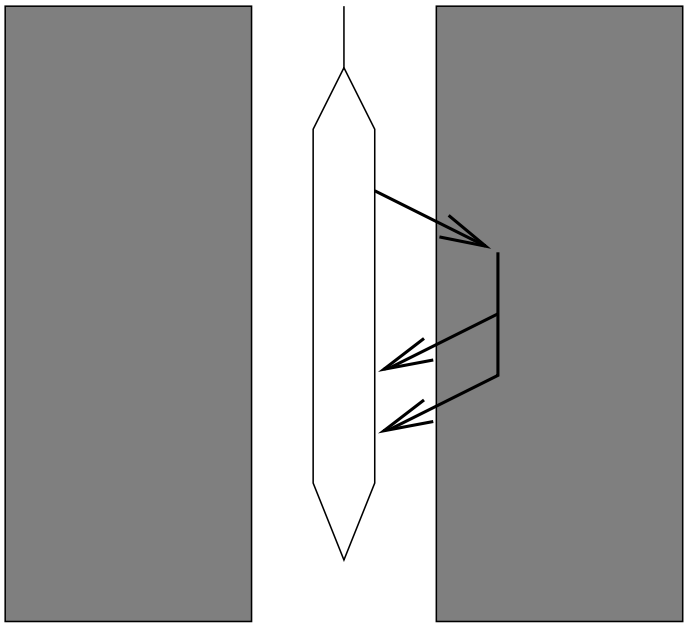

Figure F.1: The measurement tool that is lowered into the well to obtain the sonic log measurements. The recording is obtained as an average of the medium slowness.

with c_k being the 'true' velocity in the k'th section of the discretized medium. The parameters, a_i and n are associated with the tool and do not depend on the recording location. The v_k's model measurement noise and are assumed to be zero mean, uncorrelated random variables.

The physical description of the tool, suggests that $a_i = 1$ and $n = 5$ since the length between the two receivers in Figure F.1 is 2 feet and $\Delta z = .125m$. We use this model here, as was done in [21].

In order to obtain a fully specified model we need also to characterize the v_k process. To this effect, consider the variogram, shown in *Figure* F.2, associated with the sequence of slowness observations $\hat{c}_k^{-1}$. The variogram of a sequence $\{y_k\}$ is defined by

$$V(\Delta k) \quad = \quad 1/2 \sum_{k=1}^{N} (y_k - y_{k+\Delta k})^2 / N. \tag{F.1.2}$$

with $N + \Delta k$ being the length of the sequence. Note that its shape is close to linear for $\Delta k \approx 0$, with intercept at the origin. This suggests that in the measurement model $v_k \approx 0$. So we will assume $v_k = 0$ in F.1.1.

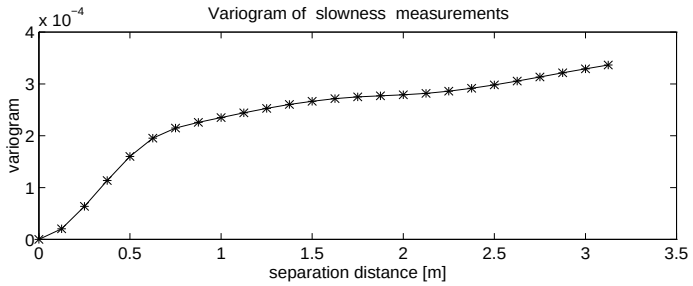

Figure F.2: Plot of the variogram associated with the sonic (slowness) log from well 10. Note the strong correlation for small lags, corresponding to small variogram-values. The tool records local averages and introduces strong correlations.

The deconvolution scheme aims at 'inverting' the effect of the measurement tool. We choose an approximate inverse as the solution to the Wiener-Hopf equations

$$\overline{c}_k^{-1} \quad = \quad \sum_{i=-n_1}^{n_2} d_i \; \hat{c}_{k+i}^{-1}. \tag{F.1.3}$$

The vector $\mathbf{d}$ of filter coefficients solves $\mathbf{A}\,\mathbf{d} = \mathbf{b}$, with $\mathbf{b}$ being a $n_1 \times 1$ vector, with coefficients defined by $b_i = a_i/(\sum_{j=1}^{n} a_j)^2$. The a_i's are the coefficients of the measurement model and are defined in F.1.1, ($a_i \equiv 0$ for $i > n$). The matrix $\mathbf{A}$ is an $n_1 \times n_1$ Toeplitz matrix. The i'th entry in the first row of $\mathbf{A}$ is

$$\sum_j a_{j+i-1} a_j / (\sum_{j=1}^{n} a_j)^2.$$

The parameter n_1 in F.1.3 defines the size of the local neighborhood on which we want to base the estimate of the c_k's. We choose $n_1 = 20$ corresponding to the length of the deconvolution filter, being 4 times that of the measurement filter.

In *Figure* F.3 we show $\tilde{I}$, the convolution of the measurement filter with the approximate inverse, in the top plot. Clearly this filter is close to the identity. The bottom plot, solid line, shows the variogram of the sequence of reflection coefficients obtained from a realization of the medium model, as defined in Section 3.3.2. The dashed line corresponds to the variogram obtained when $\tilde{I}$ is applied to the synthetic medium before we form the interface reflections. Note that even though we only have an approximate inverse, the difference between these is negligible.

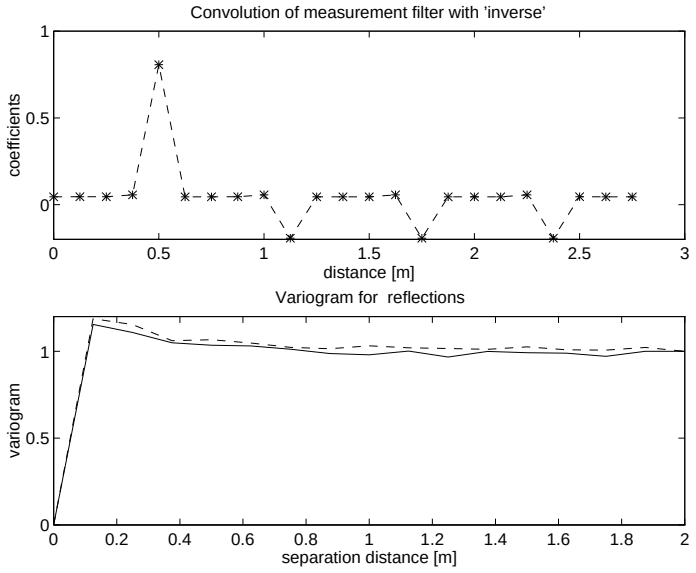

Figure F.3: The top plot shows the convolution of the measurement filter with the deconvolution filter. Note that these filters are not exact inverses. The solid line in the bottom plot is the variogram of a realization of the model. The dashed line in the plot is the variogram obtained when the speed realization is modified by convolution with the sequence shown in the top plot. The statistics are not adversely affected by this.

In [54] White et al point out, in the context of deconvolution of γ-ray logs, that a least-squares based inversion of the log sequence tends to generate unwanted high frequency components. They propose an alternative Bayesian deconvolution scheme incorporating apriori information about the stochastic structure of the underlying parameter in addition to a model for the tool. Note that in the present case Figure F.3

illustrates that the process of applying the measurement model and subsequently the deconvolution filter does not adversely change the spatial autocorrelation structure of the reflections, which is the characteristic of the process important for pulse shaping.

The density is measured by a procedure similar to that illustrated in Figure F.1. In this case the source is a directional radioactive source and γ-rays are being counted at the two receivers. The count can be related to the electron, and hence the material, density. In accordance with the discussion in [17] we will assume that the recording roughly corresponds to an average of the density between the two receivers. Thus we choose the model for the measured density, $\hat{\rho}_k$, as

$$\hat{\rho}_k \quad = \quad \sum_{i=1}^{m} b_i \ \rho_{k+i} / (\sum_{i=1}^{m} b_i) + w_k \tag{F.1.4}$$

with the interpretation of m, b_i and w_k being as for the above measurement model. Moreover, with ρ_k representing the 'true' density in section k of the material. Using an argument similar to the one presented above concerning the sonic log, we choose the model parameters as $m = 4$, $b_i = 1$ and $w_k \equiv 0$. We choose the deconvolution scheme as above.

There are certain problems with the above measurement procedures. For example, the presence of a mud-cake on the well wall may distort the reading and the process of drilling may have changed the properties of the surrounding rock. However, the tool is constructed so as to mitigate such effects and we shall assume that the above models are appropriate.

F.2 Analysis of a particular well-log.

In this appendix we show how we estimate the parameters of the medium model defined in (3.3.1). We base the analysis on the sonic log from well 10 in the Troll West Oil Province, using the observation in the depth range $500 - 1500m$. Recall that before we carry out the estimation we deconvolve the log to remove the effect of

the measurement tool as described in Appendix F.1. We do not introduce stochastic models for the macroscale components defined by the sequences $\{e_k\}$ and $\{\overline{c}_k\}$, but rather consider them as deterministic functions.

In view of the model (3.3.1) it follows, assuming ε small, that the standard deviation of $r_k \equiv (c_{k+1} - c_k)/(c_{k+1} + c_k)$ is approximately proportional to e_k. Therefore we approximate the e_k's by

$$\hat{e}_k \quad = \quad aver(r_k^2)^{1/2}/const, \tag{F.2.1}$$

where $aver(r_k^2)$ is simply unit weight local average over $40m$, and with *const* chosen so that the mean square of the sequence $\hat{e}_k$ is 1. Note that the width of the filter is primarily chosen so as to reflect the scale which can be considered as macroscopic, in the sense that features on this scale are features one can hope to identify through reflection seismology.

Based on the $\hat{e}_k$ estimate we introduce the 'standardized measured reflections' defined by

$$\tilde{r}_k \quad = \quad (c_{k+1} - c_k)/((c_{k+1} + c_k)\hat{e}_k). \tag{F.2.2}$$

Thus, we can consider $\tilde{r}_k$ to be a realization of the random variable

$$\tilde{R}_k \quad = \quad [\tilde{C}_{k+1} - \tilde{C}_k]/[\tilde{C}_{k+1} + \tilde{C}_k] \tag{F.2.3}$$

with $\tilde{C}_k$ being a standardized version of C_k such that $\overline{c}_k \equiv 1$ and $e_k \equiv 1$, but with the micro scale parameters unchanged. Hence the distribution of $\tilde{R}_k$ will be determined by the parameters ε, l and σ. We next look at some statistics of $\tilde{r}_k$ in order to determine these parameters. Every choice of these parameters defines a random variable, $\tilde{R}_k$, whose statistics we can compare with that of $\tilde{r}_k$. Hence, we choose ε, l and σ so

that the statistics associated with these sequences are comparable. Actually, since deconvolving the observations with respect to the tool only approximately inverts the effect of the measurement process, we should really compare the statistics associated with $\tilde{r}_k$ with the reflections derived from a realization of the medium model when convolved with $\tilde{I}$, the convolution of the measurement model with the approximate inverse. However, convolving the medium realization with $\tilde{I}$ does not change the statistics by much and we do not carry out this modification here.

In *Figure* F.4, the top plot, we show the histogram of the 'observed' sequence along with the histogram of the synthetic version, corresponding to the parameters $(\varepsilon, \sigma, l) = (.05, .8, .35m)$. In computing the histogram we used .0025 as the bin width. The lines in the figure connect the relative frequency in each bin for the relevant data-set. Note that the match between the marginals of the standardized observations and the model is good and we let the quoted values define the estimates of the ε, l and σ parameters. The symmetric and long tailed marginal distribution for the reflection

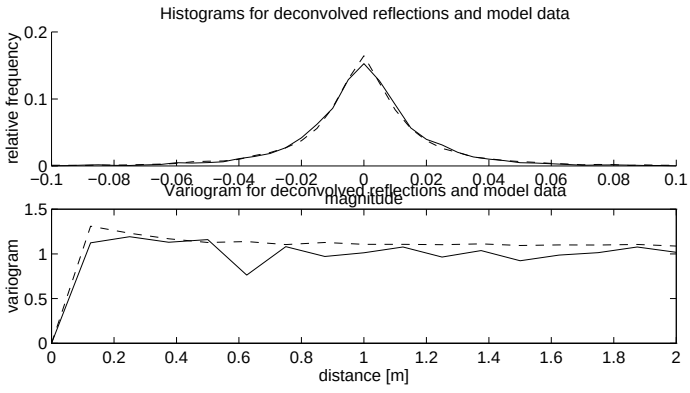

Figure F.4: Histogram, top plot, and variogram of the deconvolved speed measurement compared to that associated with a realization of the model. The dashed lines correspond to the model data using the parameter estimates $\varepsilon = .05$, $\sigma = .8$ and $l = .35m$. Note that the measurements were standardized with respect to the variability envelope.

process seen in the plot was obtained by modeling the reflections as the difference of two log-normally distributed random variables. In [52] the reflections are explicitly

modeled by a mixture of Laplacian distributions and in [19] by a generalized Gaussian distribution in order to obtain such a characteristic marginal distribution.

Since the reflections are formed by combining adjacent speed values, the marginal distribution exhibited in the top plot of Figure F.4 depends on the spatial correlation parameter l. The result (3.2.6) shows that the spatial correlation of the reflections is the important aspect of the stochastic structure of the reflections for pulse shaping. In the bottom plot we compare the spatial structure of the 'observations' with that of the synthetic version by plotting the variograms of these. Choosing the parameters as above results in the match shown in the plot, with the solid line corresponding to the sequence $\tilde{r}_k$ and the dashed line to a realization of $\tilde{R}_k$. Note the somewhat anomalous variogram value at lag $.6m$. This corresponds to the length of the measurement tool and illustrates that the deconvolution does not perfectly remove the effect of the tool. Both variograms in the plot were normalized by the estimated variance of the sequence $\tilde{r}_k$. We can also compute the variogram of the deconvolved speed recording and compare that to the variogram of the synthetic version. This we do in *Figure* F.5. Note that we normalized the speed recordings only with respect to the estimated variance. The figure corroborates that a correlation range on the order $.5m$ is reasonable.

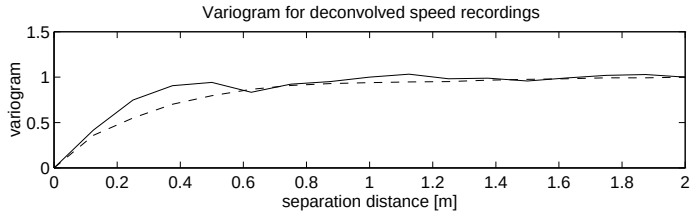

Figure F.5: Variogram of the deconvolved speed measurement compared to that associated with a realization of the model, dashed line. The parameter estimates $(\varepsilon, \sigma, l) = (.05, .8, .35m)$ led to the good match. Note that the measurements were normalized with respect to variance.

At this point it is interesting to compare the statistics of the original data, *non-deconvolved*, with those of a realization of the model when we apply the measurement filter F.1.1 to it. Consider the marginal distribution associated with $\overline{r}_k \equiv (c_{k+1} - c_k)/((c_{k+1} + c_k)\hat{e}_k)$. In the top plot of *Figure* F.6 we show the histogram of the $\overline{r}_k$ coefficients for the subrange of the well shown in the bottom plot. The solid line corresponds to the histogram of the whole sequence, whereas the dotted lines correspond to the histograms of the observations in the upper and lower halves of the sequence. Note that the lines almost coincide. Hence, by standardizing as above we have obtained a process whose marginal distribution is fairly stable with respect to depth. Also observe that the dashed line, corresponding to the marginal of the model, conforms with that of the observations. The 'observed synthetic' medium is defined by first drawing a realization from the model and then applying the measurement filter to it. The autocorrelation of the sequence $\overline{r}_k$ will be determined by the measurement process and the parameter l. This we illustrate in the bottom plot of Figure F.6 where we have plotted the variogram of the sequence $\overline{r}_k$. The interpretation of the lines is as above. That is, the solid line corresponds to all the data, the dotted lines to the data in the upper and lower halves of the well and the dashed line to the variogram of a realization of the model. Again note that the statistics of the standardized sequence are fairly stable with respect to depth, and moreover match well the statistics of the model. The somewhat peculiar shape of these variograms can be explained in terms of the measurement model and the fact that forming the interface reflection coefficients corresponds, to first order in ε, to forming the first order differences of the sequence of velocities. If the $\tilde{C}_k$ had been independent, corresponding to $l \approx 0$, the variogram of the reflection sequence would have been $< 0\ 1.5\ 1\ 1 \cdots >$, to first order in ε. The variogram value 1.5 for adjacent reflections corresponds to these being negatively correlated, and serves to 'tie down' the partial sums of the reflections, which in turn corresponds to the $\tilde{C}_k$ sequence being stationary. The variogram shape in the figure can be seen as a modification of the sequence mentioned above, the modification being induced by the measurement filter and some spatial correlation in the sequence $\tilde{C}_k$.

We now seek to illustrate how the above statistics depend on the parameter values and hence the accuracy with which we can expect to estimate these. In *Figure* F.7

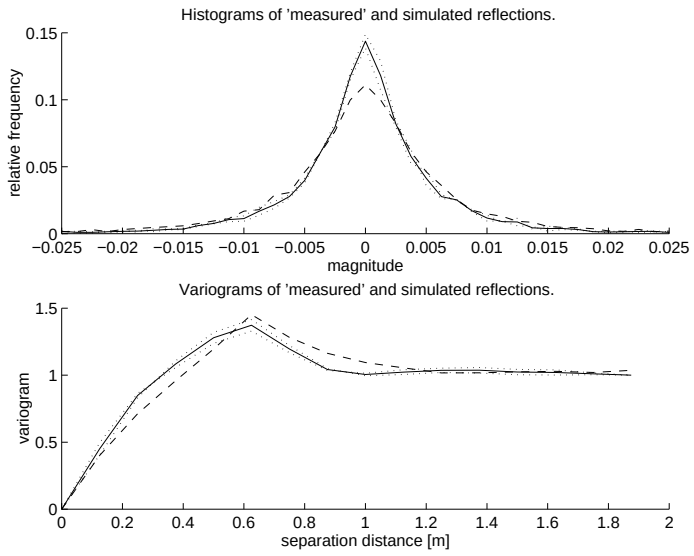

Figure F.6: The figure exhibits some statistics associated with the (non-deconvolved) sonic log in well 10 and of a realization of the estimated model having been modified by the measurement tool. The bottom plot displays the relevant subsequence of the sonic log. The top plot shows histograms of the reflection coefficients, computed assuming a constant density and standardized with respect to variability. The solid line corresponds to the entire log section, the dotted lines to data in upper/lower halves and the dashed line to a realization of the model. The marginal distribution seems to be stable with respect to depth, furthermore match that of the model. The interpretation of the second plot is similar except that the variogram rather than the histogram has been computed.

we plot, dashed lines, the histogram of the simulated multistep reflections we obtain when we perturb the value of σ by $\pm 20\%$ from the base case value quoted above. Note that the associated value of ε is chosen such that the variance of the sequences is unchanged. Since the observed sequence is only weakly spatially correlated the precision of the variance estimate will be high. We see that the statistics differ markedly from the statistics associated with the base case parameter set plotted by the solid line.

Similarly, in *Figure* F.8 we perturb the value of the parameter l by $\pm 20\%$. The resulting statistics are plotted by the dashed lines and do not differ strongly from

the statistics associated with the base case parameter set displayed by the solid line. Consequently, we cannot in general expect to estimate this parameter with high relative precision.

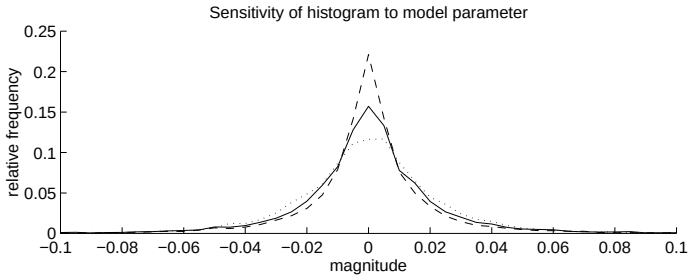

Figure F.7: We base the estimate of the parameter σ on the shape of the histogram. The dashed lines illustrate the sensitivity in the histogram of the reflections to variations in σ. We perturbed the parameter σ by $\pm 20\%$.

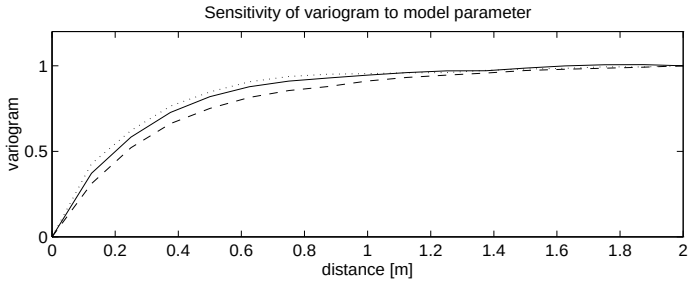

Figure F.8: The correlation range l is estimated partly based on the variogram of the speed recordings. The dashed lines illustrate the sensitivity in the variogram to variations in the parameter l. We perturbed the parameter l by $\pm 20\%$.

Bibliography

[1] K. Aki and P. G. Richards. *Quantitative Seismology-Theory and Methods*, volume 1. W. Freeman, 1980.

[2] L. Arnold, G. Papanicolaou, and V. Wihstutz. Asymptotic analysis of the lyapunov exponent and rotation number of random oscillator and applications. *SIAM J. Appl. Math.*, 46:427–450, 1986.

[3] M. Ash, W. Kohler, G. C. Papanicolaou, M. Postel, and B. White. Frequency content of randomly scattered signals. *SIAM Review*, 33:519–625, 1991.

[4] N. C. Banik, I. Lerche, and R. T Shuey. Stratigraphic filtering, part I: Derivation of the O'Doherty-Anstey formula. *Geophysics*, 50:2768–2774, 1985.

[5] N. C. Banik, I. Lerche, and R. T Shuey. Stratigraphic filtering, part II: Model spectra. *Geophysics*, 50:2775–2783, 1985.

[6] N. Bleistein and R. Handelsman. *Asymptotic expansions of integrals.* Dover Publications, 1986.

[7] E. Bølviken, G. Storvik E. Nilsen, E. Siring, and D. Van Der Wel. Stochastic regime models and wireline log data. In C. Griffiths, editor, *Proceedings of GAWL II.* Special publications of the Geological Society, 1991.

[8] R. Burridge and H. W. Chang. Multimode, one-dimensional wave propagation in a highly discontinuous medium. *Wave Motion*, 11:231–249, 1988.

[9] R. Burridge, H. W. Chang, and M. V. de Hoop. Wave propagation with tunneling in a highly discontinuous medium. *Wave Motion*, 13:307–327, 1991.

[10] R. Burridge, H. W. Chang, and M. V. De Hoop. The pseudo-primary field due to a point source in a finely layered medium. *Geophysical Journal International*, 104:489–506, 1991.

[11] R. Burridge, P. Lewicki, and G. C. Papanicolaou. Pulse stabilization in a strongly heterogeneous layered medium. *Wave Motion*, 20:177–195, 1994.

[12] R. Burridge, G. C. Papanicolaou, and B. White. One dimensional wave propagation in a highly discontinuous medium. *Wave Motion*, 10:19–44, 1988.

[13] J. Chillan and J. P. Fouque. *Pressure fields generated by acoustical pulses propagating in randomly layered media.* SIAM J. Appl. Math, to appear, 1998.

[14] J. Claerbout. *Earth Sounding Analysis. Processing versus inversion.* Blackweld Scientific Publications., 1992.

[15] J. F. Clouet and J. P. Fouque. Spreading of a pulse travelling in random media. *Annals of Applied Probability*, 4:1083–1097, 1994.

[16] W. Feller. *An Introduction to Probabilty Theory and Its Applications, Volume II.* Wiley, 1971.

[17] C. Flaum, J. Holenka, and C. Case. Eliminating the effect of rugosity on density logs by geometrical response matching. *Presented at the 64th SPE Ann. Tech. Conference and Exhibition.*, 1989.

[18] A. Frankel and R. W. Clayton. Finite difference simulations of seismic scattering: implications for the propagation of short-period seismic waves in the crust and models of heterogeneity. *J. Geophys. Res.*, 91:6465–6489, 1986.

[19] W. Gray. *Variable norm deconvolution.* Ph.D. thesis, Staford University, 1979.

[20] T. Høye, E. Damsleth, and K. Hollund. Stochastic structural modeling of Troll West with special emphasis on the thin oil zone. In J. M. Yarus and R. L. Chambers, editors, *Stochastic Modeling and Geostatistics: Practical Applications and Case Studies.* American Association of Petroleum Geologists, Special Publication, 1994.

[21] K. Hsu and R. Burridge. Effects of averaging and sampling on the statistics of reflection coefficients. *Geophysics*, 56:50–58, 1991.

[22] J. B. Keller. Stochastic equations and wave propagation in random media. *Proc. Symp. Appl. Math.*, 16, 1964.

[23] J. B. Keller and R. Lewis. Asymptotic methods for partial differential equations: The reduced wave equation and maxwell's equations. In D. McLaughlin J. B. Keller and G. Papanicolaou, editors, *Surveys in applied mathematics*. Plenum Press, New York, 1995.

[24] C. Kerner and P. E. Harris. Scattering attenuation in sediments modeled by arma processes-validation of simple q models. *Geophysics*, 59:1813–1826, 1994.

[25] G. Kneib. The statistical nature of the upper continental crystalline crust derived from in situ seismic measurements. *Geophysical Journal International*, 122:594–616, 1995.

[26] W. Kohler and G. Papanicolaou. Asymptotic theory of mixing stochastic ordinary differential equations. *Comm. Pure Appl. Math.*, 27:614–668, 1974.

[27] W. Kohler, G. Papanicolaou, and B. White. Localization and mode conversion for elastic waves in randomly layered media I & II. *Wave Motion*, 23:1–22,181–201, 1996.

[28] P. Lewicki. Long time evolution of wavefronts in random media. *SIAM J. Appl. Math.*, 54:907–934, 1994.

[29] P. Lewicki, R. Burridge, and M. V. de Hoop. Beyond effective medium theory: Pulse stabilization for multimode wave propagation in high contrast layered media. *SIAM Journal on Applied Math.*, 56:256–276, 1996.

[30] S. Mallat, G. Papanicolaou, and Z. Zhang. Adaptive covariance estimation of locally stationary processes. *Submitted to Annales of Statistics*, 1996.

[31] S. Mallat and Z. Zhang. Matching pursuit with time-frequency dictionaries. *IEEE Transactions on Signal Processing*, 41:3397–3415, 1993.

[32] L. Nirenberg. *Topics in nonlinear functional analysis.* Lecture notes; Courant Institute, 1973.

[33] R. F. O'Doherty and N. A. Anstey. Reflections on amplitudes. *Geophysical Prospecting*, 19:430–458, 1971.

[34] G. Papanicolaou. Stochastic differential equations with applications to random harmonic oscillators and wave propagation in random media. *SIAM J. Appl. Math.*, 21:287–305, 1971.

[35] G. Papanicolaou and P. Lewicki. Reflection of wavefronts by randomly layered media. *Wave Motion*, 20:245–266, 1994.

[36] G. Papanicolaou, D. Stroock, and S. Varadhan. Martingale approach to some limit theorems. *Duke Turbulence conference, Duke University Mathematics series III.*, 1976.

[37] G. Papanicolaou and S. Weinryb. A functional limit theorem for waves reflected by a random medium. *Applied Mathematics & Optimization*, 30:307 – 334, 1994.

[38] J. R. Resnick, I. Lerche, and R. T. Shuey. Reflection, transmission, and the generalized primary wave. *Geophys. J. R. Astr. Soc.*, 87:349–377, 1986.

[39] P. G. Richards and W. Menke. The apparent attenuation of a scattering medium. *Bull Seism. Soc. Amer.*, 73:1005–1021, 1983.

[40] M. Schoenberger and F. K. Levin. Apparent attenuation due to intrabed multiples. *Geophysics*, 39:278–291, 1974.

[41] M. Schoenberger and F. K. Levin. Apparent attenuation due to intrabed multiples, II. *Geophysics*, 43:730–737, 1978.

[42] N. Serakiotou. Partial suppression of multiples caused by a sequence of thin layers. *SEP*, 57:365–382, 1988.

[43] S. A. Shapiro, P. Hubral, and B. Ursin. Reflectivity/transmissivity for 1-d inhomogeneous random elastic media: dynamic-equivalent-medium approach. *Geophysical Journal International*, 126:184–196, 1996.

[44] S. A. Shapiro and H. Zhien. Transmission of wavefields through finely layered media: attenuation, velocity, fluctuations. *62nd Ann. Internat. Mtg., Soc. Expl. Geophys., Expanded Abstracts*, 1:820–823, 1992.

[45] S. A. Shapiro and H. Zhien. The O'Doherty-Anstey formula and localization of seismic waves. *Geophysics*, 58:736–740, 1993.

[46] P. Sheng, B. White, and B. Nair. Lithological correlation and seismic wave localization in the earth's subsurface. *Inverse Problems*, 5, 1989.

[47] P. Sheng, B. White, Z. Zhang, and G. Papanicolaou. Wave localization and multiple scattering in randomly-layered media. In P. Sheng, editor, *Scattering and localization of classical waves in random media.* World Scientific, 1990.

[48] P. Sheng, B. White, Z. Q. Zhang, and G. C. Papanicolaou. Minimum wave-localization length in a one-dimensional random medoium. *Phys. Rev. B*, 34:4757–4761, 1986.

[49] K. Sølna and G. C. Papanicolaou. Propagation of pulses from a point source in a locally layered medium. *In preparation*, 1997.

[50] J. P. Todoeschuck, O. G. Jensen, and S. Labonte. Gaussian scaling noise model of seismic reflection sequences: Evidence from well logs. *Geophysics*, 55:480–484, 1990.

[51] A. T. Walden and J. W. J. Hosken. An investigation of the spectral properties of primary reflection coefficients. *Geophysical Prospecting*, 33:400–435, 1985.

[52] A. T. Walden and J. W. J. Hosken. The nature of the non-gaussianity of primary reflection coefficients and its significance for deconvolution. *Geophysical Prospecting*, 34:1038–1066, 1986.

[53] B. White, P. Sheng, and B. Nair. Localization and backscattering spectrum of seismic waves in stratified lithology. *Geophysics*, 55:1158–1165, 1990.

[54] B. White, P. Sheng, B. Nair, and S. Kerford. Bayesian deconvolution of gamma-ray logs. *Geophysics*, 52:1535–1546, 1987.

[55] M. Widmaier, T. Muller, S. A. Shapiro, and P. Hubral. Amplitude-preserving migration and elastic p-wave avo corrected for thin layering. *J. Seis. Expl.*, 4:169–177, 1995.

[56] R. Wong. *Asymptotic approximations of integrals.* Academic Press, 1989.

[57] R. S. Wu and K. Aki. Elastic wave scattering by a random medium and the small-scale inhomogeneities in the lithosphere. *J. Geophys. Res.*, 90:10261–10273, 1985.

[58] R. S. Wu, Z. Xu, and X. P. Li. Heterogeneity spectrum and scale-anisotropy in the upper crust revealed by the German continental deep-drilling (KTB) holes. *Geophys. Res. Lett.*, 21:911–914, 1994.